

MODELLING OF COUNTER ROTATING TWIN SCREW EXTRUSION

MODELLING OF COUNTER ROTATING TWIN SCREW EXTRUSION

By

ALI GOGER

A Thesis

Submitted to the School of Graduate Studies

in Partial Fulfilment of the Requirements

for the Degree

Master of Applied Science

McMaster University

MASTER OF APPLIED SCIENCE (2013)

(CHEMICAL ENGINEERING)

TITLE: Modelling of Counter Rotating Twin Screw Extrusion

AUTHOR: Ali Goger

BSc. (Yildiz Technical University, Turkey)

SUPERVISORS: Dr. John Vlachopoulos and Dr. Michael R. Thompson

NUMBER OF PAGES: XX, 124

ABSTRACT

Intermeshing counter-rotating twin screw extruders (ICRTSE) are used extensively in the polymer processing industry for pelletizing, devolatilization and extrusion of various plastic products. ICRTSE have better positive displacement ability and are more suitable for shear sensitive materials compared to other types of twin screw extruders.

The present study started with an extensive literature search of both co-rotating and counter-rotating twin screw extruders. Surprisingly, it was noticed that several authors have reported negative pressure (as large as -13bar) in the simulation of twin screw extruders. Of course, negative pressure is meaningless. It is presented that negative pressure was due to the poor choice of boundary conditions. Several suggestions were provided to explain how to overcome this problem.

The objectives of this thesis are to understand the flow mechanism and the effects of screw geometries and processing conditions in the conveying element of ICRTSE. This is done by two different methods. First, a simple flow model based on a volume of the conveying element of ICRTSE was used to calculate flow rate. Since ICRTSE do not give complete positive displacement, the various leakage flows were identified and taken into account in the simple flow model. Although the simple flow model provided reasonable results in terms of flow rate, computer simulations were found necessary due to the limitations of simple flow model. Second, a 3D computer simulation of ICRTSE was developed for various screw pitch lengths, ratios of flight width-to-channel width and the screw speeds. Both Newtonian and non-Newtonian fluids were examined. A quasi-steady state finite element method was used to avoid

time dependent moving boundaries. A number of sequential geometries were used to present a complete screw rotation in the ICRTSE. The flow behaviour in the conveying element of ICRTSE was characterized by its axial velocity distribution and flow rate. In addition, dispersive mixing in the conveying element of ICRTSE was characterized by using shear stress distribution and a mixing parameter λ , which quantified the elongational flow components. Comparison of flow behaviour and dispersive mixing were also discussed for different screw pitch lengths, ratios of flight width-to-channel width and screw speeds.

It was shown the simple model based on geometrical parameters for pumping behaviour give reasonable prediction of flow rate. It was found that determination of negative pressure should be taken into account in numerical simulations. The pumping efficiency is influenced positively by the ratio of flight width-to-channel width but it is affected negatively by the screw pitch length. It is negligibly changed with screw speed. Finally, the dominant flow is shear flow in ICRTSE and therefore, dispersive mixing capacity is very limited due to a lack of elongational effects.

ACKNOWLEDGEMENTS

My first gratitude goes to my academic supervisors, Dr. J. Vlachopoulos and Dr. M. R. Thompson, for the years of academic training, thoughtful support and continuous encouragements.

I also would like to thank everyone in MIKROSAN INC., especially R&D coordinator Abdullah Demirci, for the useful discussions and suggestions to improve my study.

Finally, I can never begin to thank my wife, Aysenur Safa, for her love and peaceful support. Without her, none of this would have been possible.

TABLE OF CONTENT

ABSTRACT.....	III
ACKNOWLEDGMENT	V
TABLE OF CONTENT	VI
LIST OF FIGURES	XI
LIST OF TABLES	XVI
LIST OF SYMBOLS	XVIII
Chapter 1	
INTRODUCTION AND BACKGROUND	1
1.1. Overview of the Twin Screw Extruders	1
1.2. Intermeshing Counter-Rotating Twin Screw Extruders (ICRTSE).....	3
1.3. Modelling Twin Screw Extrusion	5
 1.3.1. Analytical Modelling	5
 1.3.2. Flow Analysis Network	5
 1.3.3. Quasi Steady State Approximation	6
 1.3.4. Moving Reference Frame Method	7
 1.3.5. Mesh Superimposition Technique	9
1.4. Objectives	10
1.5. Outline	11

Chapter 2

GEOMETRICAL PARAMETERS AND MATERIAL PROPERTIES	12
2.1. Introduction	12
2.2. Geometrical Parameters	12
2.3. Material Properties and Processing Conditions	14

Chapter 3

A SIMPLE FLOW MODEL OF COUNTER-ROTATING TWIN SCREW EXTRUDERS	19
3.1. Introduction	19
3.2. Simple Calculation of Output without Leakage Flow	21
3.3. Simple Calculation of Leakage Flows.....	24
3.3.1. Calender Leakage Flow	27
3.3.2. Tetrahedral Leakage Flow	29
3.3.3. Flight Gap Leakage Flow	31
3.3.4. Side Gap Leakage Flow	32
3.4. Simple Model of Total Output	34
3.5. Limitations of the Simple Model	41

Chapter 4

COMPUTER SIMULATION USING OPENFOAM®	42
4.1. Introduction	42
4.2. Numerical Analysis	43
4.2.1. Solvers	43
4.2.2. Utilities	45
4.3. Boundary Conditions	46
4.4. Mesh Independency	49
4.5. Parallel Running	50
4.6. Converges of Computer Simulation	52

Chapter 5

NEGATIVE PRESSURE IN MODELLING ROTATING POLYMER PROCESSING MACHINERY	53
5.1. Introduction	53
5.2. Reviewing Modelling Results	54
5.3. Explaining the Phenomenon	60
5.4. Conclusion	61

Chapter 6

NUMERICAL RESULTS.....	63
6.1. Introduction	63
6.2. Description of Method	63
6.3. Flow Pattern in ICRTSE	67
6.3.1. Axial Velocity in ICRTSE	67
6.3.2. Pumping Behaviour of ICRTSE	76
6.3.2.1. The Effect of Screw Pitch Length	76
6.3.2.2. The Effect of the Ratio of Flight Width-to-channel Width...76	
6.3.2.3. The Effect of Screw Speed	77
6.4. Dispersive Mixing Behaviour of ICRTSE	83
6.4.1. Shear Stress Distribution	83
6.4.2. Mixing Parameter Lamda	98

Chapter 7

COMPARASION OF SIMPLE FLOW MODEL AND COMPUTER SIMULATION	111
7.1. Introduction	111
7.2. Comparison of the Effect of the Screw Pitch Length	111

7.3. Comparison of the Effect of Flight Width-to-channel Width Ratio	111
7.4. Comparison of the Effect of Screw Speeds	112
Chapter 8	
CONCLUSION AND FUTURE WORK	117
8.1. Conclusion	117
8.2. Recommendations	119
REFERENCES	120

LIST OF FIGURES

Figure	Page
Figure 1.1. Classification of Twin Screw Extruders (Cheremisinoff, 1987)	2
Figure 1.2. Physical Interpretation of Moving Reference System (MRF) (Potriefke, 2007) (An observer who is always at the tip of the flight of the screws, moves with the velocity of moving frame of reference.)	9
Figure 2.1. Schematic View of ICRTSE from MIKROSAN INC. I: Left Hand Screw II: Right Hand Screw Detail A: Conveying Element Detail B: Mixing Element	13
Figure 2.2. Screw Design Parameter	15
Figure 2.3. Viscosity Curve of Typical PVC (As Measured in a Rotational Viscometer)	18
Figure 3.1. C-shaped Chamber (Fitzpatrick, 2009)	20
Figure 3.2. Overlapping Angle (Janssen, 1978)	20
Figure 3.3. Geometrical Parameters for Simple Model of Theoretical Output	23
Figure 3.4. Leakage Flows (Fitzpatrick, 2009).....	26
Figure 3.5. Calender Gap in ICRTSE (Janssen, 1978)	26
Figure 3.6. Geometrical Parameters in Tetrahedral Gap Leakage Flow (Janssen, 1978).....	30
Figure 3.7. Schematic View of Flight Gap (Janssen, 1978)	30

Figure 3.8. Pumping Efficiency for Various Screw Pitch Lengths for Simple Model	37
Figure 3.9. Pumping Efficiency for Various Flight Width-to-channel Width Ratios	39
Figure 3.10. Pumping Efficiency for Various Screw Speeds for Simple Model	40
Figure 4.1. Working Procedure of Current Study	44
Figure 4.2. Mesh Appearance of 105mm Screw Pitch Length	51
Figure 4.3. Converging Residuals with Iteration Number for 105 mm Screw Pitch Length	52
Figure 5.1. Pressure Development between Two Co-rotating Cylinders	58
Figure 5.2. Pressure Development between Two Counter-rotating Cylinders	59
Figure 5.3. Pressure Distribution in a Journal Bearing	62
Figure 6.1. Sequential Geometries Representing Complete Cycle	65
Figure 6.2. Schematic View of the Location of Cross Sections and Boundaries	66
Figure 6.3. Axial Velocity Distribution at Plane 1 $\alpha=90^\circ$ for 105 mm Screw Pitch Length	72
Figure 6.4. Axial Velocity Distribution at Plane 2 $\alpha=90^\circ$ for 105 mm Screw Pitch Length	73
Figure 6.5. Axial Velocity Distribution at Plane 3 $\alpha=90^\circ$ for 105 mm Screw Pitch Length	74

Figure 6.6. Axial Velocity Distribution at Plane 4 $\alpha=90^\circ$ for 105 mm Screw Pitch Length	75
Figure 6.7. The Effect of Screw Pitch Length on Pumping Efficiency	78
Figure 6.8. The Effect of Flight Width-to-channel Width Ratio on Pumping Efficiency for Power Index 1, 0.7 and 0.3	79
Figure 6.9. The Effect of Screw Speed on Pumping Efficiency for Power Index 1	80
Figure 6.10. The Effect of Screw Speed on Pumping Efficiency for Power Index 0.7.....	81
Figure 6.11. The Effect of Screw Speed on Pumping Efficiency for Power Index 0.3.....	82
Figure 6.12. Shear Stress Distribution at Plane 1 $\alpha=90^\circ$ for 105 mm Screw Pitch Length Power Index 0.7	86
Figure 6.13. Shear Stress Distribution at Plane 2 $\alpha=90^\circ$ for 105 mm Screw Pitch Length Power Index 0.7	87
Figure 6.14. Shear Stress Distribution at Plane 3 $\alpha=90^\circ$ for 105 mm Screw Pitch Length Power Index 0.7	88
Figure 6.15. Shear Stress Distribution at Plane 4 $\alpha=90^\circ$ for 105 mm Screw Pitch Length Power Index 0.7	89
Figure 6.16. The Volume Distribution of Shear Stress for 75 mm Screw Pitch Length for Power Index 0.7	92

Figure 6.17. The Volume Distribution of Shear Stress for 105 mm Screw Pitch Length for Power Index 0.7	93
Figure 6.18. The Volume Distribution of Shear Stress for 75 mm Screw Pitch Length for Power Index 0.3	94
Figure 6.19. The Volume Distribution of Shear Stress for 105 mm Screw Pitch Length for Power Index 0.3	95
Figure 6.20. The Average Shear Stress for Various Screw Speed and Screw Pitch Length Power Index 0.7	96
Figure 6.21. The Average Shear Stress for Various Screw Speed and Screw Pitch Length Power Index 0.3.....	97
Figure 6.22. Mixing Parameter λ Distribution at Plane 1 $\alpha=90^\circ$ for 105 mm Screw Pitch Length Power Index 0.7	101
Figure 6.23. Mixing Parameter λ Distribution at Plane 2 $\alpha=90^\circ$ for 105 mm Screw Pitch Length Power Index 0.7	102
Figure 6.24. Mixing Parameter λ Distribution at Plane 3 $\alpha=90^\circ$ for 105 mm Screw Pitch Length Power Index 0.7	103
Figure 6.25. Mixing Parameter λ Distribution at Plane 4 $\alpha=90^\circ$ for 105 mm Screw Pitch Length Power Index 0.7	104
Figure 6.26. The Volume Distribution of Mixing Parameter λ for 75 mm Screw Pitch Length for Power Index 0.7	105

Figure 6.27. The Volume Distribution of Mixing Parameter λ for 105 mm Screw Pitch Length for Power Index 0.7	106
Figure 6.28. The Volume Distribution of Mixing Parameter λ for 75 mm Screw Pitch Length for Power Index 0.3	107
Figure 6.29. The Volume Distribution of Mixing Parameter λ for 105 mm Screw Pitch Length for Power Index 0.3	108
Figure 6.30. The Average Mixing Parameter λ for Various Screw Speed and Screw Pitch Length Power Index 0.7	109
Figure 6.31. The Average Mixing Parameter λ for Various Screw Speed and Screw Pitch Length Power Index 0.3	110
Figure 7.1. Comparison of the Effect of Screw Pitch Length for Computer Simulation and Simple Flow Model	113
Figure 7.2. Comparison of the Effect of the Flight Width-to-channel Width Ratio for Computer Simulation and Simple Flow Model	114
Figure 7.3. Comparison of the Effect of Screw Speed for 75 mm and 90 mm Screw Pitch Length for Computer Simulation and Simple Flow Model	115
Figure 7.4. Comparison of the Effect of Screw Speed for 105 mm and 135 mm Screw Pitch Length for Computer Simulation and Simple Flow Model	116

LIST OF TABLES

Table	Page
Table 2.1 ICRTSE Geometrical Design Parameters	16
Table 3.1. Geometrical Parameters and Mass Flow Rate Results without Leakage Flow	24
Table 3.2. Parameters for Simple Model of Leakage Flows.....	27
Table 3.3. Total Calender Leakage Flow for Various Screw Pitch Lengths	28
Table 3.4. Total Tetrahedral Gap Leakage Flow for Various Screw Pitch Lengths	29
Table 3.5. Total Flight Gap Leakage Flow for Various Screw Pitch Lengths	32
Table 3.6. Total Side Gap Leakage Flow for Various Screw Pitch Lengths	33
Table 3.7. Total Mass Flow Rate (Including Leakage Flows) for Various Screw Pitch Lengths	34
Table 3.8. Total Mass Flow Rate (Including Leakage Flows) For Various Flight Width-to-channel Width Ratios	38
Table 3.9. Total Mass Flow Rate (Including Leakage Flows) for Various Screw Speeds	38
Table 4.1. Boundary Conditions for Velocity and Pressure	48
Table 4.2. Different Number of Cells and Results for Various Cases	50

Table 5.1. Parameters Used in the Co- and Counter-rotating Cylinder Examples Reported in Figures 5.1 and 5.2	57
Table 6.1. Average Axial Velocities for Various α and for Screw Pitch Length for Power Index 1	69
Table 6.2. Average Axial Velocities for Various α and for Screw Pitch Length for Power Index 0.7	70
Table 6.3. Average Axial Velocities for Various α and for Screw Pitch Length for Power Index 0.3	71
Table 6.4. Average Shear Stress and Average Mixing Parameter for Various α and Screw Pitch Length for Power Index 0.7	90
Table 6.5. Average Shear Stress and Average Mixing Parameter for Various α and Screw Pitch Length for Power Index 0.3	91

LIST OF SYMBOLS

\bar{V}	Velocity Vector
$\dot{\gamma}$	Rate of the Strain Tensor
$\bar{\tau}$	Stress tensor
A	Center Distance
C_p	Specific Heat Capacity
e_θ	Unit Vector in θ direction
H	Screw Channel Depth
i	Number of Screw Flights
Π_D	Second invariant of the Strain Rate Tensor
k	Thermal Conductivity
n	Power index
N	Screw Speed
P	Pressure
Q_c	Calender Leakage Flow
Q_f	Flight Gap Leakage Flow
Q_s	Side Gap Leakage Flow
Q_t	Tetrahedral Leakage Flow

Q_{th}	Theoretical Flow Rate
Q_{total}	Total Flow Rate
R	Screw Radius
r	Radial Position of the Element
S	Screw Pitch Length
U_x	Velocity at x Direction
U_y	Velocity at y Direction
U_z	Velocity at z Direction
V	Circular Path Velocity
V_1	Volume of the One Barrel Half over One Pitch Length
V_2	Volume of the Screw Root over One Pitch Length
V_3	Volume of the Screw Flight
V_{axial}	Axial Velocity
V_c	C-shaped chamber Volume
W_c	Screw Channel width
W_f	Screw Flight Width
α	Overlapping Angle
δ	Clearance Between Screw and Barrel

Δp	Local Pressure Difference Between Opposite C-shaped Chamber
ΔP	Pressure Drop due to the Die
ϵ	Side Gap Width
η	Viscosity
η_0	Viscosity at Zero Shear Rate
η_{inf}	Viscosity at Infinity Shear Rate
θ	Helix Angle
λ	Dispersive Mixing Parameter
ρ	Density
σ	Calender Gap
ω	Rate of the Vorticity Tensor

Chapter One

INTRODUCTION AND BACKGROUND

1.1. Overview of the Twin Screw Extruders

Twin screw extruders are used extensively for pelletizing, compounding and extrusion of various plastic products in polymer processing. A twin screw extruder entails two side by side screws used to convey, melt and pump the polymers. Twin screw extruders can be classified according to the screw rotation direction and relative positions of the screws. The categorization of twin screw extruders are shown in Figure 1.1. First, the types of twin screw extruders can be divided into two groups: co- or counter rotating twin screw extruders in terms of direction of screw rotation. Second, they can be categorized as intermeshing and non-intermeshing twin screw extruders according to the relative position of the screws. Furthermore, the intermeshing type of twin screw extruder is divided into two as fully and partially intermeshing twin screw extruders. Non-intermeshing twin screw extruders can be categorized as tangential and separated as well.

One of the main differences between the single screw and twin screw extruder is the type of transport mechanism. Material transport in a single screw extruder is viscous drag in the melt conveying zone. On the other hand, the mechanism of







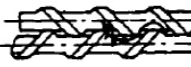

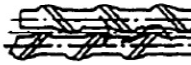

SCREW ENGAGEMENT		SYSTEM	COUNTER-ROTATING	CO-ROTATING
INTERMESHING	FULLY INTERMESHING	LENGTHWISE AND CROSSWISE CLOSED	1 	2 THEORETICALLY NOT POSSIBLE
		LENGTHWISE OPEN AND CROSSWISE CLOSED	3 THEORETICALLY NOT POSSIBLE	4 
		LENGTHWISE AND CROSSWISE OPEN	5 THEORETICALLY POSSIBLE BUT PRACTICALLY NOT REALIZED	6 
	PARTIALLY INTERMESHING	LENGTHWISE OPEN AND CROSSWISE CLOSED	7 	8 THEORETICALLY NOT POSSIBLE
		LENGTHWISE AND CROSSWISE OPEN	9A 	10A 
			9B 	10B 
NOT INTERMESHING	NOT INTERMESHING	LENGTHWISE AND CROSSWISE OPEN	11 	12 

Figure 1.1. Classification of Twin Screw Extruders (Cheremisinoff, 1987)

of transport in a twin screw extruder is positive displacement for its fluid transport. Another main difference between single and twin screw extruders is the velocity profile in the screw channel. The flow in twin screw is more complex than in the single screw extruder. This complexity of the flow provides better mixing, heat transfer and devolatilization.

Intermeshing counter-rotating twin screw extruders (ICRTSE) have better positive displacement ability and are more suitable for shear sensitive materials compare to other types of extruders. In addition, Eggen and Syre (2004) implied that having counter-rotating screws are advantageous because they can be made shorter than co-rotating machines. A shorter extruder gives an opportunity to save material and space. It also simplifies the screw design because it is hard to prevent long screws from flexing under load.

1.2. Intermeshing Counter-Rotating Twin Screw Extruders (ICRTSE)

Intermeshing counter-rotating twin screw extruders (ICRTSE) have their origins in the 19th century as positive displacement pumps. Positive displacement is defined in this case as material transportation within a fully filled C-shaped chamber that only allows bulk motion in one axial direction. ICRTSE are mainly utilized for pelletizing, devolatilizing, polyvinyl chloride (PVC) pipes and profiles. ICRTSE have an advantage by exhibiting a superior constant throughput compare to the other extruders.

The ratio between the total throughput and theoretical throughput based on its C-shaped chamber volume is called *pumping efficiency*. Pumping efficiency is the main parameter for measuring performance of an ICRTSE. Doboczky (1965²) suggested the application of this factor by which the theoretical output must be multiplied in order to arrive at experimental values. Doboczky (1965²) stated that pumping efficiencies varied for different screws from 0.17 to 0.64. Schenkel (1966) mentioned that the efficiency of twin screw extruder lies between 34% and 41% for various extruders. Menges and Klenk (1966) and Klenk (1971) improved the process, using polyvinylchloride. It was reported that the experimental output versus the theoretical prediction was in the range of 37 to 41% in their case.

Jiang (2008) investigated the pumping behaviour of ICRTSE for different ratios of flight width-to-channel width, clearances between screw and barrel and helix angles in his PhD thesis. It was found that thicker flighted elements had better pumping efficiency. According to that author the pumping efficiency decreased with decreasing power law index. It was also argued that a larger clearance between screw and barrel caused lower pumping efficiency due to higher leakage flows. Finally, he mentioned that there was little variation in pumping efficiency with changing helix angle.

Janssen et al. (1975) revealed that the throughput of ICRTSE increased linearly with increasing screw speed for a 70mm screw diameter. Doboczky (1965¹, 1965²) stated that ICRTSE has about three times higher output capacity than the single screw extruder for same size and the screw speed. Li and Manas-Zloczower (1994) stated that pumping efficiency hardly ever changes with screw speed. Sakai et al. (1987) made an experimental comparison between counter-rotation and co-rotation on the

twin screw extrusion performance. They mentioned that sharper residence time distribution can be obtained when using the counter-rotating twin screw extruder for a 69 mm diameter twin screw extruder. Wolf et al. (1986) concluded that counter-rotating twin screw extruders tend to behave like plug flow almost the entire extruder length for a 90 mm diameter extruder. Shon et al. (1999) indicated that the lowest mean residence time was obtained for the intermeshing twin screw extruder compare to the buss kneader, continuous mixer, co-rotating twin screw extruder and counter-rotating twin screw extruder. They showed that ICRTSE have near plug flow which indicates a positive displacement mechanism. In present study, different geometries of ICRTSE will be examined and effects on the pumping behaviour and dispersive mixing will be discussed.

1.3. Modelling Twin Screw Extrusion

1.3.1. Analytical Modelling

Analytical models have been presented by various authors and these have been reviewed by Janssen (1978) and White (1990). The analytical models are derived from simply determination of positive displacement capacity on the basis of twin screw geometry. The relevant models to this thesis and their limitations will be discussed in Chapter 3.

1.3.2. Flow Analysis Network

A common simplified numerical method to simulate this twin screw extruder is the Flow Analysis Network (FAN) method. The basic idea of the FAN method is to divide the region into control volumes (CV) and carry out flux balances on each. One

of the first users of FAN method for modelling fluid flow in kneading elements of a co-rotating twin screw extruder was Szydlowski et al. (1987). Sebastian and Rakos (1990) compared FAN method and finite element method (FEM) for the mixing section of the co-rotating twin screw extruder. Hong and White (1998) presented a FAN method to understand a pumping characteristic of thick and thin flight elements of counter-rotating twin screw extruder. However, this method is generally too restrictive in both the geometries it can be applied to as well as the information obtained, and hence other methods have been considered over time. What follows are a series of techniques used to apply the finite element method (FEM) to numerically simulate flow in a twin screw extruder – a system made complex due to its moving screws. In FEM, the geometry of the fluid domain is divided into a number of cells. Each cell is defined by nodal points and the neighbouring points connect to each other. Flow patterns are described by the equations of continuity and momentum as discretized partial differential equations in matrix form. The non-linear system of equation is then solved to determine the velocity and pressure components.

1.3.3. Quasi Steady State Approximation

Twin screw extruders cannot reach a truly steady state condition because the flow geometry being modelled is in constant motion rather than being fixed in space. Lee and Castro (1989) mentioned that if the Reynolds number is very small, the time dependent part of the continuum equation is negligible. The resulting quasi-steady state solution is dependent only on instantaneous material properties and boundary conditions. By this approximation, different relative positions of the screws into the barrel are selected and simulated as a fixed, steady state system. Different meshes are

necessary for each relative position of the screw as it rotates and the results are compiled together.

Yang and Manas-Zloczower (1992) used this method to simulate the dispersive mixing behaviour of a Banbury mixer (which is a rotating screw system). Ishikawa et al. (2000) applied this approach to simulate the pressure distribution of a 30 mm diameter co-rotating twin screw extruder. Bravo (1998) explored this method to understand the flow behaviour of a 45° stagger angle kneading element. Yao and Manas-Zloczower (1997) followed the quasi-steady state approximation for the mixing behaviour of the clearance mixer. Wang and Manas-Zloczower (1994) also applied quasi-steady state for the mixing behaviour of cavity mixer. Li (1995) simulated the intermeshing counter-rotating twin screw extruder and tangential counter-rotating twin screw extruder in terms of mixing efficiency by using quasi-steady state approximation in his PhD thesis. Recently, Sobhani et al. (2010) analyzed the flow behaviour of co-rotating twin screw extruder with the same method.

There are two main disadvantages for quasi-steady state approximation. First, a lot of meshing studies have to be done to accurately capture as many positions of screws as possible. Second, this method does not work properly because the energy equation is truly transient. Lee and Castro (1989) stated that neglecting the transient term in the equation of motion was justified but not the transient term of the energy equation.

1.3.4. Moving Reference Frame (MRF) Method

The alternative to the quasi-steady state approximation is to simulate the twin screw extrusion by the moving reference frame (MRF) method. In the MRF

approximation, an observer who is always at the tip of the flight of the screws, moves with the velocity of moving frame of reference. Physical interpretation of the MRF system is shown in Figure 1.2. There are two systems in MRF which are the absolute and the relative systems. In the absolute system, a point on a screw rotates in a circular path with the velocity in Equation 1.1.

$$V = N * R \quad (1.1)$$

where N is the screw speed and R is the screw radius. In the relative system, the velocity vector has an additional axial component which is shown Equation 1.2.

$$V_{axial} = -N * S \quad (1.2)$$

where N is the screw speed and S is the screw pitch. In this system, an observer is always moving on the tip of screws and the geometry stays the same.

Ortiz-Rodriquez and Tzoganakis (2009) used the MRF method in their study of reactive extrusion within 33.70 mm and 95.60 mm diameter co-rotating twin screw extruders. Similarly, Potriefke (2007) applied the MRF approach to understand the flow behaviour of 58 mm diameter partially filled co-rotating twin screw extrusion. And Ortiz-Rodriquez (2009) mentioned that the capability of predicting the flow behaviour of double flighted screw by MRF has limitation because two different radial vectors are defined. The one of the disadvantages, according to Ortiz-Rodriquez (2009), of MRF is its restricted capability for describing the distributive mixing of twin screw extruders.

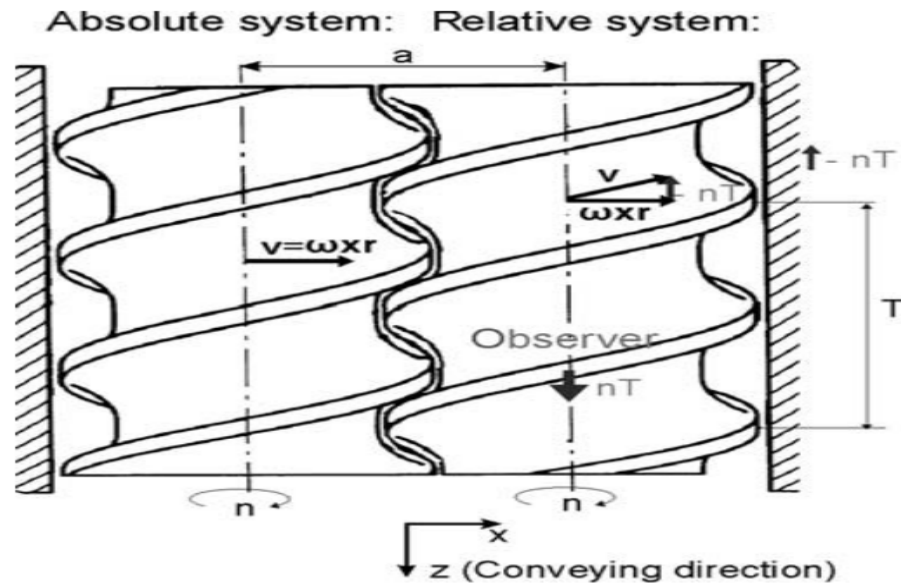


Figure 1.2. Physical Interpretation of Moving Reference System (MRF) (Potriefke, 2007) (An observer who is always at the tip of the flight of the screws, moves with the velocity of moving frame of reference.)

1.3.5. Mesh Superimposition Technique

A technique close to the quasi-steady state approximation method but more sensitive to transient effects is the Mesh Superimposition technique. Avalosse and Rubin (2000) described mesh superimposition technique by the following sequence. First, build a mesh for the available inner volume of the barrel and a mesh of the volume occupied by the screws independently. Then, these meshes are superimposed to reveal the flow domain of the process. At each time step, the screw meshes are updated and replaced at their nominal position. For the actual fluid domain, the Navier-Stokes equation is solved. Then, for each node within this domain a penalty formulation is used to correct the velocity so that it matches the rotation of the local screw. Gotsis et al. (1990) used this method to simulate the flow behaviour in a set of

kneading discs within a co-rotating twin screw extruder. Alsteens et al. (2004) evaluated this method to understand the mixing efficiency for said kneading elements of a co-rotating twin screw extruder. Gupta et al. (2009) compared 30 mm diameter co-rotating and counter-rotating twin screw extruders by this approach. The mesh generation required for this method can very simple when a coarse pattern is used; however, very coarse meshes can cause poor results for complex flow regions. Considering the complexities inside a twin screw extrusion this is extremely complicated and therefore was not chosen for the present thesis.

1.4. Objectives

There are three main objectives in this dissertation.

1. Carryout a comprehensive analysis of the flow mechanism in the conveying element of counter-rotating twin screw extruder for various screw pitch lengths, ratios of flight width-to-channel width and screw speeds to determine the pumping efficiency. The objective is to understand the effects of geometrical parameters and processing conditions in better detail than found in previous literature. The quasi-steady state approximation has been used for modelling the flow within an ICRTSE. A number of sequential geometries at defined angles of position are selected to represent a complete cycle of rotation in the time dependent moving boundary condition. This approach assumes that the polymer melt flows at very low Reynolds number, such that it is reasonable to neglect the transient term of motion equation. It is also assumed that the flow channel of the extruder is fully filled with polymer melt.

2. Evaluate how a simple (analytical) model predicts flow rate for the extruder relative to different operational/geometric parameters. Compare the computer simulation and simple flow model in order to determine whether the simple flow model is useful or not.
3. Characterize the dispersive mixing through the determination of shear stress and mixing parameter λ . Investigate the effect of the geometrical parameters and processing conditions on the dispersive mixing.

1.5. Outline

The thesis is divided into 7 chapters in addition to this introduction and background. Chapter 2 is devoted to a description of geometrical parameters and processing conditions that are used for the simple flow model and computer simulations. Chapter 3 contains a simple flow model for various screw geometry and processing conditions. Limitations of the simple model are discussed in Chapter 3 as well. In Chapter 4, information is given setting up a computational fluid dynamics simulation of the extruder with OpenFOAM® (CFD software). Chapter 5 is dedicated to explaining negative pressures in rotating polymer processing machinery, obtained by various researchers. Chapter 6 includes numerical results to understand the flow behaviour and dispersive mixing for different screw geometries and processing conditions. The simple flow model and computer simulations are compared in terms of flow rate in Chapter 7. Conclusions and recommendations for future studies are presented in Chapter 8.

Chapter Two

GEOMETRICAL PARAMETERS AND MATERIAL PROPERTIES

2.1. Introduction

Before the simple model and computer simulation of intermeshing counter rotating twin screw extruders (ICRTSE) are considered precisely, it is useful to discuss screw geometries, material properties and processing conditions in detail. ICRTSE include two screws which rotate in opposite directions. One screw has a left hand flight while the other has a right hand flight as is shown in Figure 2.1.

2.2. Geometrical Parameters

A schematic presentation of ICRTSE is shown in Figure 2.1. It is clear from Figure 2.1 that the conveying element is the major type of screw element in ICRTSE. The polymer material in the C-shaped chamber is pushed towards the die by positive displacement in conveying elements. The polymer melt recirculates with the C-shaped chamber, converging towards a narrow intermeshing region and then it diverges. The geometrical parameters of ICRTSE that were used in this study are shown in Figure 2.2 and Table 2.1. Screw radius, R , channel depth, H , screw pitch length, S , flight width, W_f , channel width, W_c , clearance between flight and barrel, δ , number of flights, i , center distance, A , helix angle, θ , and flight width-to-channel width ratio are the crucial design parameters for ICRTSE.

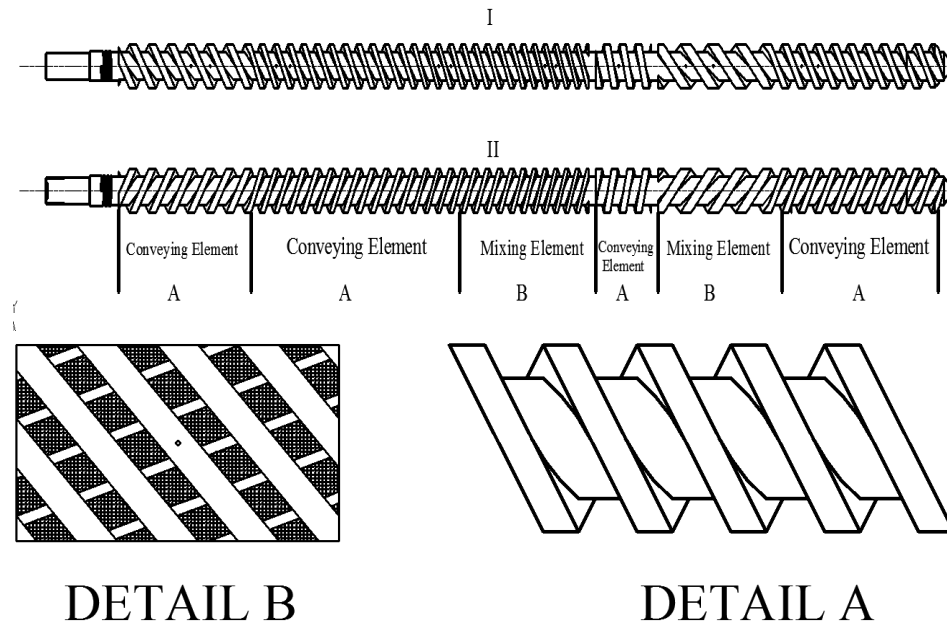


Figure 2.1. Schematic View of ICRTSE from MIKROSAN INC. I: Left Hand Screw II: Right Hand Screw

Detail A: Conveying Element Detail B: Mixing Element

All these important parameters can be seen in Figure 2.2 and Table 2.1. Theoretically, the flight width-to-channel width ratio lies between 0 and 1. If the flight width-to-channel width ratio is bigger than 0.6, it is called a thick conveying element. On the other hand, it is called a thin conveying element. Helix angle, θ , can be calculated as:

$$\theta = \tan^{-1}\left(\frac{2\pi R}{S}\right) \quad (2.1)$$

Screw channel width, W_c , can be calculated as:

$$W_c = \frac{S}{i} - W_f \quad (2.2)$$

2.3. Material Properties and Processing Conditions

ICRTSE are used primarily for the unplasticized (rigid) polyvinyl chloride (R-PVC) pipe and profile industry. For the simple model and computer simulations, it was decided to use typical material data (R-PVC). The material used in this study was R-PVC provided by MIKROSAN Inc., and its viscosity was measured on a rotational viscometer. Result of the measurement and Carreau viscosity model fitting are shown in Figure 2.3.

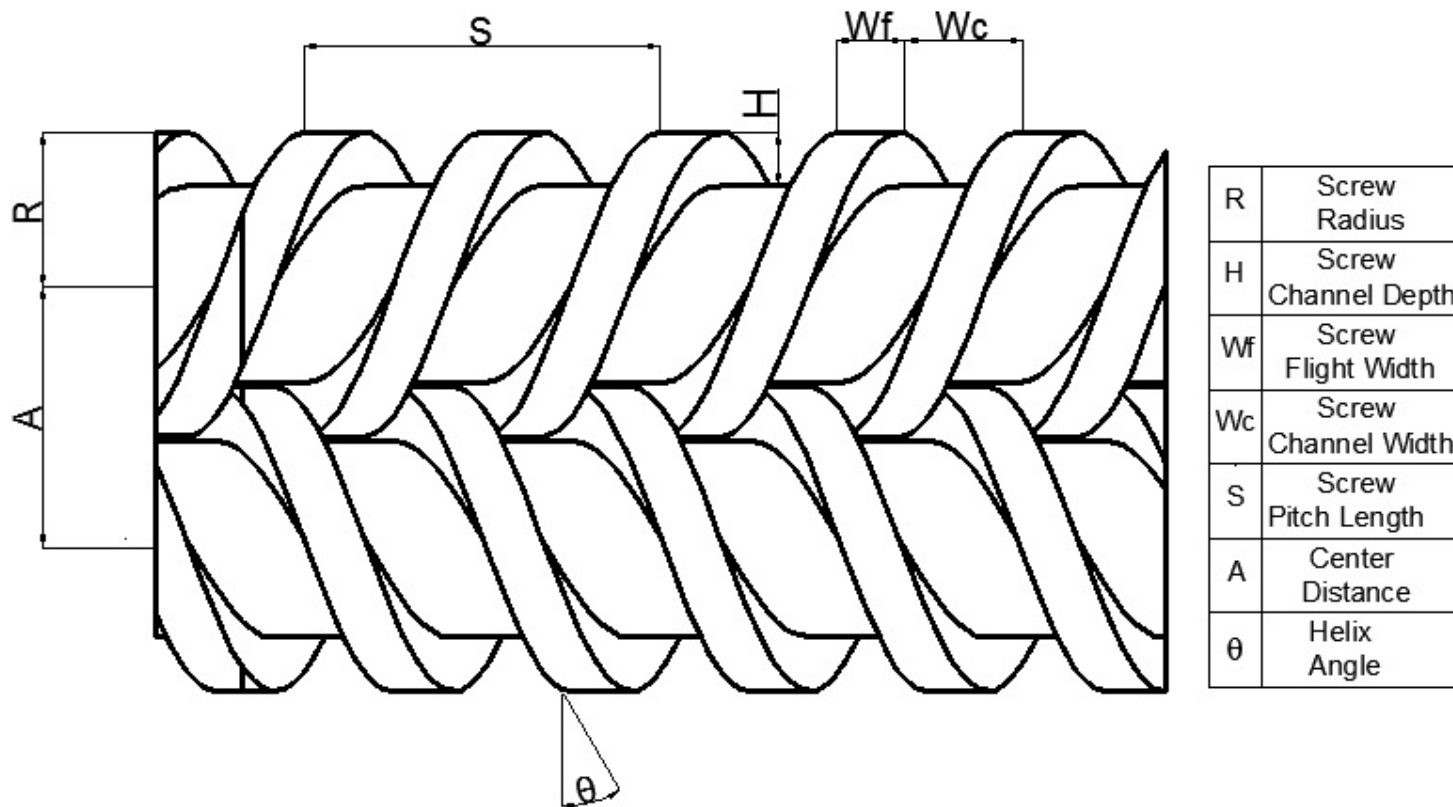


Figure 2.2. Screw Design Parameters

Table 2.1 ICRTSE Geometrical Design Parameters

R	<i>Screw Radius</i>	$[mm]$	44.85	
H	<i>Screw Channel Depth</i>	$[mm]$	15.85	
W_f	<i>Screw Flight Width</i>	$[mm]$	17.5	
i	<i>Number of Screw Flight</i>	$[-]$	2	
A	<i>Center Distance</i>	$[mm]$	75	
δ	<i>Clearance Between Screw and Barrel</i>	$[mm]$	0.5	
S	<i>Screw Pitch Length</i>	$[mm]$	Case 1	75
			Case 2	90
			Case 3	105
			Case 4	135
θ	<i>Helix Angle</i>	$[^\circ]$	Case 1	14.90
			Case 2	17.71
			Case 3	20.44
			Case 4	25.60
$\frac{W_f}{W_c}$	<i>Flight Width / Channel Width Ratio</i>	$[-]$	Case 1	0.875
			Case 2	0.636
			Case 3	0.500
			Case 4	0.350

The Carreau viscosity model in Equation 2.3 was used for the shear rate dependency of viscosity. In the Carreau model, η_0 is the viscosity at zero shear rate, η_{inf} is the viscosity at very high shear rates (important for solutions, but not for melts), n is the power index, and λ is a relaxation time. Fitting of the data shown in Figure 2.3 gave $\eta_0=12800$ Pa.s (approximately), $\eta_{inf}=10^{-12}$ Pa.s (assumed), $n=0.47$ and $\lambda=1.4$ s (approximately). It was subsequently decided to use $\eta_0=10000$ Pa.s, $\lambda=2$ and $n=1, 0.7, 0.3$ to cover the usual range of polymer melts, likely to be processed in an ICRTSE. Specific heat capacity, C_p , is assumed 1530 J/kg/°K and the melt density, ρ , is assumed 1300 kg/m³.

$$\eta_{eff} = \eta_{inf} + (\eta_0 - \eta_{inf})(1 + (\lambda\dot{\gamma})^2)^{\frac{n-1}{2}} \quad (2.3)$$

Figure 2.3 shows the viscosity curve of the typical R-PVC provided by Mikrosan Inc. It has a zero shear viscosity, η_0 , of 10000 Pa.s and power index, n , of 0.47 at temperature 170°C. For the thesis study, the power index was not used but rather altered. A power index of 1 was used for the Newtonian fluid simulations and power indexes of 0.7 and 0.3 were used for Non-Newtonian fluid simulations.

Screw speed, N , is normally the main processing variable for controlling an ICRTSE. Speeds of 30, 60 and 120 rpm were chosen to investigate. In this study, left screw was rotated in the clockwise direction while right screw was rotated in the counter-clockwise direction. Temperature dependency was never studied in this work.

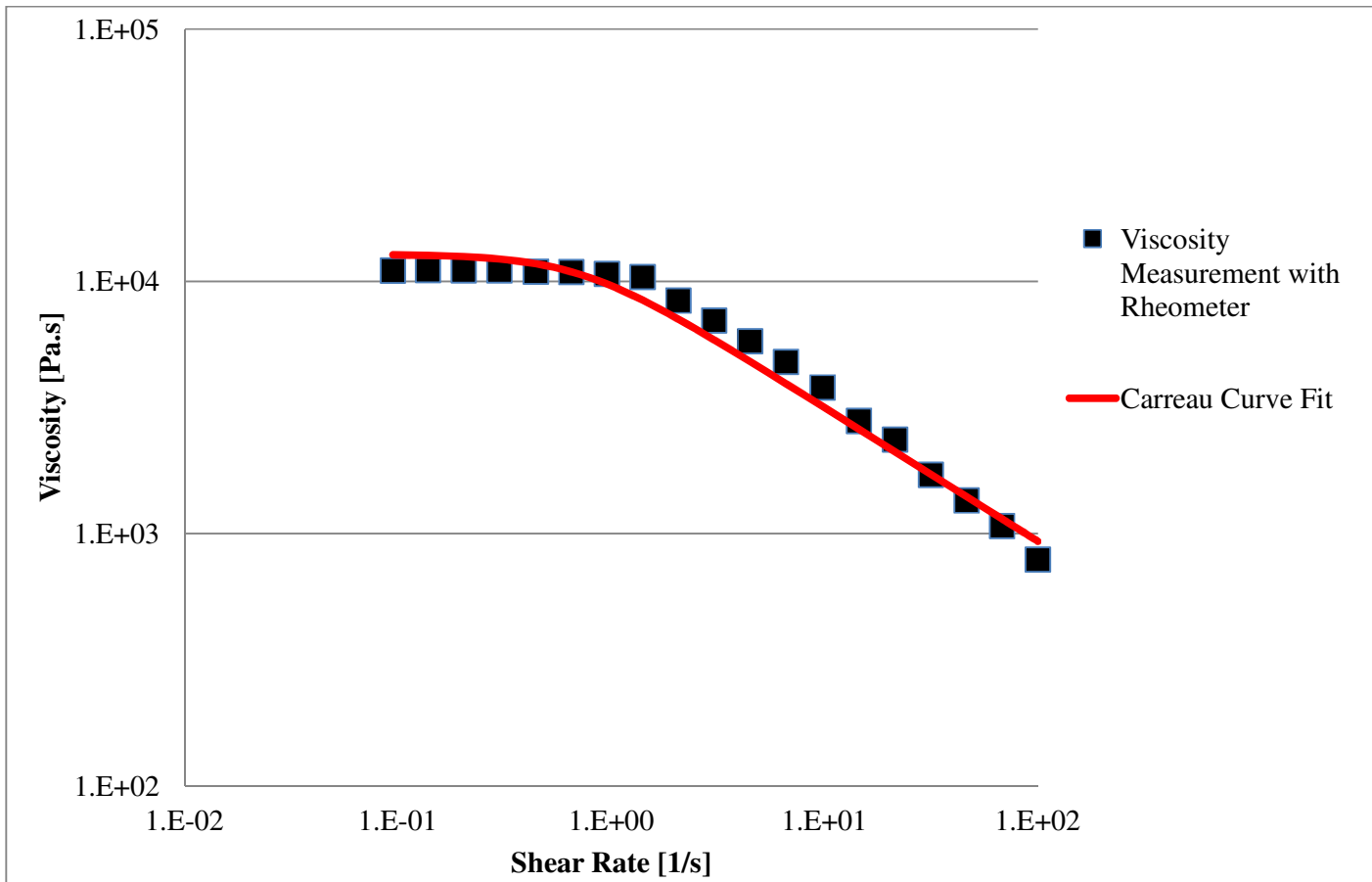


Figure 2.3. Viscosity Curve of Typical PVC (As measured in a Rotational Viscometer)

Chapter Three

A SIMPLE FLOW MODEL OF COUNTER-ROTATING TWIN SCREW EXTRUDERS

3.1. Introduction

Intermeshing counter-rotating twin screw extruders (ICRTSE) are the closest of this type of machine to exhibiting positive displacement while conveying process material. Ideally, this means that all of the material in the system is pushed constantly forwards no matter what the discharge pressure. In ICRTSE, the discrete volumes that are filled by the polymers are called C-shaped chambers. The ICRTSE have been modelled as a succession of C-shaped chambers by Janssen (1978). This simple flow model is used to obtain throughput of ICRTSE. In this simple model, the C-shaped chamber volume that is shown in Figure 3.1 combined with screw speed gives the theoretical flow rate. By subtracting the total leakage flow from the theoretical flow rate, the actual calculated output is obtained.

In this simple model, the chambers are assumed to be completely filled with Newtonian fluid. The screws are also assumed to have uniform profiles in this zone which means that the chamber and leakage gaps do not change as fluid moves along the screws. Schenkel (1966), Doboczky (1965¹) analyzed the flow of a Newtonian fluid within C-shaped chambers of an ICRTSE while neglecting leakage flows. Janssen (1978) and White (1990) improved the accuracy of the simple flow calculation by considering leakage flows.

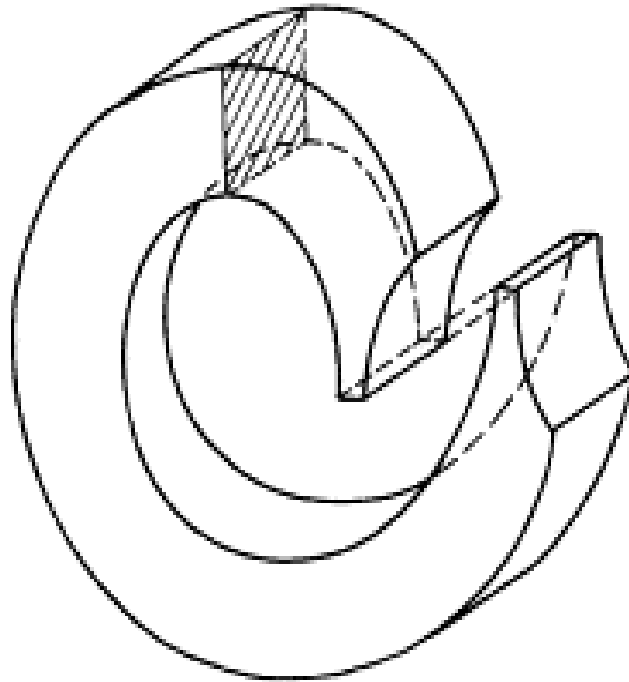


Figure 3.1. C-shaped Chamber (Fitzpatrick, 2009)

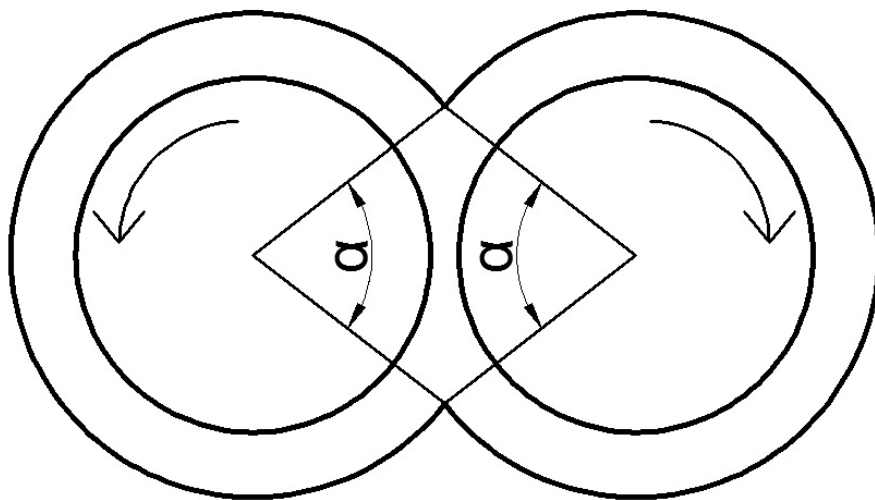


Figure 3.2. Overlapping Angle (Janssen, 1978)

3.2. Simple Calculation of Output without Leakage Flow

Apparently, the first attempt to calculate the output of the intermeshing counter-rotating multiple screw extruders for thermoplastics in the open literature was by Schenkel (1963) who wrote:

$$Q_{th} = m N V_c \rho \quad (3.1)$$

where Q_{th} is the theoretical mass throughput, m is the number of screws, N is the screw rotation speed, V_c is the C-shaped chamber volume per screw and ρ is the melt density.

Doboczky (1965¹) modified Eq. (3.1) for twin screw machines as follows:

$$Q_{th} = 2 i N V_c \rho \quad (3.2)$$

where i is the number of flights. Eq. (3.2) was also used by Janssen (1978) to develop a more detailed analytical model for the ICRTSE. Janssen (1978) mentioned that the C-shaped chamber volume can be calculated by subtracting the volume of a given length of screw from the same length of the empty barrel.

The volume, V_1 , of one side of the inner barrel bore over one flight pitch length was calculated as:

$$V_1 = \left\{ \left(\pi - \frac{\alpha}{2} \right) R^2 + \left(R - \frac{H}{2} \right) \sqrt{RH - \frac{H^2}{4}} \right\} S \quad (3.3)$$

where the variables of R , H and S for typical ICRTSE are shown in Figure 3.3 and values for these variables are presented in Table 3.1. α is defined as the overlapping angle in radians (See Figure 3.2). It is given by the formula:

$$\alpha = 2 \tan^{-1} \left[\frac{\sqrt{RH - H^2/4}}{R - H/2} \right] \quad (3.4)$$

The volume, V_2 , of the screw root over one pitch length is:

$$V_2 = \pi(R - H)^2 S \quad (3.5)$$

The volume, V_3 , of one screw flight is:

$$V_3 = 2\pi \left\{ \left(RH - \frac{H^2}{2} \right) W_f + \left(RH^2 - \frac{2}{3} H^3 \right) \tan(\theta) \right\} \quad (3.6)$$

where W_f and θ for typical ICRTSE are shown in Figure 3.3 and values for them are presented in Table 3.1.

The total volume of C-shaped chamber is:

$$V_c = \frac{V_1 - V_2 - iV_3}{i} \quad (3.7)$$

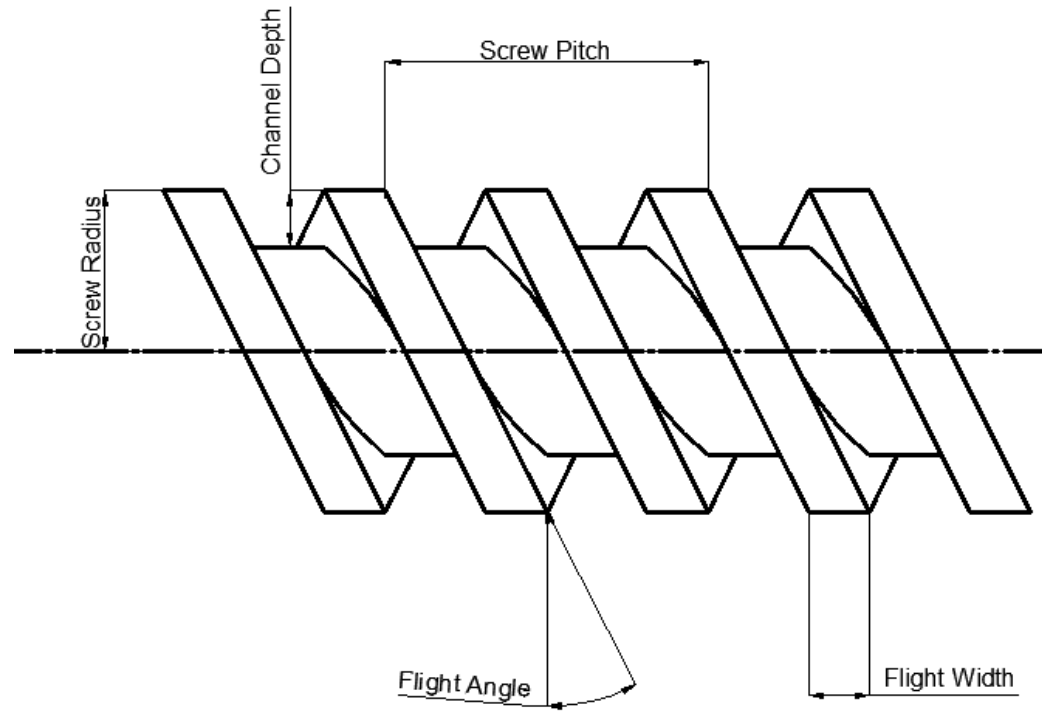


Figure 3.3. Geometrical Parameters for Simple Model of Theoretical Output

Table 3.1. Geometrical Parameters and Mass Flow Rate Results without Leakage

Flow

INPUT	P	Melt Density	[kg/m ³]	1300	
	i	Number of Screw Flight	[-]	2	
	R	Screw Radius	[mm]	44.85	
	H	Channel Depth	[mm]	15.85	
	S	Screw Pitch Length	[mm]	Case 1	75
				Case 2	90
				Case 3	105
				Case 4	135
	W_f	Flight Width	[mm]	17.5	
	θ	Flight Angle	[°]		14.9
				17.7	
				20.04	
				25.6	
RESULT	Q_{th}	Theoretical Mass Flow Rate without Leakage Flow	[kg/h]	Case 1	457.8
				Case 2	669.7
				Case 3	881.0
				Case 4	1304.8

Janssen (1978) verified the equations by weighing the water needed to fill an extruder. The calculated values were within the spread of the measured values, which was less than two percent, and so the calculations can be regarded as accurate.

3.3. Simple Calculation of Leakage Flows

Counter-rotating twin screws configurations cannot display perfectly positive displacement else metal will rub on metal, and so there is leakage between the subsequent C-shaped chambers along the length of the barrel. Leakage flows were initially addressed by Doboczky (1965²) and Klenk (1966) for an ICRTSE. Doboczky

(1965²) indicated that leakage flows occur in the four areas that are shown in Figure 3.4. The first of these leakage flows is the calender leakage flow, Q_c . This is the leakage between the screw flight and the screw root. The second type of leakage is tetrahedral gap leakage flow, Q_t , which is the back flow through the tetrahedral gap between the flanks of screws. The third type of leakage flow is the flight gap leakage which is defined as flow of material over the flights of screws, Q_f . Flight gap leakage flow occurs between the barrel and screw flight, away from the intermeshing region. The fourth is the side gap leakage flow, Q_s , which is flow between the flanks of two screws flight. Two pressure sources were identified by Janssen (1978) for this simple model. The first source is the pressure which is developed at the die. This source from the die is assumed zero in this simple model due to the isolating effect of each chamber from the next. Janssen (1978) explained the second source of pressure as moving wall of the extruder and the flow which occurs within the chamber itself. Janssen (1978) wrote the second source of pressure as:

$$\Delta p = 6\eta \frac{2\pi RN}{H^2} \left(\frac{S}{i} - W_f \right) \quad (3.8)$$

where Δp is the local pressure difference between opposite C-shaped chambers, R is the screw radius, S is the screw pitch length, i is the number of screw flight, W_f is the flight width and N is the screw speed. All the geometrical parameters for a typical ICRTSE are given in Table 3.2.

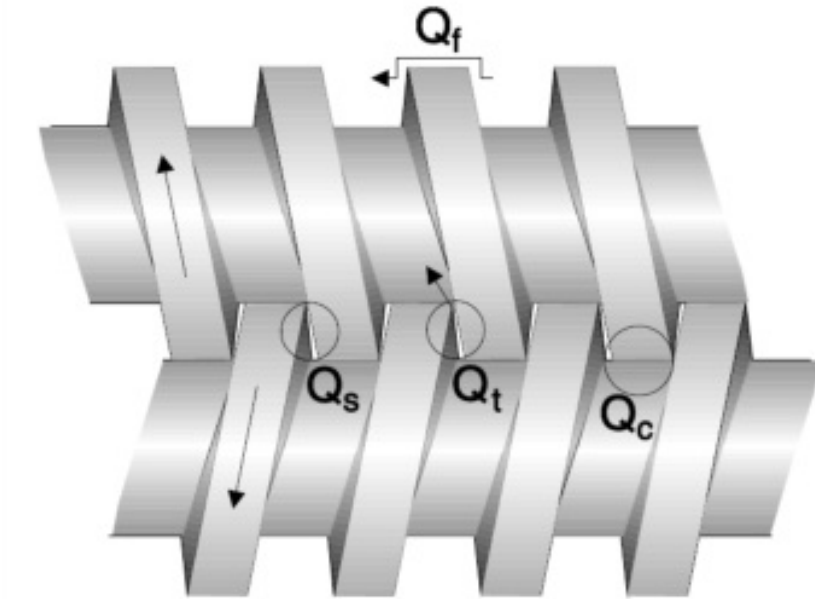


Figure 3.4. Leakage Flows (Fitzpatrick, 2009)

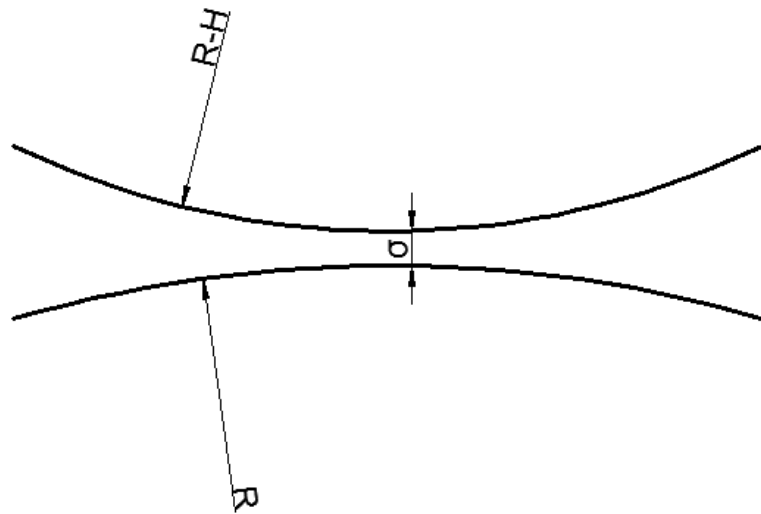


Figure 3.5. Calender Gap in ICRTSE (Janssen, 1978)

Table 3.2. Parameters for Simple Model of Leakage Flows

INPUTS FOR LEAKAGE FLOWS	R	Screw Radius	[mm]	44.85	
	H	Screw Channel Depth	[mm]	15.85	
	W_f	Screw Flight Width	[mm]	17.5	
	i	Number of Screw Flight	[-]	2	
	α	Overlapping Angle	[radians]	1.207	
	S	Screw Pitch Length	[mm]	Case 1	75
				Case 2	90
				Case 3	105
				Case 4	135
	θ	Helix Angle	[radians]	Case 1	0.26
				Case 2	0.31
				Case 3	0.40
				Case 4	0.45
	ϵ	Side Gap Width	[mm]	Case 1	1.25
				Case 2	5.00
				Case 3	8.75
Case 4				16.25	
σ	Calendering Gap	[mm]	1.15		
δ	Clearance between Screw and Barrel	[mm]	0.5		
N	Screw Speed	[rpm]	30		
η	Viscosity	[Pa.s]	10000		
ρ	Melt Density	[kg/m ³]	1300		

3.3.1. Calender Leakage Flow

In ICRTSE, the gap between screws is called the calender gap. Calender leakage flow, Q_c , is the flow between the intermeshing screws. Janssen (1978) derived the simple equation for a Newtonian fluid as:

$$Q_c = \frac{4(S - W_f i)}{3i} * \left\{ N\pi(2R - H)\sigma - \frac{\Delta p \sigma^3}{6\pi\eta\sqrt{(2R - H)\sigma/2}} \right\} \quad (3.9)$$

Since there are four calender gaps in ICRTSE for the two flights per screw pitch, the Q_c in Equation 3.9 should be multiplied by four to obtain the total calender leakage flow per C-shaped chamber. The calculated total calendar leakage flows for the conditions examined in this work are shown in Table 3.3.

Speur et al. (1987) determined that the calender leakage flow rate over theoretical flow rate changed between 10 to 44% for various geometries. Li (1995) found that calender leakage flow was around 11% of the theoretical output for a 34 mm diameter ICRTSE while Kajiwara et al. (1996) found it to be 5% of the total flow rate for a smaller one flight 40 mm diameter ICRTSE. As shown in Table 3.3, the total calender leakage flow over theoretical mass flow rate varies between 12.5 to 14.4% for different screw pitch lengths of 90 mm diameter ICRTSE. This ratio does not change sufficiently with increasing screw pitch length; however, the amount of total calender leakage flow increases with increasing screw pitch length.

Table 3.3. Calender Leakage Flow for Various Screw Pitch Lengths

S	Screw Pitch Length	[mm]	Case 1	75
			Case 2	90
			Case 3	105
			Case 4	135
Q_c	Total Calender Leakage Flow	[kg/h]	Case 1	66.14
			Case 2	90.7
			Case 3	115.2
			Case 4	163.8
Q_c/Q_{th}	Total Calender Leakage Flow / Theoretical Mass Flow Rate	[-]	Case 1	0.144
			Case 2	0.135
			Case 3	0.130
			Case 4	0.125

3.3.2. Tetrahedral Gap Leakage Flow

In ICRTSE, another gap exists between screw flight walls. As can be seen in Figure 3.4, the gap is approximately tetrahedral, Q_t . Janssen (1978) developed a simple model for tetrahedral gap leakage flow by using dimensional analysis and regression analysis of the measurements. That simple model can be written as:

$$Q_t = \frac{\Delta p * R^3}{\eta} * 0.0054 * \left(\frac{H}{R}\right)^{1.8} * \left(\theta + 2 * \left(\frac{\epsilon + \sigma * \tan\theta}{H}\right)^2\right) \quad (3.10)$$

where ϵ is the width of the side gap and σ is the calender gap. There is only one tetrahedral gap per C-shaped chamber. All the parameters used in the calculation can be seen in Figure 3.6 with representative values given in Table 3.2.

Table 3.4. Tetrahedral Gap Leakage Flow for Various Screw Pitch Lengths

S	Screw Pitch Length	[mm]	Case 1	75
			Case 2	90
			Case 3	105
			Case 4	135
Q_t	Tetrahedral Gap Leakage Flow	[kg/h]	Case 1	6.59
			Case 2	17.56
			Case 3	42.40
			Case 4	158.84
Q_t/Q_{th}	Total Tetrahedral Gap Leakage Flow / Theoretical Mass Flow Rate	[-]	Case 1	0.014
			Case 2	0.026
			Case 3	0.048
			Case 4	0.12

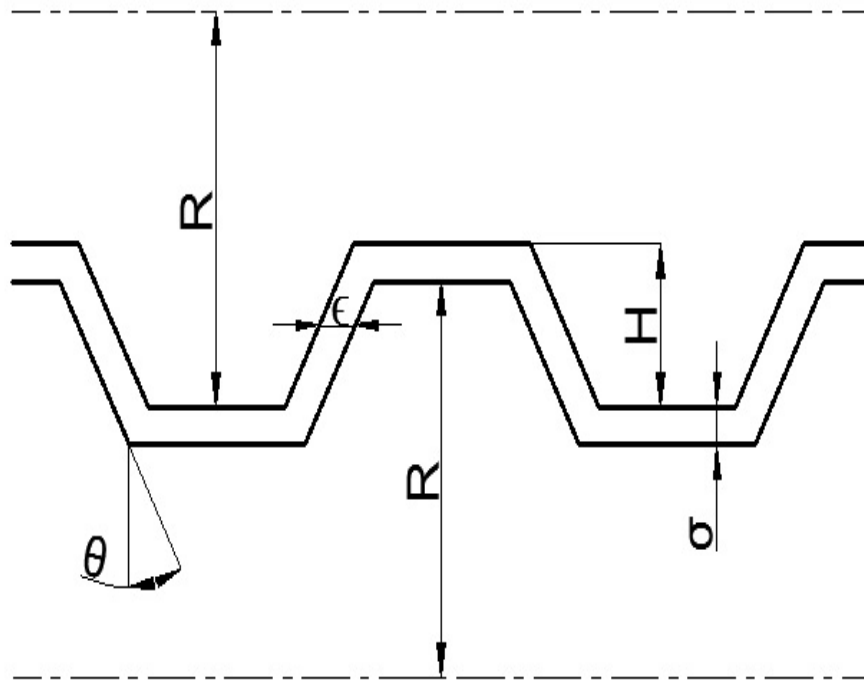


Figure 3.6. Geometrical Parameters in Tetrahedral Gap Leakage Flow (Janssen, 1978)

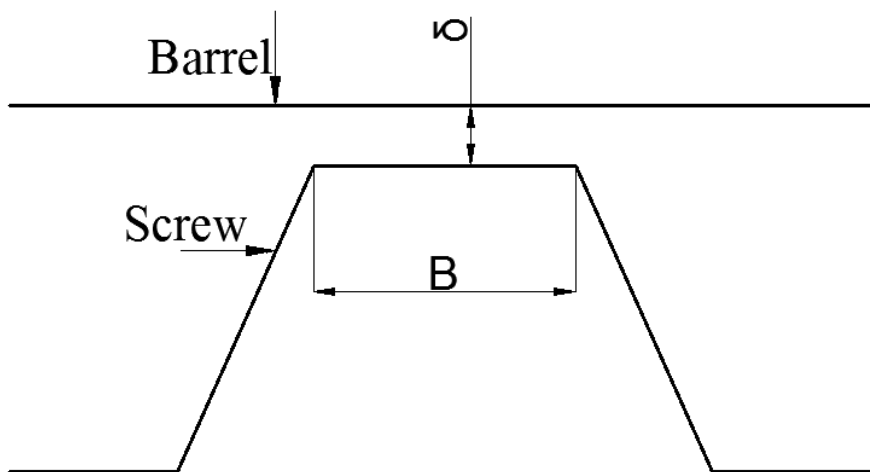


Figure 3.7. Schematic View of Flight Gap (Janssen, 1978)

Li (1995) mentioned in his PhD thesis that tetrahedral leakage flow was around 1% of the theoretical output for a 34 mm diameter ICRTSE. Similarly, Kajiwara et al. (1996) found that tetrahedral gap flow was 1.6 % of the total mass flow rate for one flight 40 mm diameter ICRTSE. It was found that tetrahedral leakage flow over theoretical mass flow rate varied between 1.4 to 12% for different screw pitch lengths within a 90 mm diameter ICRTSE. This ratio becomes higher with increasing screw pitch length, especially for thin screw flight elements.

3.3.3. Flight Gap Leakage Flow

Flight leakage flow, Q_f , occurs in clearances, which is between the screws and barrel. Janssen (1978) developed an analytical model to predict the flight leakage flow. The analytical equation can be written as:

$$Q_f = (2\pi - \alpha) R \left\{ \frac{2\pi RN\delta}{2} + \frac{\delta^3}{6\eta W_f} \left[3\eta \frac{2\pi RN}{H^2} * \left(\frac{S}{i} - W_f \right) + \Delta P \right] \right\} \quad (3.11)$$

where α (See Figure 3.2.) is the overlapping angle in radians and ΔP is the pressure drop due to the die. ΔP will be zero if there is no die at the end of the extruder. Q_f in Equation 3.11 should be multiplied by two to obtain total flight leakage flow because of the two screws. The geometrical parameters and processing parameter are shown in Figure 3.7 and Table 3.2.

Li and Manas-Zloczower (1994) stated that flight gap leakage flow was around 7% of the theoretical flow rate for a 34 mm diameter ICRTSE. It was noted that total flight gap leakage flow over theoretical mass flow rate varied between 5.7 to 16.4% for different screw pitch lengths of 90 mm diameter ICRTSE. This ratio

increased with decreasing screw pitch length especially for thick screw flight elements.

Table 3.5. Total Flight Gap Leakage Flow for Various Screw Pitch Lengths

S	Screw Pitch Length	[mm]	Case 1	75
			Case 2	90
			Case 3	105
			Case 4	135
Q_f	Total Flight Gap Leakage Flow	[kg/h]	Case 1	75.14
			Case 2	75.18
			Case 3	75.24
			Case 4	75.27
Q_f/Q_{th}	Total Flight Gap Leakage Flow / Theoretical Mass Flow Rate	[-]	Case 1	0.164
			Case 2	0.112
			Case 3	0.085
			Case 4	0.057

3.3.4. Side Gap Leakage Flow

The last type of gap yielding leakage is the side gap which is between the flanks of the flights in ICRTSE. Janssen (1978) developed a simple analytical model for this side gap leakage flow, Q_s . The calculation can be made as:

$$Q_s = \pi N(2R - H) (H - \sigma)(\epsilon + \sigma \tan(\theta)) \quad (3.12)$$

The geometrical parameters and processing parameters are shown in Figure 3.6 with values given in Table 3.2. Since there are four side gaps per C-shaped chamber, the Q_s in Equation 3.12 should be multiplied by four to obtain total side gap leakage flow.

Table 3.6. Total Side Gap Leakage Flow for Various Screw Pitch Lengths

S	Screw Pitch Length	[mm]	Case 1	75
			Case 2	90
			Case 3	105
			Case 4	135
Q_s	Total Side Gap Leakage Flow	[kg/h]	Case 1	49.68
			Case 2	171.34
			Case 3	294.00
			Case 4	536.33
Q_s/Q_{th}	Total Side Gap Leakage Flow / Theoretical Mass Flow Rate	[-]	Case 1	0.10
			Case 2	0.25
			Case 3	0.33
			Case 4	0.41

Kajiwarra et al. (1996) mentioned that the side gap leakage flow is 91% of the total mass flow rate for 40 mm diameter ICRTSE. Side gap leakage flow becomes very dominant in ICRTSE when the ratio between flight width and channel width decreases, i.e. a thinner conveying element is used. In this study, the screw conveying elements were thick conveying elements for Case 1 and 2 but they are thin conveying elements for Case 3 and 4. It is obvious in Table 3.6 that the influence of side gap leakage flow becomes dramatically important for thin conveying elements. Total side gap leakage flow over theoretical mass flow rate varies between 10 to 41% for different screw pitch lengths of 90 mm diameter ICRTSE. This ratio increases with increasing screw pitch length. In addition, side gap leakage flow is the most dominant leakage flow among the other type of leakage flows especially for thin flight elements.

3.4. Simple Model of Total Output

Ideally, the total output of the ICRTSE for double flighted screws (i.e. two screw flights per turn) follows a mass balance equation:

$$Q_{total} = Q_{th} - Q_t - 2Q_f - 4Q_c - 4Q_s \quad (3.13)$$

where Q_{total} is the total mass throughput, Q_t is the tetrahedral leakage flow, Q_f is the flight gap leakage flow, Q_c is the calender leakage flow and Q_s is the side gap leakage flows. Total mass throughputs are shown in Table 3.7 for various screw pitch length.

Table 3.7. Total Mass Flow Rate (Including Leakage Flows) for Various Screw Pitch Lengths

S	Screw Pitch Length	[mm]	Case 1	75
			Case 2	90
			Case 3	105
			Case 4	135
Q_{total}	Total Mass Flow Rate (Including Leakage Flows)	[kg/h]	Case 1	259.32
			Case 2	313.63
			Case 3	353.82
			Case 4	367.79
Q_{total}/Q_{th}	Total Mass Flow Rate (Including Leakage Flows)/Theoretical Mass Flow Rate	[-]	Case 1	0.566
			Case 2	0.468
			Case 3	0.401
			Case 4	0.281

It can be seen in Table 3.7 that total mass flow rate increase gradually by increasing screw pitch length. The pumping efficiency of an ICRTSE is a critical parameter for measuring its performance. The pumping efficiency is defined as the ratio between total mass flow rate and the theoretical throughput. Total mass flow

over theoretical mass flow rate (pumping efficiency) varies between 28 to 56% for different screw pitch lengths of 90 mm diameter ICRTSE in Figure 3.8. In addition, the results for pumping efficiency are plotted decreasing with increasing screw pitch length. This is because the tetrahedral and side gaps become larger as the screw pitch length increases. Hence, those gaps cause more leakage flow. The pumping efficiencies of simple model of ICRTSE are same range as Doboczky (1965²), Schenkel (1966), Klenk (1971) and Li and Manas-Zloczower (1994).

The ratio of flight width and channel width is the one of the important geometrical parameters. In this work flight width-to-channel width ratios of 0.875, 0.636, 0.500 and 0.350 were used. Table 3.8 indicated that the total mass flow rate increases slightly by decreasing the ratio of the flight width to the channel width. In addition Figure 3.9 shows that the pumping efficiency goes up with increasing flight width-to-channel width ratio. Thicker flight elements have a better pumping behaviour than the thin flight elements.

Another parameter that was investigated in this study is screw speed. Screw speeds of 30, 60, and 120 rpm were selected in order to understand their influence on the pumping behaviour of an ICRTSE. Total mass flow rates, Q_{total} , are shown in Table 3.9 for various screw speeds. It can be seen in Table 3.9 and Figure 3.10 that the total mass throughput, Q_{total} , increased linearly with screw speed; however, the pumping efficiency did not change with screw speed. It is because while the total throughput, Q_{total} , increased linearly with screw speed, the theoretical output, Q_{th} , increased in the same manner.

Li and Manas-Zloczower (1994) showed that the ratio between leakage flow and total leakage flow hardly ever changes with screw speed for a 34 mm diameter ICRTSE.

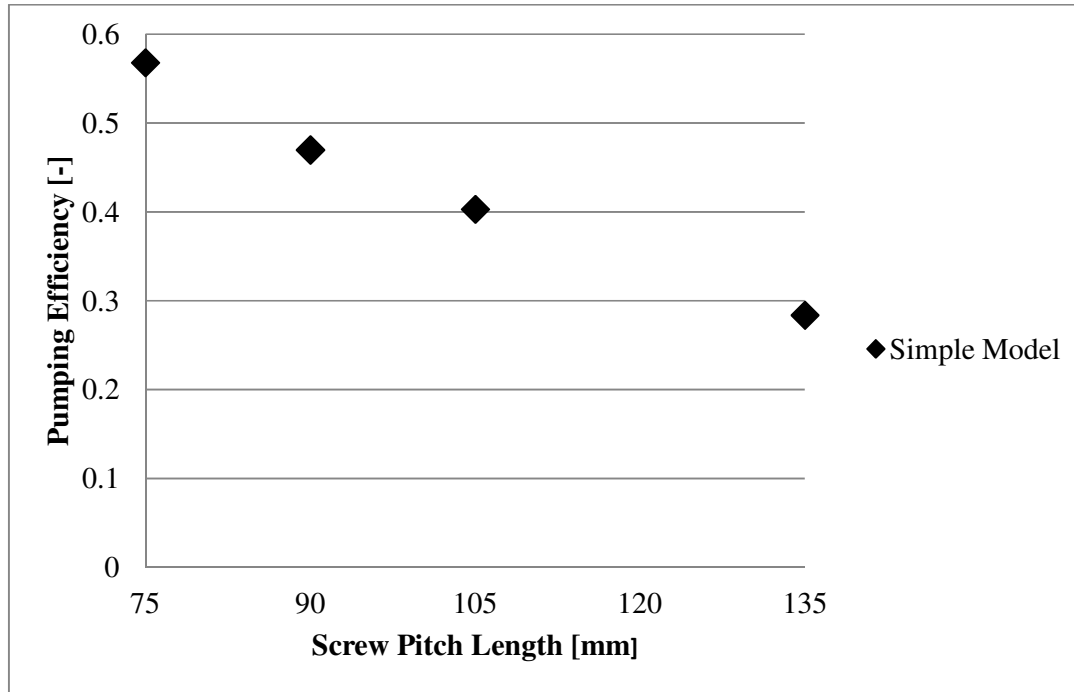


Figure 3.8. Pumping Efficiency for Various Screw Pitch Lengths for Simple Model

Table 3.8. Total Mass Flow Rate (Including Leakage Flows) For Various Flight Width-to-channel Width Ratios

W_f/W_c	Flight Width/Channel Width	[-]	Case 1	0.875
			Case 2	0.636
			Case 3	0.500
			Case 4	0.350
Q_{total}	Total Mass Flow Rate (Including Leakage Flows)	[kg/h]	Case 1	259.32
			Case 2	313.63
			Case 3	353.82
			Case 4	367.79

Table 3.9. Total Mass Flow Rate (Including Leakage Flows) for Various Screw Speeds

Screw Speed	Screw Pitch Length	Total Mass Flow Rate (Including Leakage Flows)
N	S	Q_{total}
[rpm]	[mm]	[kg/h]
30	75	259.32
60		519.53
120		1039.08
30	90	313.63
60		628.93
120		1257.86
30	105	353.82
60		710.31
120		1420.63
30	135	367.79
60		740.96
120		1481.93

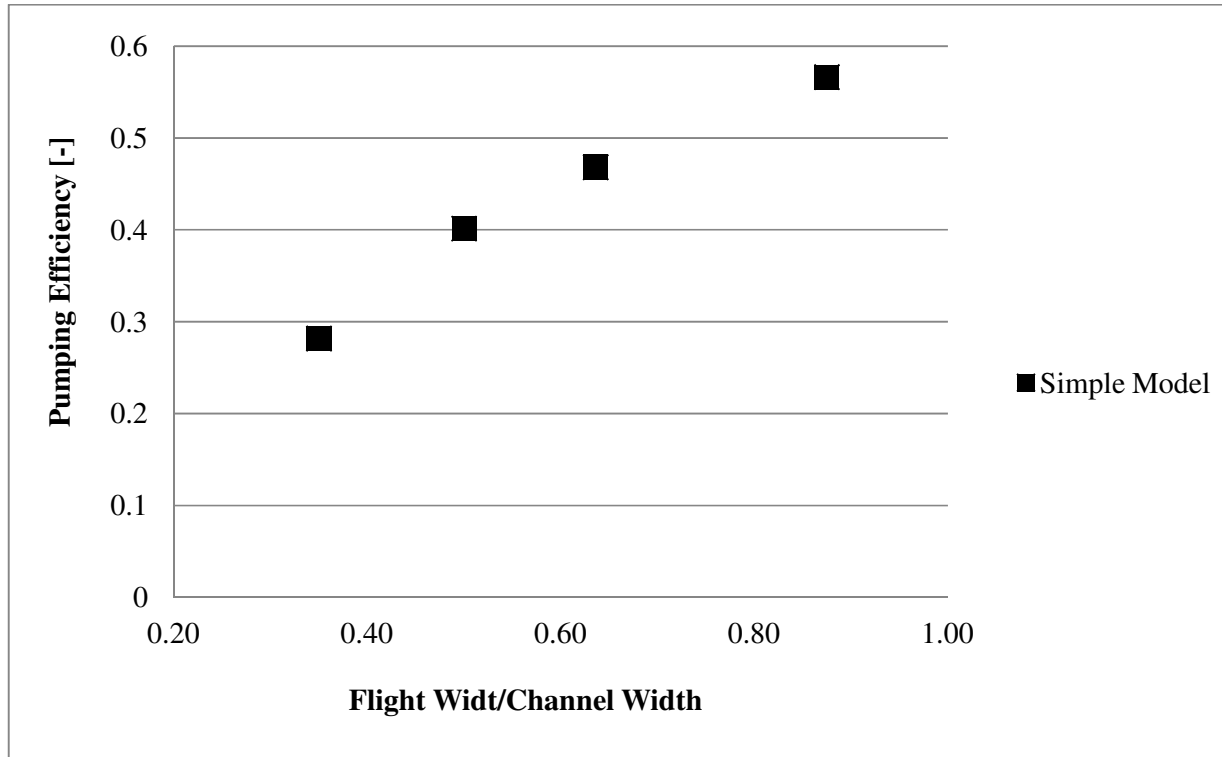


Figure 3.9. Pumping Efficiency for Various Flight Width-to-channel Width Ratios

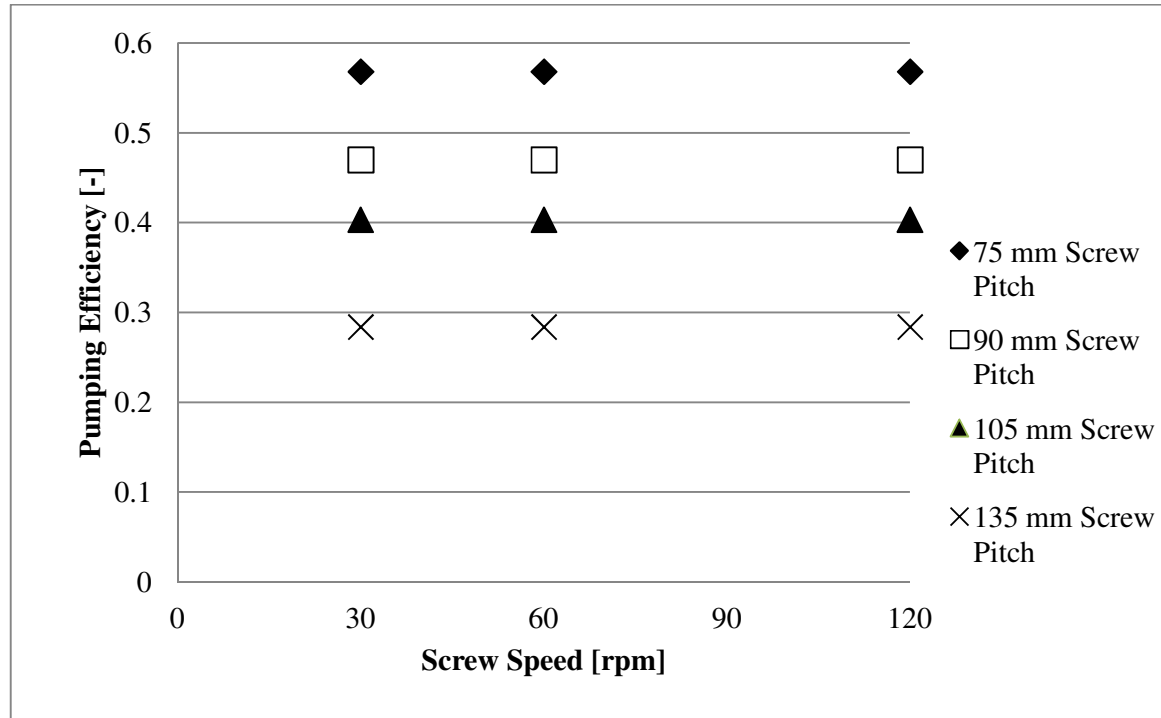


Figure 3.10. Pumping Efficiency for Various Screw Speeds for Simple Model

3.5. Limitations of the Simple Model

The simple model provides a reasonable result about the pumping behaviour of ICRTSE, yet it has some limitations. First and foremost, the simple model is valid for Newtonian fluids but the materials used in the polymer processing industry are non-Newtonian. Pressure due to the die in leakage flows is not taken into account and these negative flows are also affected by non-Newtonian behavior. Then, the simple model of ICRTSE can only predict throughput but the shear stress distribution, velocity distribution, etc., are important as well to better understanding the ICRTSE. Last but not least, the simple model of ICRTSE is only valid for parallel ICRTSE but conical ICRTSE is also very common in polymer processing industry; however, this issue has no relevance to the present thesis. Finally, the simple model assumes that there is no die at the end of extruder, which neglects pressure effects and the screw channels are fully filled with molten polymer, which is perhaps the least erroneous of all stated assumptions.

To conclude, the simple model for ICRTSE can be an excellent starting point but numerical models are necessary to better understand flow behaviour and ICRTSE performance.

Chapter Four

COMPUTER SIMULATION USING OPENFOAM®

4.1. Introduction

Computational fluid dynamics (CFD) use numerical schemes to solve and analyze problems related to fluid flow in complex environments. Availability of high speed computers has made solving huge numbers of equations simultaneously quite routine.

Basically, using CFD follows three steps. Pre-processing is the first step that includes mesh generation, boundary condition determination as well as designation of fluid properties. Secondly, numerical equations are solved based on the properties that are determined in pre-processing step. Finally, the results are visualized in the post-processing step.

Open Field Operation and Manipulation (OpenFOAM®) is the open source CFD package developed by Open CFD Ltd. It was released in 2004 under the General Public Licence. Fundamentally, the OpenFOAM® package use libraries to create executable files, defined as applications, to solve the numerical equations. Since two types of applications are valid in OpenFOAM®, solvers are used to solve numerical equations while utilities are used to manipulate the data.

4.2. Numerical Analysis

The various screw geometries to be meshed and solved were provided by MIKROSAN Inc. In this study, the procedure was followed is shown in Figure 4.1. GAMBIT® is geometry and mesh generation software. Firstly, 3D meshes were created for the various screw pitch lengths in GAMBIT®. Secondly, the created GAMBIT® mesh files were converted to OpenFOAM® mesh file style. Furthermore, boundary conditions (mentioned in Sec. 4.3) and controlling parameters (iteration numbers, discretisation methods etc.) were set. Then, the solver was executed on Canada's supercomputer network, Sharcnet, using four processors. The CPU time required to perform the flow simulations varied between 80000 and 100000 s, depending on the flow conditions and different type of geometries of ICRTSE employed. Lastly, the results were examined and presented by using open source scientific visualization software, ParaView®.

4.2.1. Solvers

OpenFOAM® includes around 80 standard solvers for different kind of problems. In addition, OpenFOAM® has the ability to develop a new solver or modify an existing solver for customized cases. In this study, the solver was chosen for steady, incompressible fluid flow under laminar conditions. The chosen solver used the SIMPLE algorithm, which stands for Semi Implicit Methods Pressure Linked Equations, to solve mass and momentum as shown in Equations 4.1 and 4.2. This algorithm minimizes simulation instabilities that otherwise arise when solving velocity and pressure simultaneously.

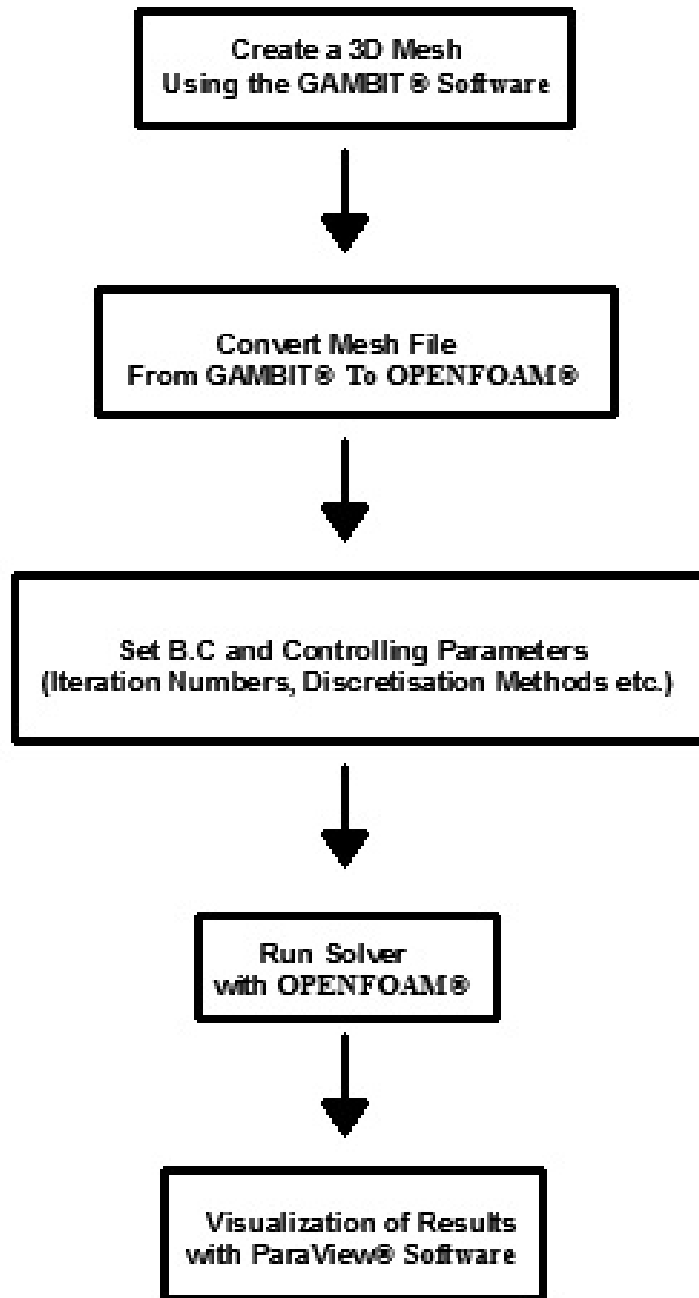


Figure 4.1. Working Procedure of Current Study

Conservation of mass for an incompressible fluid and conservation of momentum for laminar creeping flow (Reynolds number much smaller than 1) are shown in Equations 4.1 and 4.2 respectively. Shear thinning viscosity model and strain rate tensor are given in Equations 4.3 and 4.4.

$$\nabla \cdot \bar{V} = 0 \quad (4.1)$$

$$-\nabla P + \nabla \cdot \bar{\tau} = 0 \quad (4.2)$$

$$\bar{\tau} = \eta(I_{II_D})2\bar{D} \quad (4.3)$$

$$\bar{D} = \frac{1}{2}(\nabla \bar{V} + \nabla \bar{V}^T) = \frac{1}{2}\left(\frac{\partial V_i}{\partial x_j} + \frac{\partial V_j}{\partial x_i}\right) \quad (4.4)$$

where \bar{V} is the velocity vector, P is the pressure, $\bar{\tau}$ is the stress tensor, I_{II_D} is the second (scalar) invariant of the strain rate tensor, i and j equals 1, 2, 3. Juretic (2004) explained the SIMPLE algorithm as follows: First of all, the initial guess is determined. Secondly, the velocity field is calculated from the momentum equation by the using initial guess. The momentum equation is solved under relaxation in order to decrease non-linearity effect. Since the resulting velocity does not satisfy the momentum equation, the pressure equation is solved by using the predicted velocity to obtain new pressure field. Finally, it is repeated until the solution converges. The chosen solver was modified to compute shear stress, shear rate and vorticity tensor.

4.2.2. Utilities

Utilities in OpenFOAM® provide data transformation and manipulation. More than two hundreds utilities are present for different purposes. On top of that, OpenFOAM® has the ability to develop new utilities or to modify current utilities for

customized cases. In this study, a lot of utilities were used but the most frequent ones will be explained.

The first common utility is to convert to a GAMBIT® mesh file to an OpenFOAM® mesh file, including multiple region and boundaries. The second useful utility is to check mesh quality. This utility provides mesh statics, topology checking, geometry checking and the sufficiency of a mesh for a simulation run. In this study, the results showed that the mesh quality, which was obtained by this utility, was always good. Another useful utility was used to calculate mass flow through selected face sets or boundary patches for incompressible flow. This utility should be used after the numerical solution converged. Last but not least, a utility was used to extract data such as final residuals, iteration number etc., for plotting the profile of data over time. Figure 4.3, for example, was created by using this utility.

4.3. Boundary Conditions

Four different boundary conditions are specified for velocity and pressure. The boundary conditions that were used in this study are listed in Table 4.1.

Firstly, the standard no-slip boundary condition was used since slip concerns with PVC are unlikely to be important far from the die. This meant that the barrel velocity boundary condition was:

$$U_x = U_y = U_z = 0 \quad (4.5)$$

$$\vec{U} = N.r\vec{e}_\theta \quad (4.6)$$

Secondly, boundary condition for rotating screws follows the Equation 4.6 for. This boundary condition is specified Where N is the rotational speed, r is the radial position and \vec{e}_θ is the unit vector in θ direction.

Table 4.1. Boundary Conditions for Velocity and Pressure

Boundary		Barrel	Screws	Inlet	Outlet
Velocity	U	No-slip	Rotating Wall Velocity	Zero Gradient	Zero Gradient
Pressure	P	Zero Gradient	Zero Gradient	Fixed Value	Fixed Value

4.4. Mesh Independency

The mesh of the typical fluid domain and the cross-section of fluid domain are shown in Figure 4.2 for a 105 mm screw pitch length. Tetrahedral elements (cells) were chosen for the analysis. Shah and Gupta (2004) found that using tetrahedral finite elements permitted the most accurate mesh generation for a complex fluid domain like the ICRTSE. Similarly, Ilinca and Hetu (2010) used tetrahedral elements to get reasonable flow data for a 20.3 mm diameter co-rotating twin screw conveying element. They subsequently used the same tetrahedral finite elements to understand the mixing behaviour of a 20.3 mm diameter twin screw extruder (Ilinca and Hetu 2012). Sobhani et al. (2010) stated that their numerical experiments have shown that the tetrahedral elements were preferable for twin screw extruder simulations.

In CFD, the simulation results must be independent of mesh density. The different numbers of tetrahedral cells used in the mesh of a conveying element are shown in Table 4.2, which were used to verify that the numerical solutions produced were not dependent on mesh density. This re-meshing exercise was done for screw pitch lengths of 75 mm, 90 mm, 105 mm and 135 mm. According to Lawal et al. (1999), volumetric flow rates fluctuation between 1 to 8% should be considered to be indicating that the mesh dependency is negligible. The results found that the calculated mass flow rate changed between 0.5 to 5% within agreement Lawal et al. (1999). Therefore, the presented results in this thesis always corresponded to the highest mesh density value shown in Table 4.2.

Table 4.2. Different Number of Cells and Results for Various Cases

Number of Case	Screw Pitch Length	Number of Cells	Mass Flow Rate
	[mm]	[unit]	[kg/h]
Case 1	75	2068734	287.9
		4205205	280.14
Case 2	90	2212445	310.8
		3853651	305.8
Case 3	105	1659119	343.3
		3531209	338.15
Case 4	135	1804323	348.1
		4730938	340.69

4.5. Parallel Running

Parallelized simulation runs were carried out on the computer cluster ‘kraken’ which is part of Canada’s Sharcnet supercomputing network. There are three steps for parallelizing the runs in this study. The first step was domain decomposition where the geometry and associated fields were divided into pieces and saved to the different processors for solution. The number of processors, decomposition method and other parameters should be adjusted in the decomposition step. The second step was to set runs with a solver on four different processors. The last step was domain reconstitution. In this step, the solved decomposed fields were reassembled into a new folder. In the present academic work, 144 different cases were used and each case took 30 hours on average to complete on SharcNet.

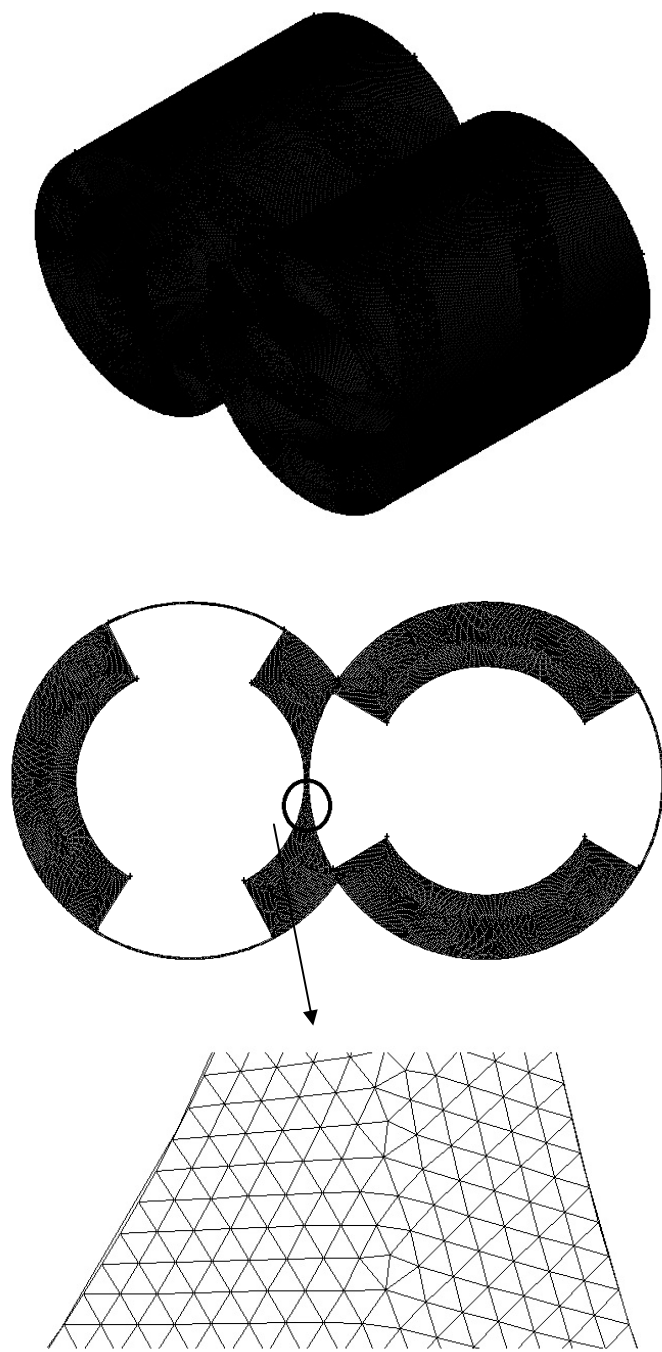


Figure 4.2. Mesh Appearance of 105mm Screw Pitch Length (The number of cells is 3531209.)

4.6. Converges of Computer Simulation

The residuals are simply the differences between two iterations by the solver. In this specific study, acceptable residuals to terminate the simulation were set at 5×10^{-5} . It means that when the residuals for velocity and pressure fields fall below 5×10^{-5} , the simulation stopped. Plotting the residuals with iteration number is the best way to show the convergence of a computer simulation. In Figure 4.3, velocity and pressure fields convergence are shown. It can be seen in Figure 4.3 that simulation converged at around 4000 iterations for 5×10^{-5} residuals for a 105 mm screw pitch length.

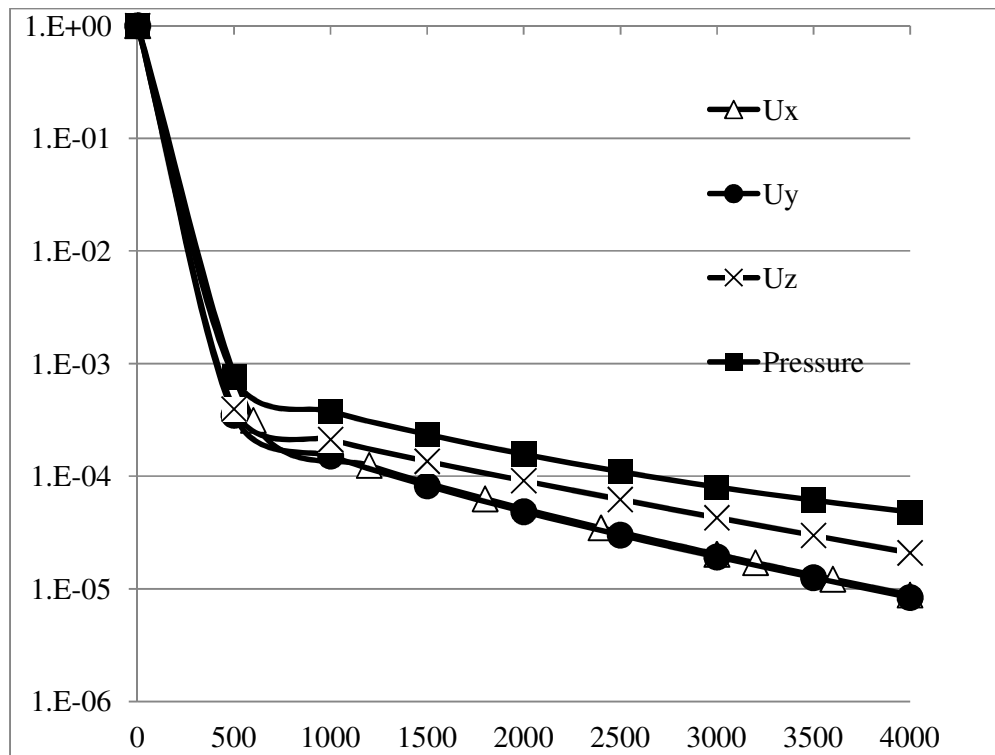


Figure 4.3. Converging Residuals with Iteration Number for 105 mm Screw Pitch

Length

Chapter Five

NEGATIVE PRESSURE IN MODELLING ROTATING POLYMER PROCESSING MACHINERY

5.1. Introduction

Rotating polymer processing machinery frequently involves melt flow between two non-parallel surfaces. The melt is usually dragged and compressed towards a narrow gap and then it expands. As a result of the drag flow in the non-parallel narrow gap, the pressure reaches a maximum in the compression region and then a minimum in the expansion region. Modelling is usually carried out with the help of the lubrication approximation or with fully 3D momentum equations for creeping (inertialess, viscous) flow. If the baseline pressure at both ends of the compression-expansion flow field is zero, then negative pressures will be calculated in the expansion region. Figure 5.1 shows positive and negative pressure development between two co-rotating cylinders. In the counter-rotating case, both compression and expansion are greater in magnitude than in the co-rotating case and consequently the positive and negative pressures calculated are higher, as shown in Figure 5.2. Of course, negative pressures are meaningless. However, with so many machines operating at or near ambient pressure, boundary conditions at or close to zero values are quite realistic and so these negative results should occur quite frequently in modelling. It is argued in this chapter that these negative pressures are telling researchers important information about their modeled environment.

5.2. Reviewing Modelling Results

An extensive literature search was carried out regarding the calculation and reporting of negative pressures in flow simulations of twin screw extruders and other types of rotating polymer processing equipment. In the vast majority of publications there is never any mention that negative pressures were ever calculated when solving the conservation of mass and momentum equations. It is not clear whether this was due to the fortuitous occurrence of high baseline pressures or convenient choices of boundary conditions.

Most papers ignore negative pressure results even though the mathematical descriptions suggest such possibilities. These studies usually confine their discussions to the negative and positive pressure gradients and the implications relating to forward flow and back-mixing. This is particularly apparent when entry or exit boundary conditions are at ambient pressure (i.e. zero gauge pressure). The fact that twin screw extruders are frequently starve-fed poses additional difficulties, because the locations of free surfaces are not priori known and cannot be determined by simply solving the equations for drag induced flow and pressure development. Jiang et al. (2007) in a modelling and experimental study of counter-rotating twin screw extruders show positive pressure peaks emerging from, what appears to be, a zero pressure baseline without mentioning if any negative pressures were ever calculated. Similar results on counter-rotating twin screw extruders (positive pressure peaks only, above a zero baseline pressure) are also reported in the book by White (1990), without any mention of what was calculated between the positive pressure peaks. Although it is tempting to associate the zones between zero pressure, with unfilled channel sections, there is no

reason for that. The filling ratio is set by the machine operator and has absolutely no relation to what is predicted by the single fluid hydrodynamic analysis.

Valette et al. (2009) carried out simulations of fully filled co-rotating twin screw extrusion, which gave pressures starting at zero, without explaining how the zero pressure boundary was determined. Some papers have fortuitously worked with boundary conditions with high enough pressures and avoided seeing negative values. For example, Bravo et al. (2000) validated their simulations by actual experimental data obtained from a co-rotating twin screw extruder and determined a high “peak” and a low pressure “valley”, all above zero, because the baseline pressure was high enough to avoid negative pressures. Still other papers show results with negative pressures, but minimize their relevance to the model. Gupta et al. (2009) in their co-rotating twin screw extrusion simulations reported qualitative agreement with experiments and stated that “since the predicted pressure is zero at the exit, the pressure in a portion of the 120/120 element conveying element near the entrance is negative...the actual value of the predicted pressure is not important. It is the pressure gradient which is captured by the flow equations”. Ortiz-Rodriguez (2009) showed in a figure of his doctoral thesis with localized negative pressures along the length of a co-rotating extruder reaching -0.5 MPa, without explaining what they meant or how they could be obtained. Ilinca and Hetu (2012) in their numerical study of co-rotating twin screw extruder mixing elements avoided giving an explanation regarding their negative pressure values which reached -2 MPa, by simply stating that “the exit pressure is taken as reference and it was fixed to 0 in the numerical simulation”. Radl et al. (2010) in their computer simulations of a novel pelletizer having a rotor-stator system, observed negative pressures in the flow field reaching -13 bar, but had no

explanation why the meaningless values were obtained. Similarly, Ishikawa et al (2000) reported that some pressures were negative in simulations of co-rotating twin screw extrusion with no reason given.

Uniformly raising the baseline pressure in simulating twin screw extruders may avoid these meaningless negative values, but it is often not the appropriate solution to obtaining correct pressure gradients. The boundary conditions at entry and exit must carefully be chosen to produce physically meaningful results and not simply be done to avoid values that cannot be explained.

Table 5.1. Parameters Used in the Co- and Counter-rotating Cylinder Examples Reported in Figures 5.1 and 5.2

		Co-rotating case	Counter-rotating case
Diameter of inner cylinder	[mm]	50	50
Diameter of outer cylinder	[mm]	70	70
Minimum gap	[mm]	2	2
Viscosity	[Pa.s]	10000	10000
Density	[kg/m ³]	1000	1000
Rotational speed	[rpm]	100	100

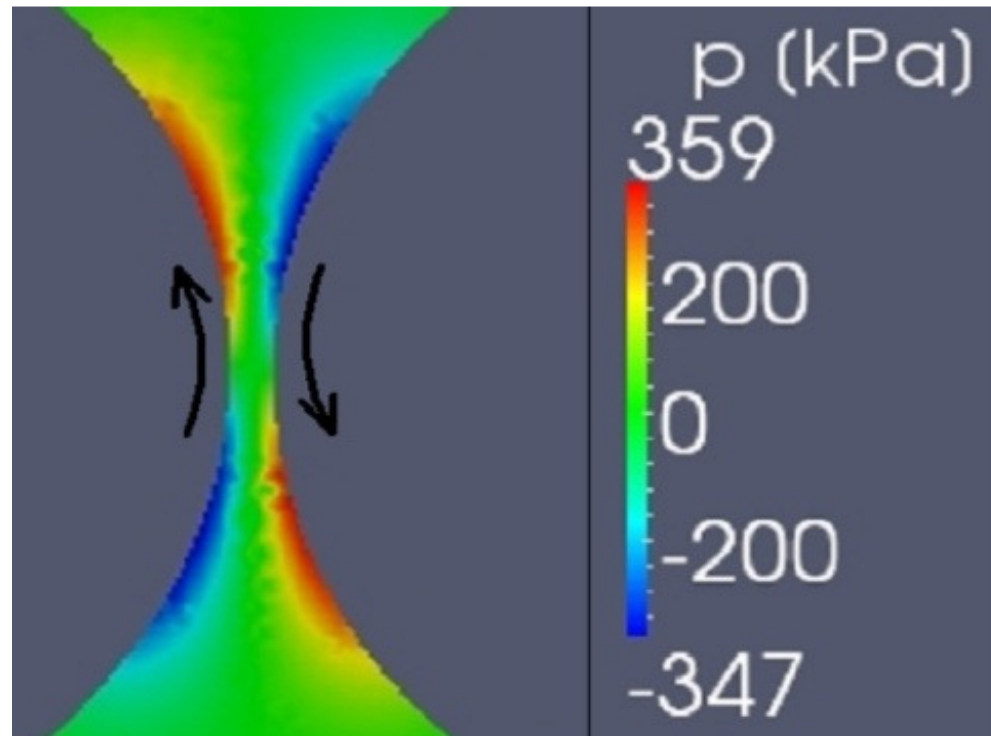


Figure 5.1. Pressure Development between Two Co-rotating Cylinders

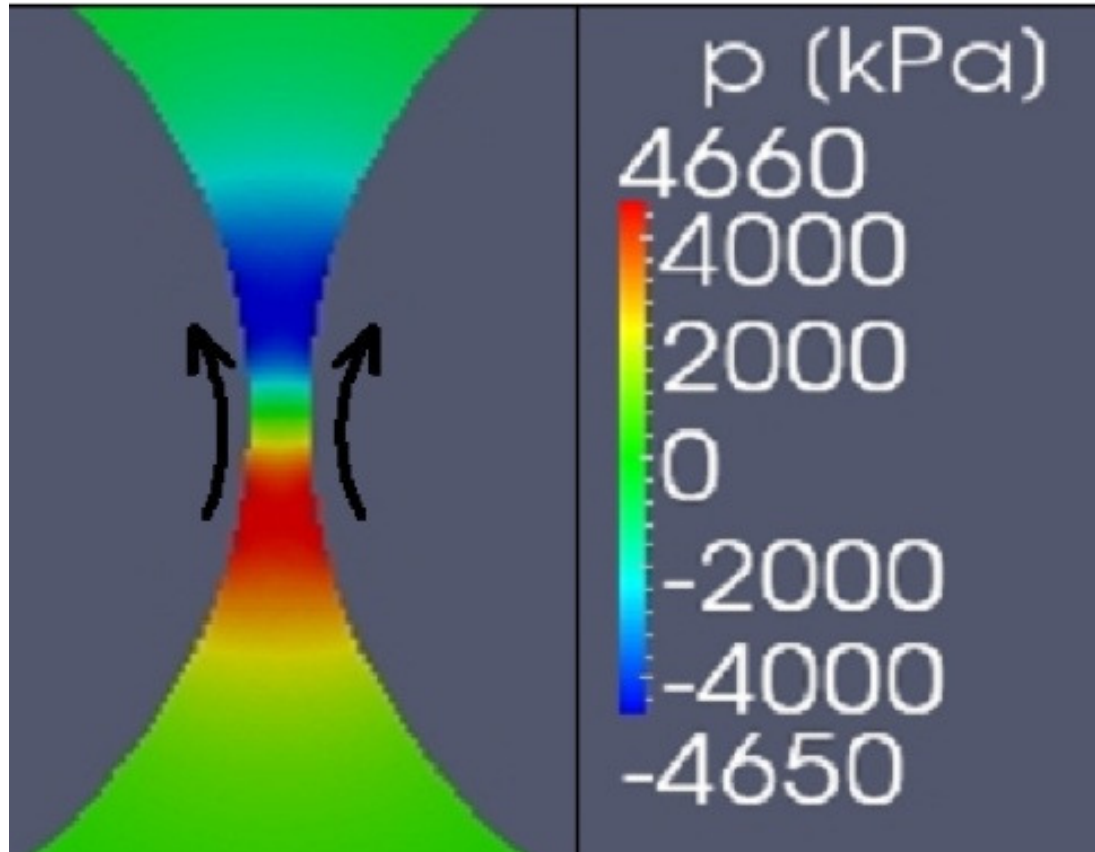


Figure 5.2. Pressure Development between Two Counter-rotating Cylinders

5.3. Explaining the Phenomenon

The non-physical result of negative pressures has been observed and properly interpreted as to its cause for more than a hundred years in the modelling of journal bearing lubrication. An example of such modeling results is shown in Figure 5.3. The results were obtained using the OpenFOAM® software package for a fluid having viscosity of 1 Pa.s, density of 1000 kg/m³, inner cylinder diameter of 40 mm rotating at 3000 rpm, outer cylinder diameter of 41 mm and a minimum gap of 0.2 mm. It is well recognized in the field of lubrication that in the expansion region, when the pressure becomes less than the vapor pressure of the lubricant and/or the saturation state of any dissolved gases, bubbles are actually forming and cavitation is taking place, as explained in a review by Dowson and Taylor (1979) and more recently by Gonzales-Avila et al. (2011). Of course, in the liquid-vapor region of the expansion, the single liquid flow modelling is no longer valid. Due to the highly localized regions where negative pressures are often reported (i.e in the nip regions of extrusion machinery), being far from barrel walls, such findings of bubbling are difficult to verify. But then the purpose of such modelling efforts is often to observe and explain phenomena inside the process that cannot be physically observed by the conventional placement of sensors. We are inferring that modellers of polymer systems within rotating machinery simply need to recognize that their negative results may be an indication of a multiphase system being incorrectly reconciled within a single phase model.

We do not mean to infer from our statements above that observing negative pressure results invalidates the relevance of the model. In most cases, the flow regions

showing negative values occupy a small portion of the overall system. However, they should be reported as they may lead to future studies with more complex phase assumptions being introduced.

5.4. Conclusion

Negative pressures obtained in modelling of rotating polymer processing machinery indicate the possibility of local bubble formation and cavitation, when the pressure drops below the vapor pressure of dissolved gases, as it is well known in journal bearing lubrication. The single fluid modelling is not valid in such flow regions. When simulations are carried out, the baseline pressure, which would prevent the meaningless negative pressures, should be clearly stated and its impact on pressure gradients and any conclusions relating to mixing or scale-up should be discussed. The purpose of numerical simulation is to produce results, which should reflect reality and could be confirmed by experimental measurements of several quantities, including pressures.

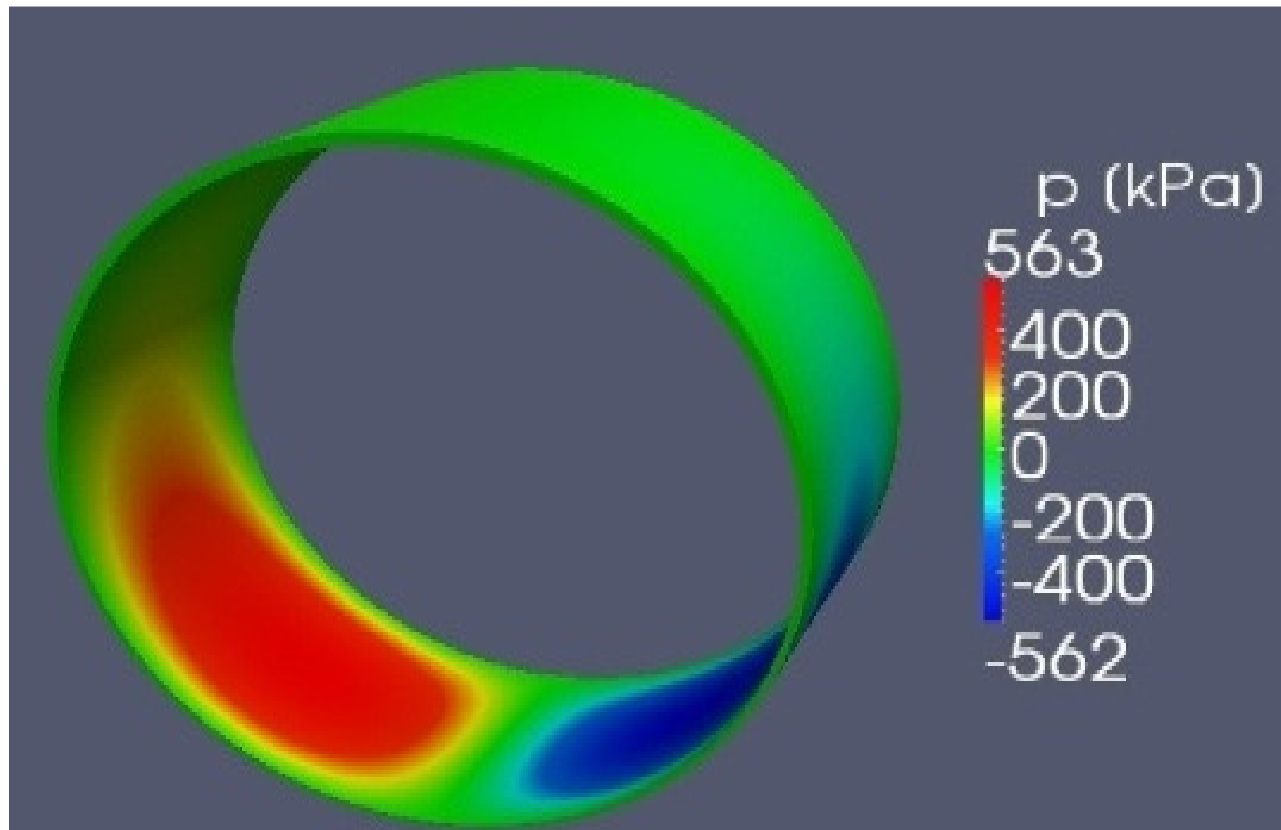


Figure 5.3. Pressure Distribution in a Journal Bearing

Chapter Six

NUMERICAL RESULTS

6.1. Introduction

Generally, twin screw extruders are divided into three zones: solid conveying zone, melting zone and metering zone. In metering zone, all the particles of polymer are at molten phase. Ideally, all screw channels are filled with molten polymer in this region. Since pumping and mixing mainly take place in metering zone, it is very important to characterize the metering region to understand the twin screw extruder process.

The purpose of this study is to investigate the pumping behaviour and mixing performance of metering zone of intermeshing counter rotating twin screw extruders (ICRTSE) for various screw pitch lengths, flight width-to-channel width ratios and screw speeds. Pumping behaviour and dispersive mixing ability of ICRTSE provide information screw designers and operators for better understanding of both screw geometries and processing conditions.

6.2. Description of Method

One of the biggest challenges in simulating ICRTSE is the time dependent flow boundaries as the screws rotate in counter direction. Lee and Castro (1989) mentioned that some extrusion processes cannot reach a truly steady state due to the start-end-repeat behaviour in polymer processing. If the Reynolds number is very small, time dependency at flow boundaries are negligible compared to other terms in the equations of motion. With this assumption, extrusion processes can only reach a

quasi-steady state which is dependent only on instantaneous material behaviour and boundary conditions of the system.

In this study, four sequential geometries were specified to present a complete cycle of rotation by the screws. A complete cycle is shown in Figure 6.1 for $\alpha = 90, 60, 30$ and 0 for the 75 mm screw pitch length. The parameter, α , represents the angle between the left screw tip and x-axis, as shown in Figure 6.1. Since ICRTSE have two identical screw tips, only one half of a revolution is sufficient to model the ICRTSE. Cross-sections through the flow domain including the inlet and outlet boundaries are shown schematically in Figure 6.2. It is well known that length equal to half of the gap is sufficient to obtain fully developed velocity profiles in creeping flows (Reynolds number is much smaller than 1). Four different cross-sections in the transport direction are used to understand the flow behaviour and dispersive mixing performance in the screw element.

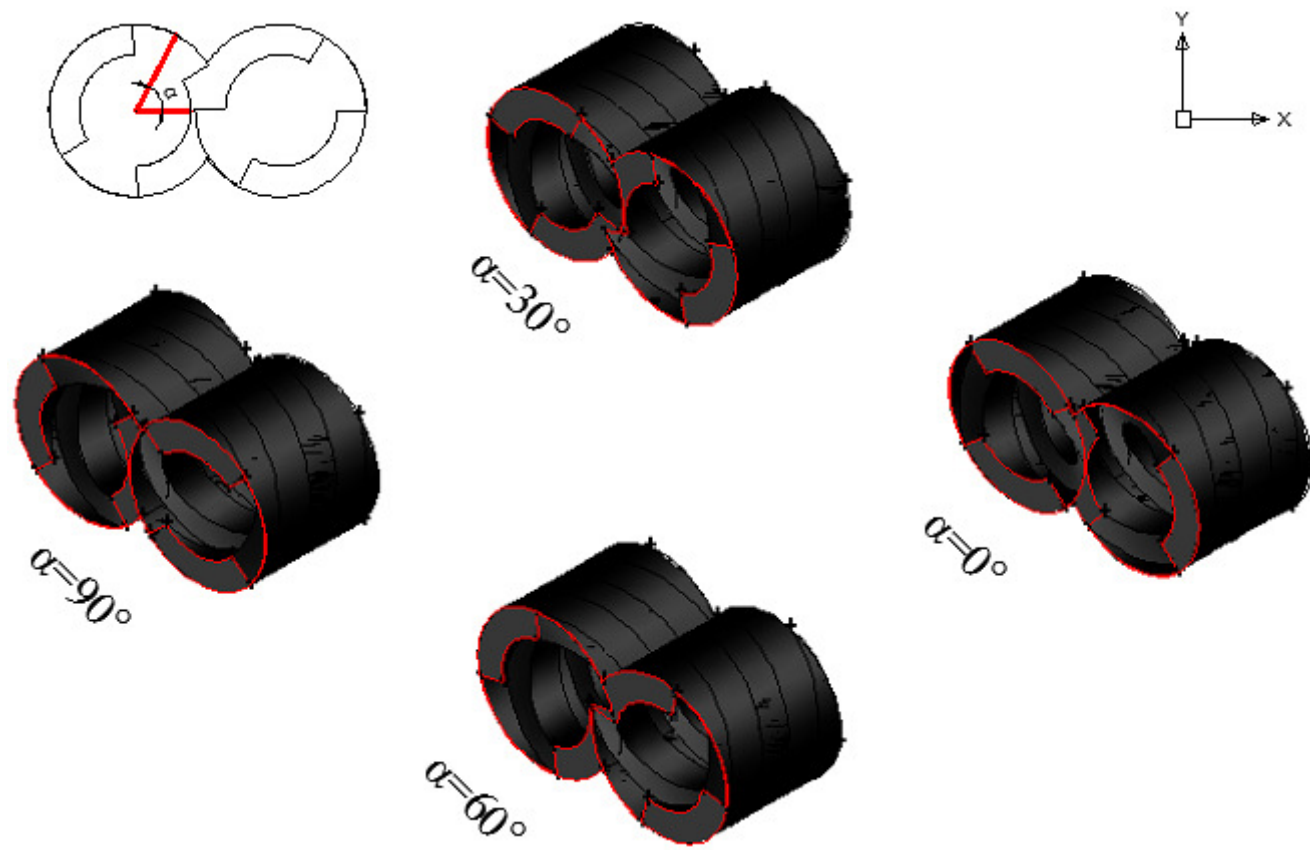


Figure 6.1. Sequential Geometries Representing Complete Cycle

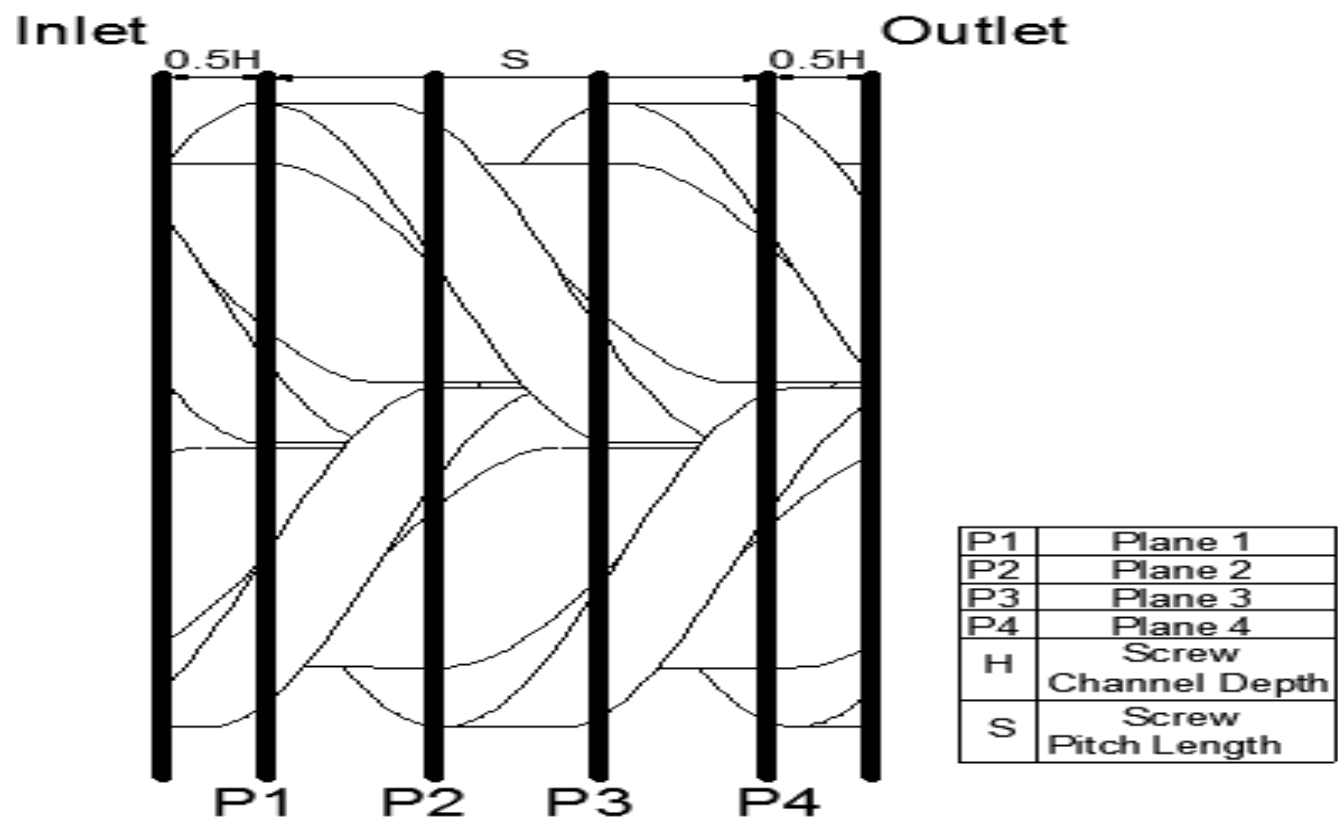


Figure 6.2. Schematic View of the Location of Cross Sections and Boundaries

6.3. Flow Pattern in ICRTSE

In this section, the axial velocities and pumping efficiency are investigated to understand the flow behaviour of ICRTSE. Different screw pitch lengths, flight width-to-channel width ratios, power indexes and screw speeds were used to study the screw geometries and processing conditions of an ICRTSE.

6.3.1. Axial Velocity in ICRTSE

Axial velocity is one of the most important parameters to understanding the flow behaviour of an ICRTSE. Axial velocity is the main component of velocity in the transport direction of flow. Axial velocities are shown in Figure 6.3 to 6.6 for various cross sections for 105 mm screw pitch length. The positive value in these figures correspond to the flow in the transport direction whereas negative values indicate that the flow in the opposite transport direction. Figure 6.3 to 6.6 reveal that most of the polymers flow was in the transport direction.

The results indicated that the maximum positive axial velocity occurred before the converging section of intermeshing region and screw tips while the maximum negative axial velocity occurred in the intermeshing region. In fact, most of the fluid in the intermeshing region exhibited negative axial velocity values. Shah and Gupta (2004) found that the maximum axial velocity occurred in a similar location as the present results for their 29.2 mm diameter ICTRSE simulations and likewise, included mention that the axial velocity was predominantly backwards in their intermeshing region. Similarly, Ma et al. (2004) noted negative velocity values in their simulation results for the intermeshing region of a 33.2 mm diameter ICRTSE.

The average values for axial velocities of all four different geometries in a complete cycle are shown in Tables 6.1 to 6.3 for power index values of 1, 0.7 and 0.3 respectively. These averages were calculated by weighing the axial velocity for each element by the area of the element itself across the entire cross section. It is noted that the average values hardly ever change from one geometry to another for the same screw pitch length. Thus, it is shown in Tables 6.1 to 6.3 that one angle for α is sufficient to use for flow rate determination of ICRTSE with fully agreement Li and Manas-Zloczower (1994). It can be seen from Tables 6.1 to 6.3 that the average axial velocity decreased with increasing screw pitch length. Since lower power index fluid has a smaller viscosity at the same shear rate which cause higher leakage flows, the average axial velocity goes down with shear thinning.

Table 6.1. Average Axial Velocities for Various α and for Screw Pitch Length for

Power Index 1

Screw Pitch Length		Average Axial Velocity
[mm]		[mm/s]
75 mm Screw Pitch Length	$\alpha=90^\circ$	16.12
	$\alpha=60^\circ$	16.33
	$\alpha=30^\circ$	16.27
	$\alpha=0^\circ$	16.08
90 mm Screw Pitch Length	$\alpha=90^\circ$	15.64
	$\alpha=60^\circ$	15.79
	$\alpha=30^\circ$	15.77
	$\alpha=0^\circ$	15.61
105 mm Screw Pitch Length	$\alpha=90^\circ$	15.18
	$\alpha=60^\circ$	15.22
	$\alpha=30^\circ$	15.24
	$\alpha=0^\circ$	15.14
135 mm Screw Pitch Length	$\alpha=90^\circ$	14.13
	$\alpha=60^\circ$	14.38
	$\alpha=30^\circ$	14.27
	$\alpha=0^\circ$	14.14

Table 6.2. Average Axial Velocities for Various α and for Screw Pitch Length for

Power Index 0.7

Screw Pitch Length		Average Axial Velocity
[mm]		[mm/s]
75 mm Screw Pitch Length	$\alpha=90^\circ$	16.06
	$\alpha=60^\circ$	16.18
	$\alpha=30^\circ$	16.16
	$\alpha=0^\circ$	16.08
90 mm Screw Pitch Length	$\alpha=90^\circ$	15.07
	$\alpha=60^\circ$	15.17
	$\alpha=30^\circ$	15.14
	$\alpha=0^\circ$	15.08
105 mm Screw Pitch Length	$\alpha=90^\circ$	14.67
	$\alpha=60^\circ$	14.71
	$\alpha=30^\circ$	14.73
	$\alpha=0^\circ$	14.68
135 mm Screw Pitch Length	$\alpha=90^\circ$	13.58
	$\alpha=60^\circ$	13.65
	$\alpha=30^\circ$	13.67
	$\alpha=0^\circ$	13.59

Table 6.3. Average Axial Velocities for Various α and for Screw Pitch Length for

Power Index 0.3

Screw Pitch Length		Average Axial Velocity
[mm]		[mm/s]
75 mm Screw Pitch Length	$\alpha=90^\circ$	13.66
	$\alpha=60^\circ$	13.65
	$\alpha=30^\circ$	13.62
	$\alpha=0^\circ$	13.66
90 mm Screw Pitch Length	$\alpha=90^\circ$	13.05
	$\alpha=60^\circ$	13.07
	$\alpha=30^\circ$	13.11
	$\alpha=0^\circ$	13.05
105 mm Screw Pitch Length	$\alpha=90^\circ$	12.49
	$\alpha=60^\circ$	12.51
	$\alpha=30^\circ$	12.53
	$\alpha=0^\circ$	12:50
135 mm Screw Pitch Length	$\alpha=90^\circ$	11.98
	$\alpha=60^\circ$	12.01
	$\alpha=30^\circ$	12.05
	$\alpha=0^\circ$	11.97

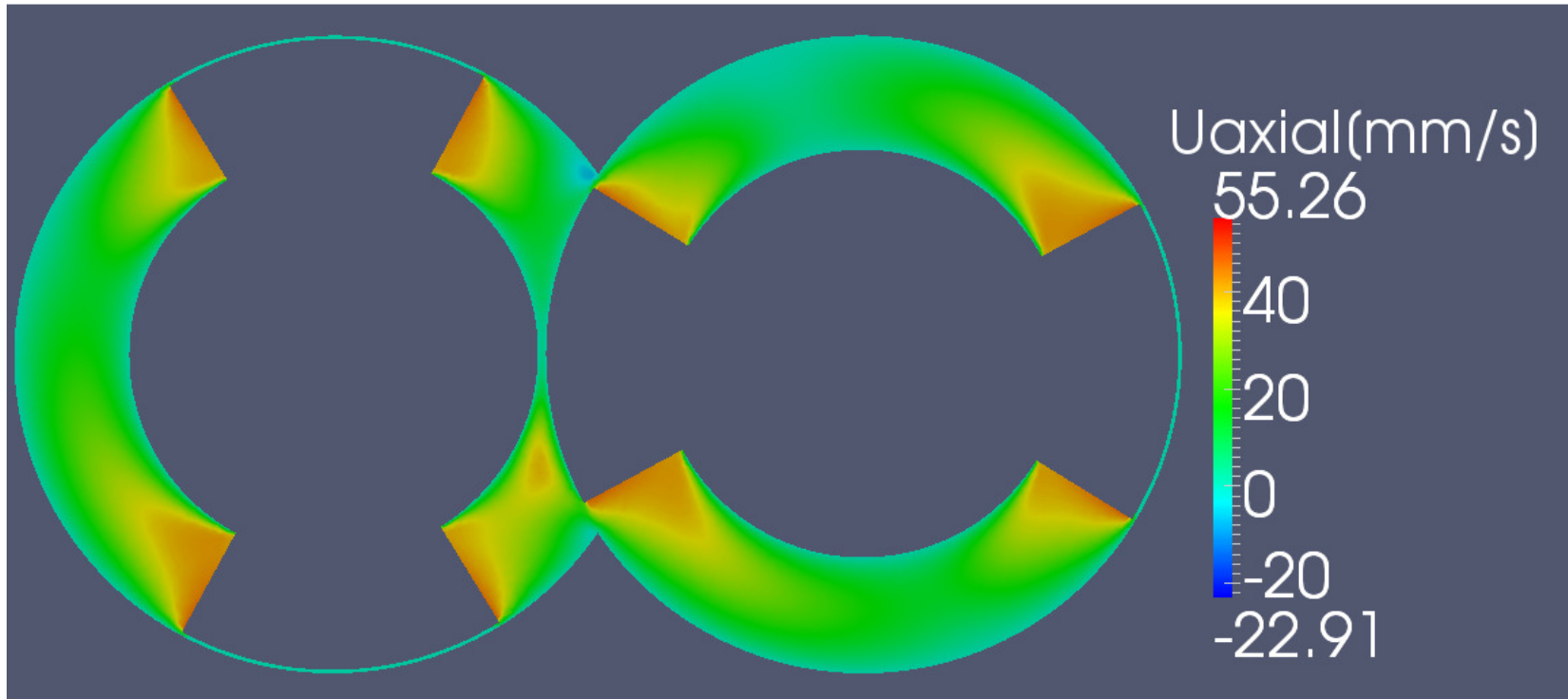


Figure 6.3. Axial Velocity Distribution at Plane 1 $\alpha=90^\circ$ for 105 mm Screw Pitch Length

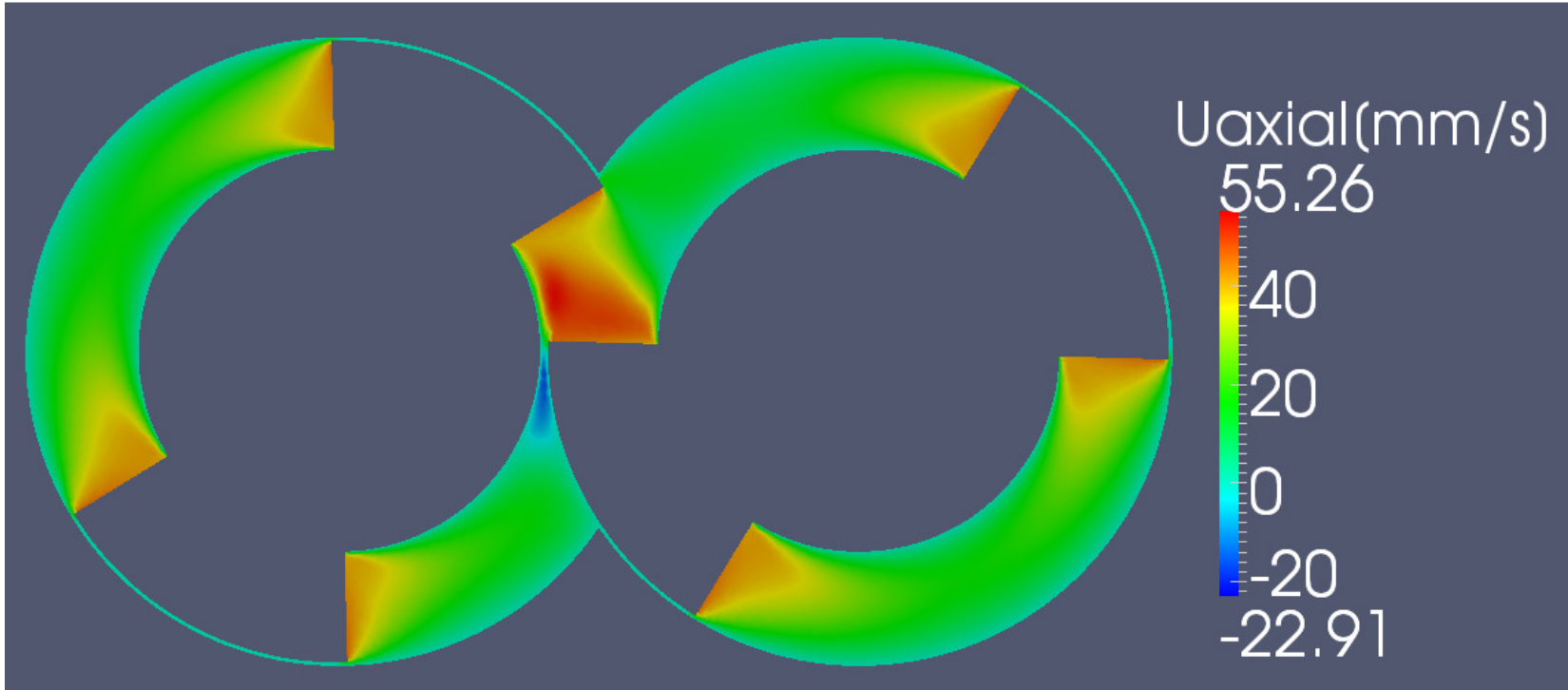


Figure 6.4. Axial Velocity Distribution at Plane 2 $\alpha=90^\circ$ for 105 mm Screw Pitch Length

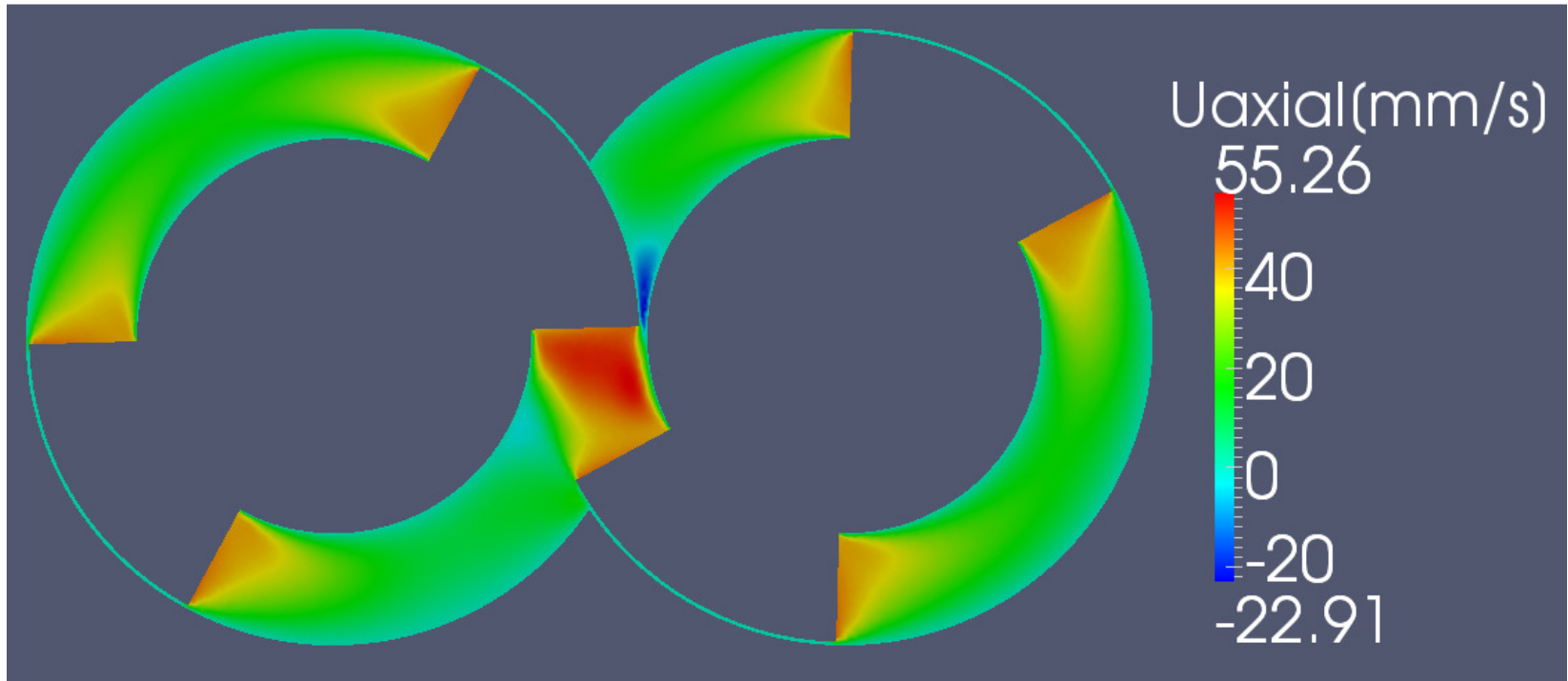


Figure 6.5. Axial Velocity Distribution at Plane 3 $\alpha=90^\circ$ for 105 mm Screw Pitch Length

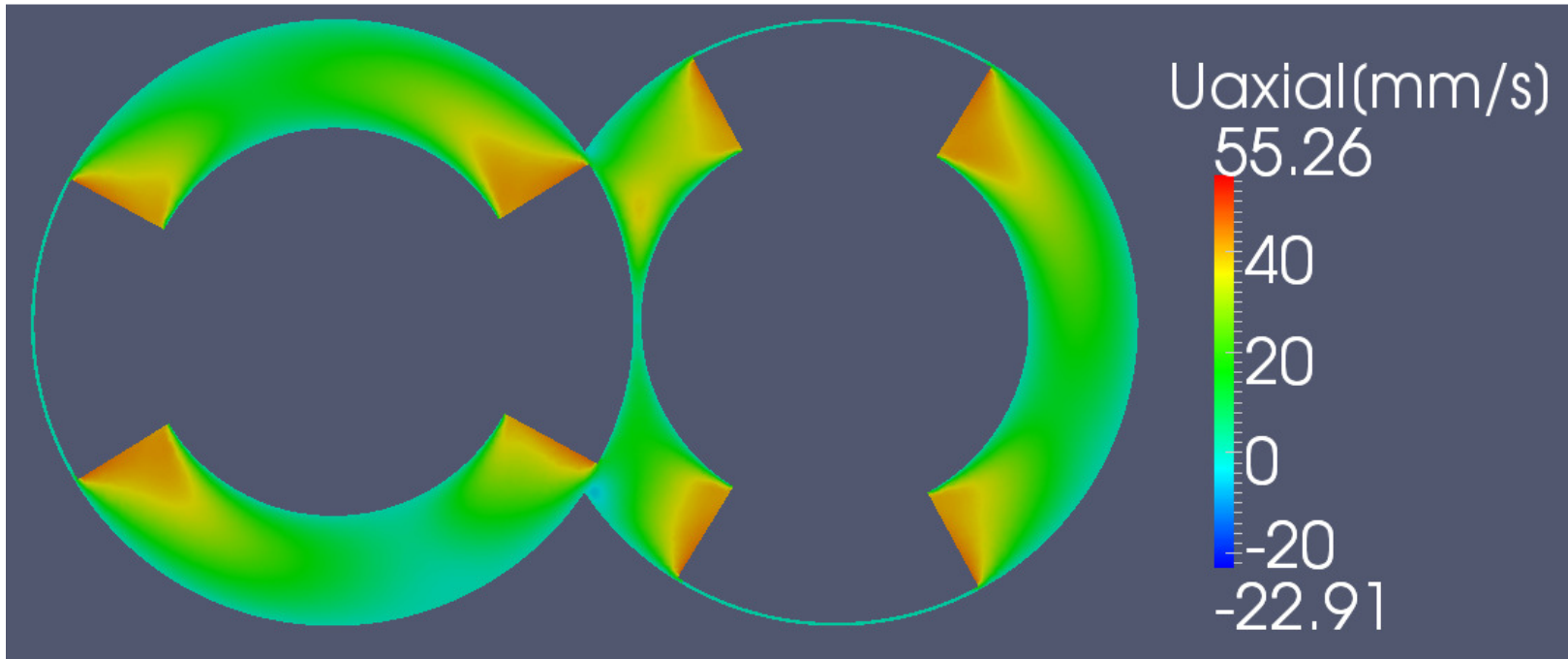


Figure 6.6. Axial Velocity Distribution at Plane 4 $\alpha=90^\circ$ for 105 mm Screw Pitch Length

6.3.2. Pumping Behaviour of ICRTSE

In this section, the effects of screw pitch length, flight width-to-channel width ratio and screw speed on the pumping behaviour were investigated for fluid with different power index values.

The *Total mass flow rate* used was calculated by OpenFOAM® whereas the *Theoretical mass flow rate* (without leakage flows) was obtained through the volume of one screw pitch length fluid domain times by screw speed and polymer density. Detailed calculations for the theoretical mass flow rate can be found from Equations 3.2 to 3.7 in Chapter 3.

6.3.2.1. The Effect of Screw Pitch Length

It can be seen in Figure 6.7 that the pumping efficiency decreases with the increasing screw pitch length. It is due to the fact that the theoretical flow rate goes up greatly by increasing screw pitch length but the real flow rate is slightly affected by the screw pitch length because of the leakage flow. Pumping efficiency is also affected by the non-Newtonian behaviour. The negative influence of non-Newtonian behaviour on pumping efficiency rises up with decreasing power index.

6.3.2.2. The Effect of the Ratio of Flight Width-to-channel Width

Flight width-to-channel width ratios of 0.875, 0.636, 0.500 and 0.350 were used in this study. Figure 6.8 shows that the pumping efficiency tended to increase linearly with an increasing ratio. A lower power index resulted in lower pumping efficiency for all of the ratios examined. This is because the lower power index fluid results in a smaller viscosity at the same shear rate which causes higher leakage flows

and lower pumping efficiency. In addition, the effect of power index on pumping efficiency increases with decreasing power index value. It is concluded that thick flighted elements have a greater pumping ability than thin flighted elements.

6.3.2.3. The Effect of Screw Speed

Screw speed has already been mentioned to be one of the most crucial processing parameters in terms of pumping behaviour for the ICRTSE. Speeds of 30, 60, and 120 rpm were investigated. Figures 6.9, 6.10 and 6.11 indicate that the influence of screw speed on pumping efficiency is almost negligible similar to the findings with the simple model. It is concluded that screw speed affects the theoretical flow rate and total flow rate at same degree.

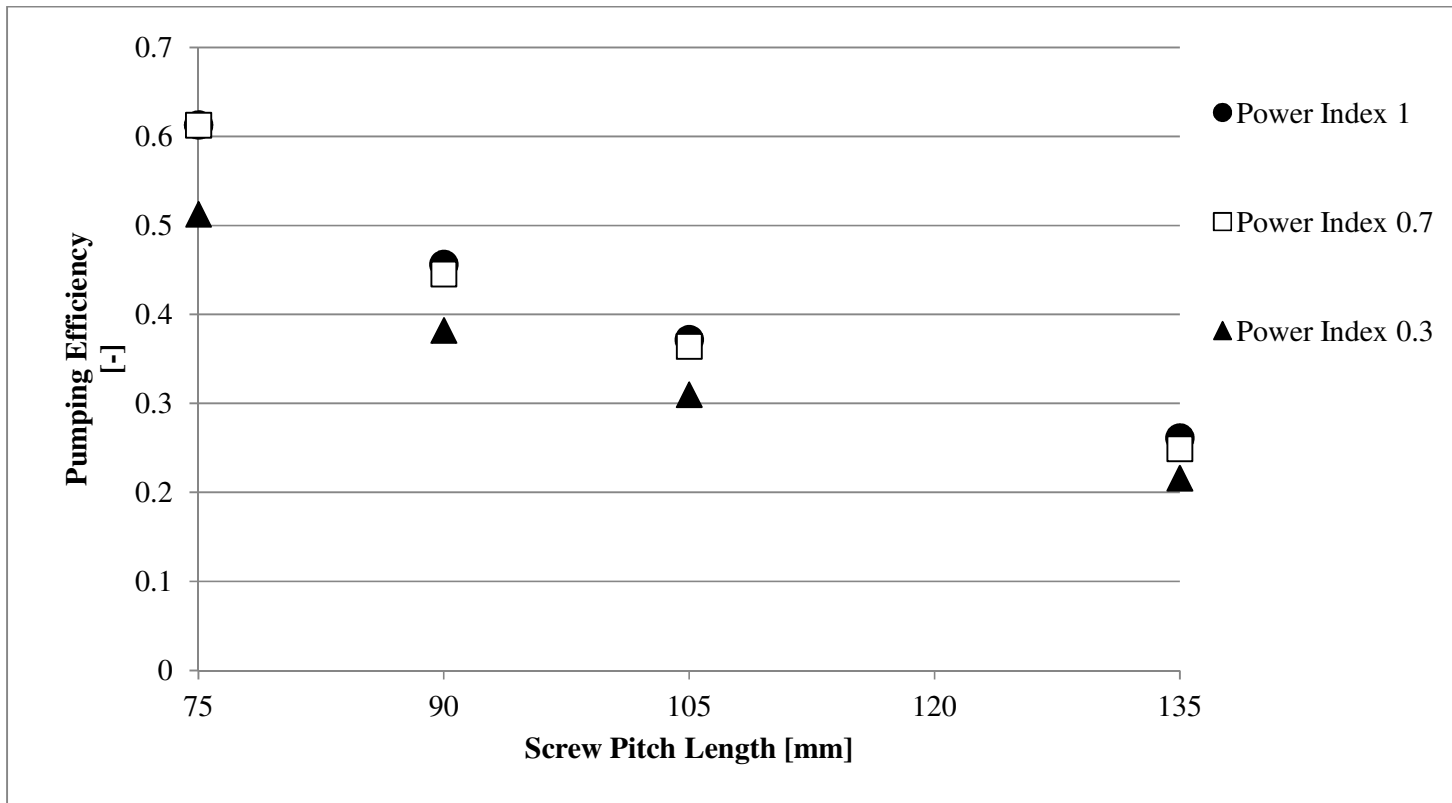


Figure 6.7. The Effect of Screw Pitch Length on Pumping Efficiency

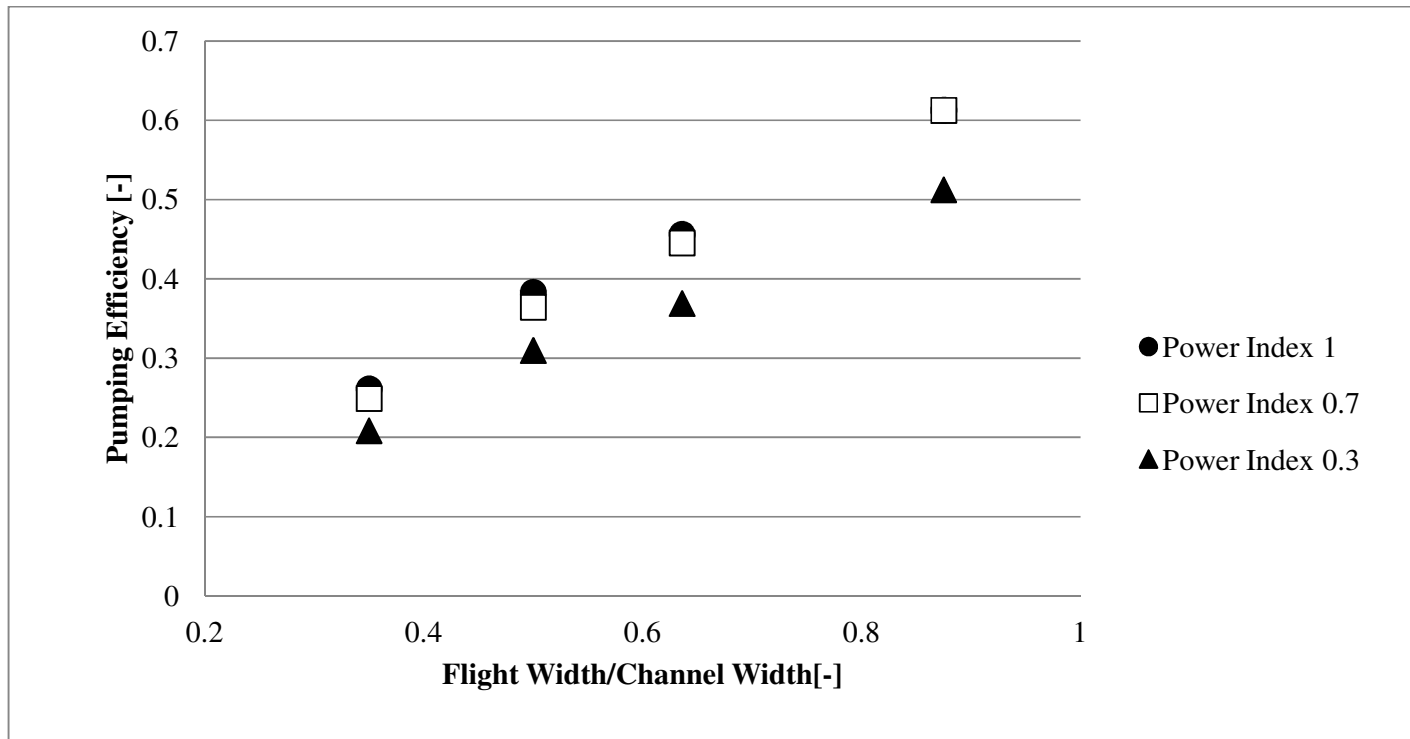


Figure 6.8. The Effect of Flight Width-to-channel Width Ratio on Pumping Efficiency for Power Index 1, 0.7 and 0.3

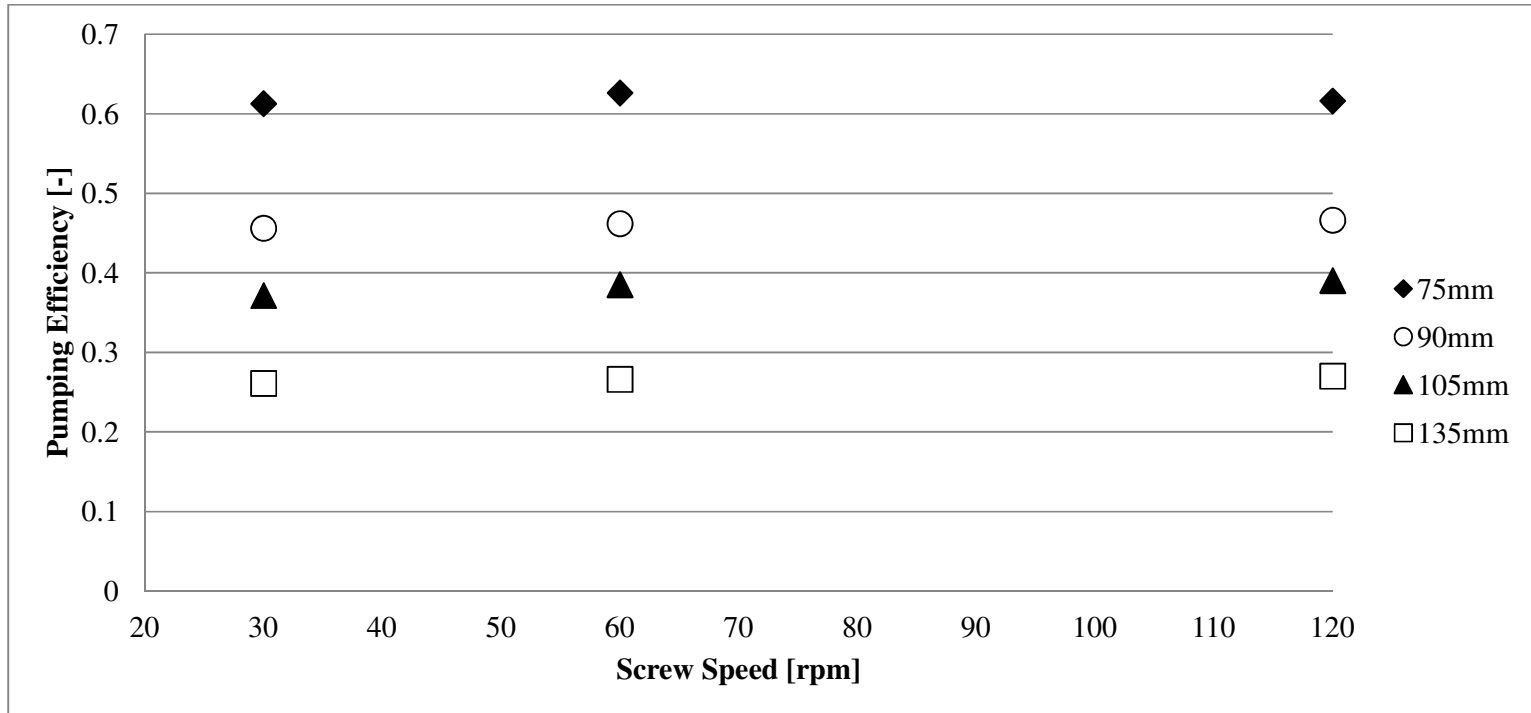


Figure 6.9. The Effect of Screw Speed on Pumping Efficiency for Power Index 1

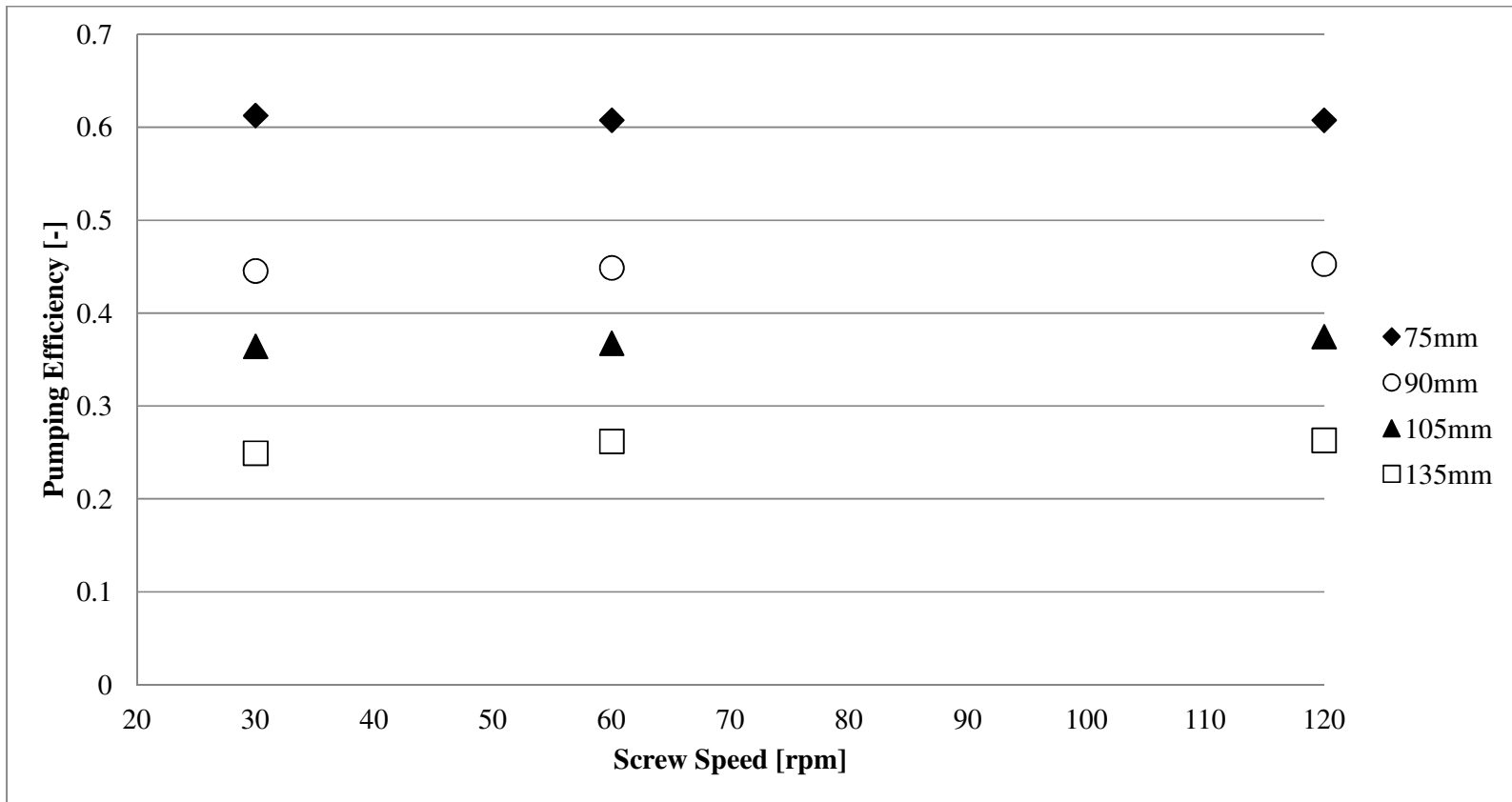


Figure 6.10. The Effect of Screw Speed on Pumping Efficiency for Power Index 0.7

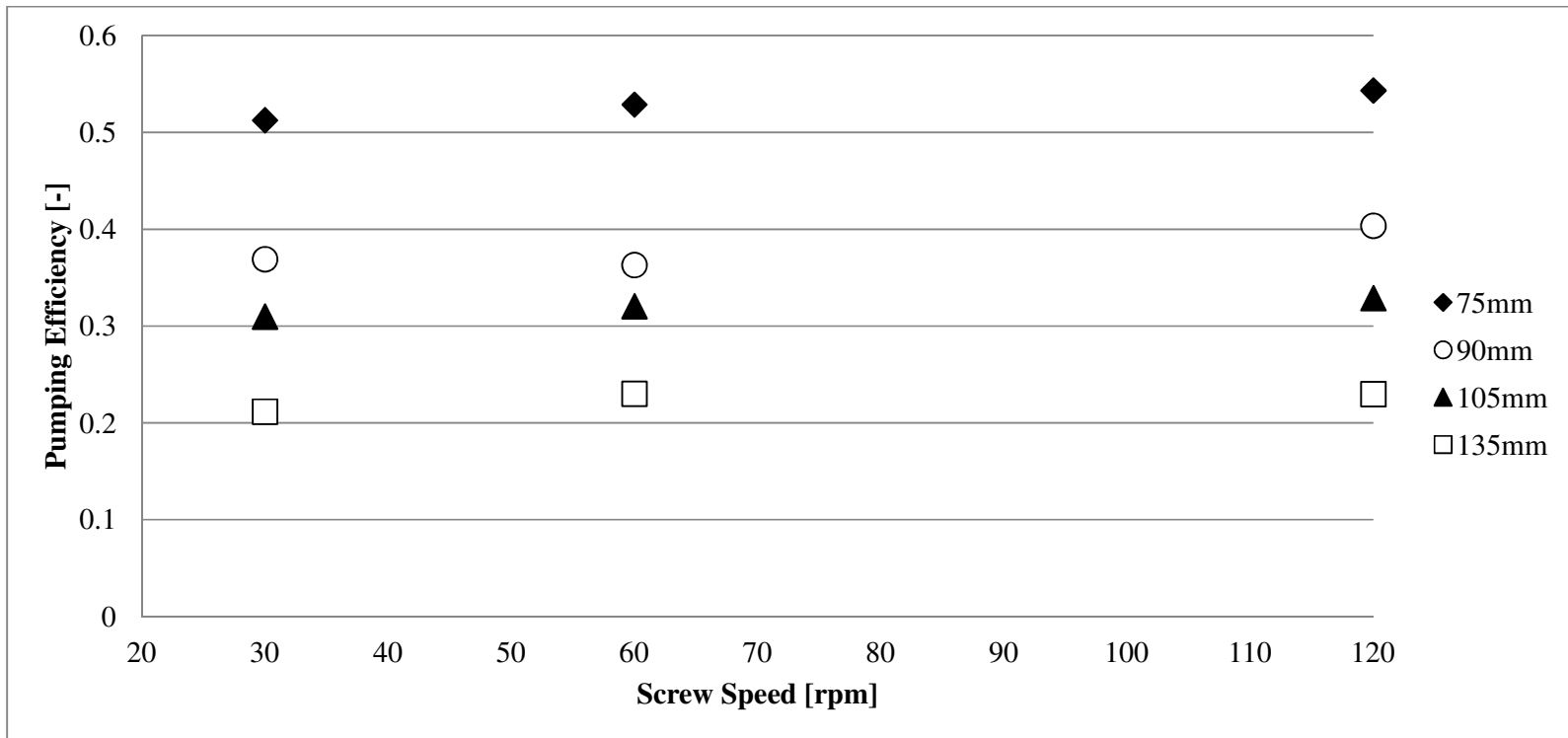


Figure 6.11. The Effect of Screw Speed on Pumping Efficiency for Power Index 0.3

6.4. Dispersive Mixing Behaviour of ICRTSE

Quantification of mixing is always challenging in polymer processing. More is the norm is to talk about mixing in terms of ‘good’ versus ‘bad’. To interpret the dispersive mixing efficiency of ICRTSE, both the shear stress distribution and dispersive mixing parameter, λ , were used in this analysis. Mixing parameter λ was defined by Manas-Zloczower et al. (1988, 1989) as in Equations 6.2 to 6.5.

Kajiwara et al. (1996) mentioned that knowing the shear stress distribution of a process was a valuable measure to evaluating the dispersive mixing of a twin screw extruder. Yang (1993) used shear stress distribution and mixing parameter λ to understand the dispersive mixing behaviour of batch mixer and co-rotating twin screw extruder. Similarly, Li and Manas-Zloczower (1994) investigated the influence of screw speed and axial pressure difference on dispersive mixing for a 34 mm diameter counter-rotating twin screw extruder. They focus on both shear stress distribution and mixing parameter λ as well to quantify the dispersive mixing.

6.4.1. Shear Stress Distribution

Shear stress distributions are shown from Figures 6.12 to 6.15 for various cross sections of the conveying element with 105 mm screw pitch length and power index of 0.7. The distributions indicate that the maximum shear stress was always at the screw tips (the region between screw and barrel) or in the intermeshing region (the region between screws). It is because of that fluid is forced to pass through small gaps in these regions. The shear stress in screw tips and intermeshing region were found to be of the same order of magnitude. In comparison, Li and Manas-Zloczower (1994) found the same results with their simulations of a 34 mm diameter ICRTSE. Kajiwara

et al. (1996) found the highest stresses only in intermeshing region for 40 mm diameter counter rotating twin screw extruder.

The average values of the shear stress for all geometries are shown in Tables 6.4 and 6.5 for power index values of 0.7 and 0.3 respectively. The average values of shear stresses and mixing parameter λ in Tables 6.4 and 6.5 were calculated by following the method of Yang and Manas-Zloczower (1992). They were calculated by weighing the corresponding parameters for each cell by the volume of the cell itself. It is noted from the tables that the average values hardly ever change from one geometry to another for the same screw pitch length. As a result, similar to axial velocity determination, it is concluded that one angle for α is sufficient to use for shear stress and mixing parameter λ determination of ICRTSE which is in agreement with Li and Manas-Zloczower (1994). It is seen in Tables 6.4 and 6.5 that average shear stress decreased with increasing screw pitch length. This was due to the fact that intermeshing region became smaller with increasing screw pitch length. Average shear stress dropped dramatically with decreasing power index, as expected.

The shear stress distributions in Figures 6.16 to 6.19 correspond to the conveying elements with 75 mm and 105 mm screw pitch lengths were determined for power indexes of 0.7 and 0.3 respectively. It can be seen in Figures 6.16 and 6.17 that shear stress distribution becomes slightly narrower with increasing screw pitch length. In addition, the shear rate distribution becomes wider while the power index decreased in Figures 6.18 and 6.19.

The effects of screw speeds on the shear stress distribution are shown in Figures 6.20 and 6.21 for power indexes of 0.7 and 0.3. Average shear stress values over the geometry showed less differences as the power index decreased from 0.7 to 0.3.

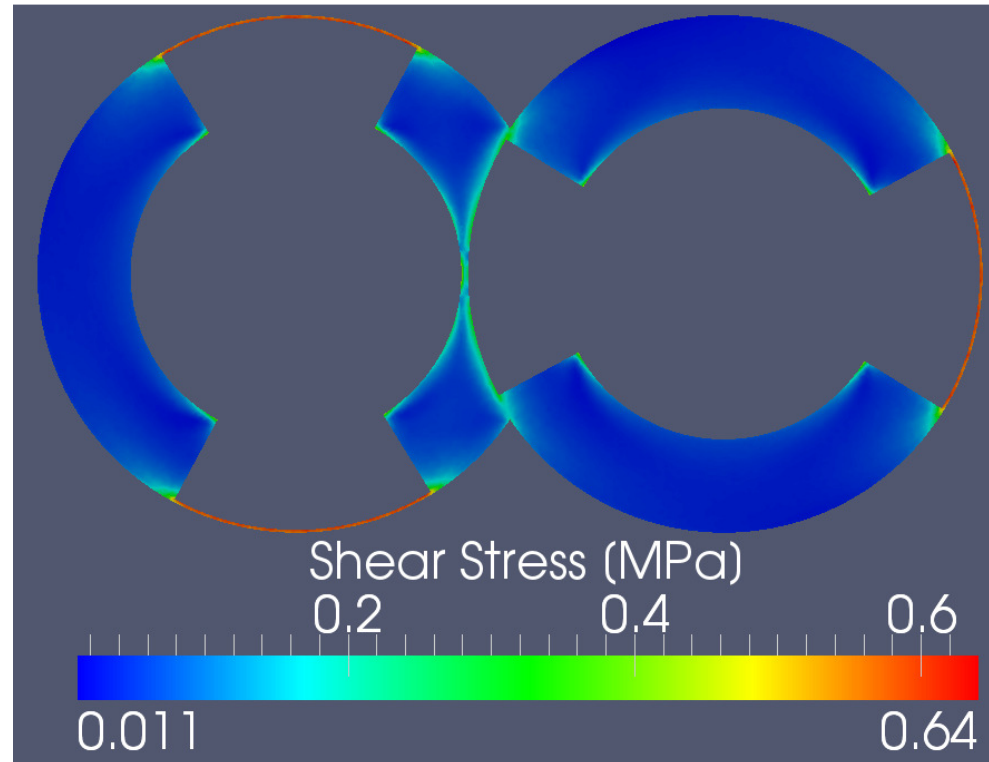


Figure 6.12. Shear Stress Distribution at Plane 1 $\alpha=90^\circ$ for 105 mm Screw Pitch Length Power Index 0.7

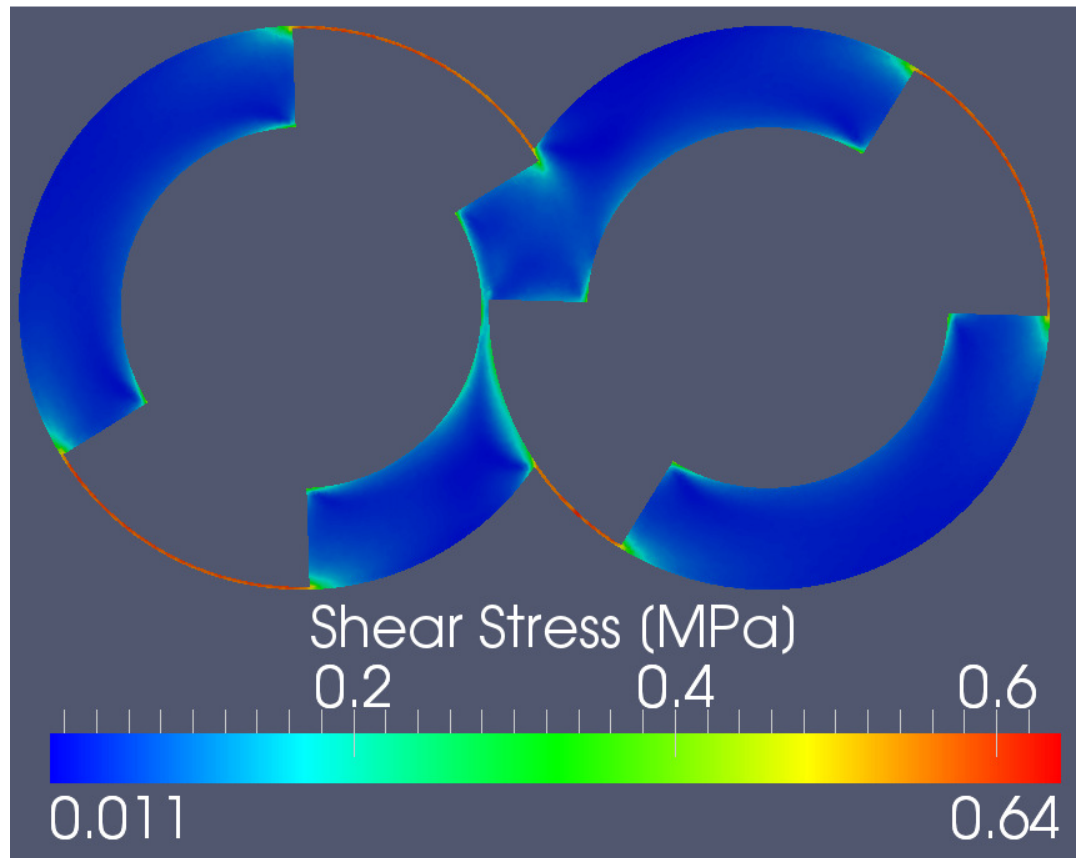


Figure 6.13. Shear Stress Distribution at Plane 2 $\alpha=90^\circ$ for 105 mm Screw Pitch Length Power Index 0.7

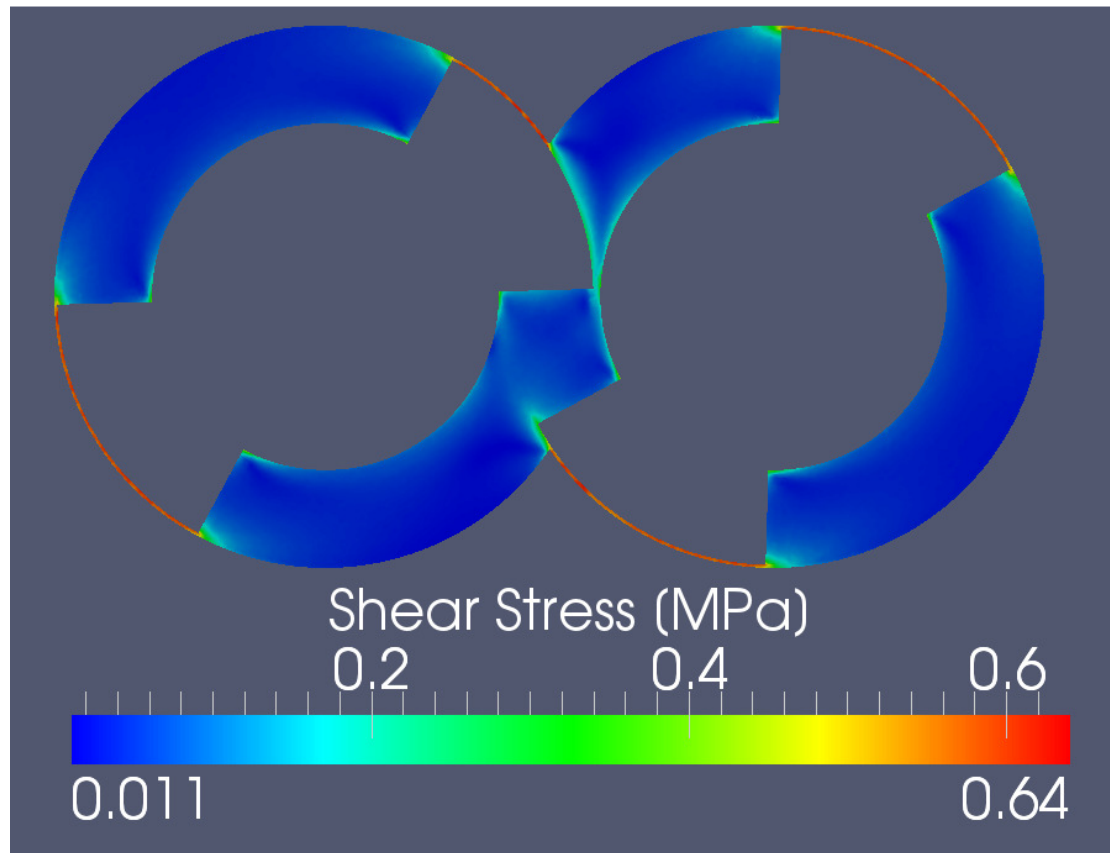


Figure 6.14. Shear Stress Distribution at Plane 3 $\alpha=90^\circ$ for 105 mm Screw Pitch Length Power Index 0.7

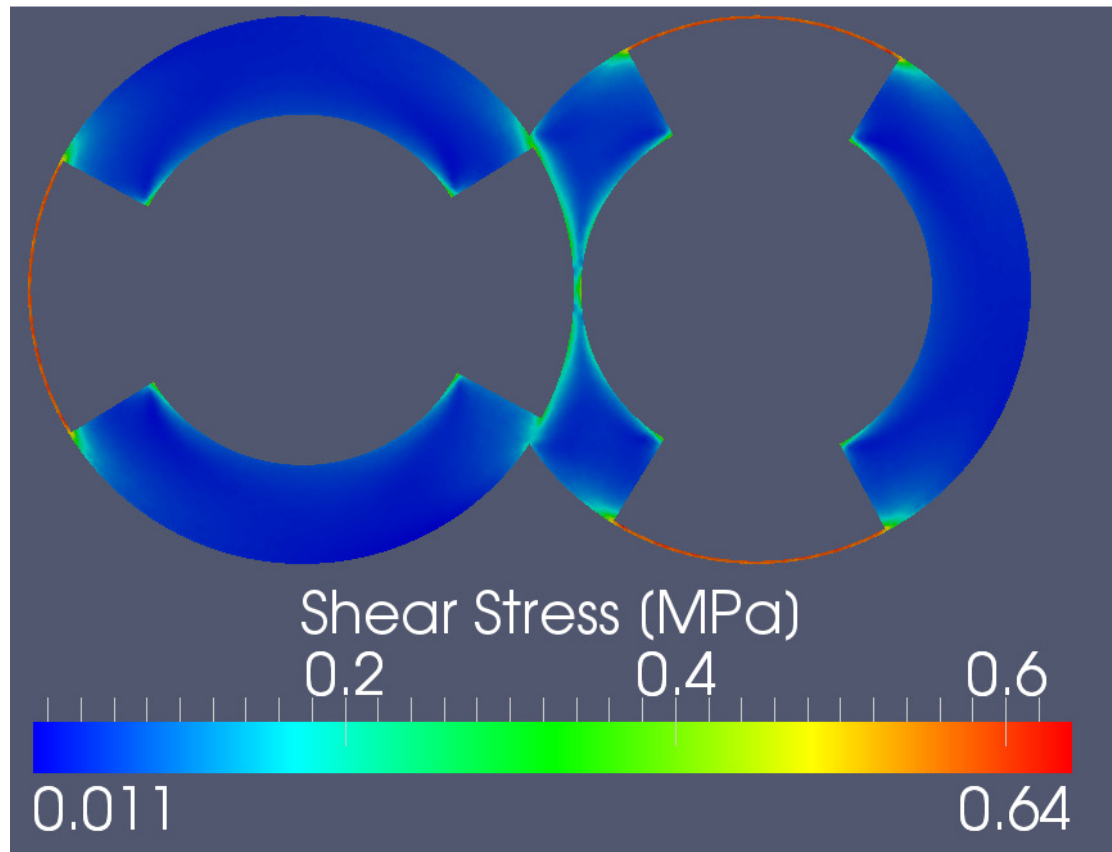


Figure 6.15. Shear Stress Distribution at Plane 4 $\alpha=90^\circ$ for 105 mm Screw Pitch Length Power Index 0.7

Table 6.4. Average Shear Stress and Average Mixing Parameter for Various α and Screw Pitch Length for Power Index 0.7

Screw Pitch Length		Shear Stress	Lamda, λ
[mm]		[MPa]	[-]
75 mm Screw Pitch Length	$\alpha=90^\circ$	0.079	0.535
	$\alpha=60^\circ$	0.075	0.537
	$\alpha=30^\circ$	0.076	0.537
	$\alpha=0^\circ$	0.079	0.534
90 mm Screw Pitch Length	$\alpha=90^\circ$	0.065	0.543
	$\alpha=60^\circ$	0.064	0.542
	$\alpha=30^\circ$	0.065	0.544
	$\alpha=0^\circ$	0.066	0.543
105 mm Screw Pitch Length	$\alpha=90^\circ$	0.060	0.547
	$\alpha=60^\circ$	0.059	0.548
	$\alpha=30^\circ$	0.059	0.549
	$\alpha=0^\circ$	0.060	0.548
135 mm Screw Pitch Length	$\alpha=90^\circ$	0.052	0.554
	$\alpha=60^\circ$	0.052	0.553
	$\alpha=30^\circ$	0.053	0.553
	$\alpha=0^\circ$	0.052	0.554

Table 6.5. Average Shear Stress and Average Mixing Parameter for Various α and Screw Pitch Length for Power Index 0.3

Screw Pitch Length		Shear Stress	Lamda, λ
[mm]		[MPa]	[-]
75 mm Screw Pitch Length	$\alpha=90^\circ$	0.0213	0.533
	$\alpha=60^\circ$	0.0213	0.533
	$\alpha=30^\circ$	0.0211	0.534
	$\alpha=0^\circ$	0.0213	0.533
90 mm Screw Pitch Length	$\alpha=90^\circ$	0.0201	0.538
	$\alpha=60^\circ$	0.0202	0.538
	$\alpha=30^\circ$	0.0201	0.537
	$\alpha=0^\circ$	0.0201	0.538
105 mm Screw Pitch Length	$\alpha=90^\circ$	0.0196	0.542
	$\alpha=60^\circ$	0.0193	0.541
	$\alpha=30^\circ$	0.0197	0.541
	$\alpha=0^\circ$	0.0196	0.541
135 mm Screw Pitch Length	$\alpha=90^\circ$	0.0182	0.546
	$\alpha=60^\circ$	0.0185	0.547
	$\alpha=30^\circ$	0.0183	0.546
	$\alpha=0^\circ$	0.0183	0.548

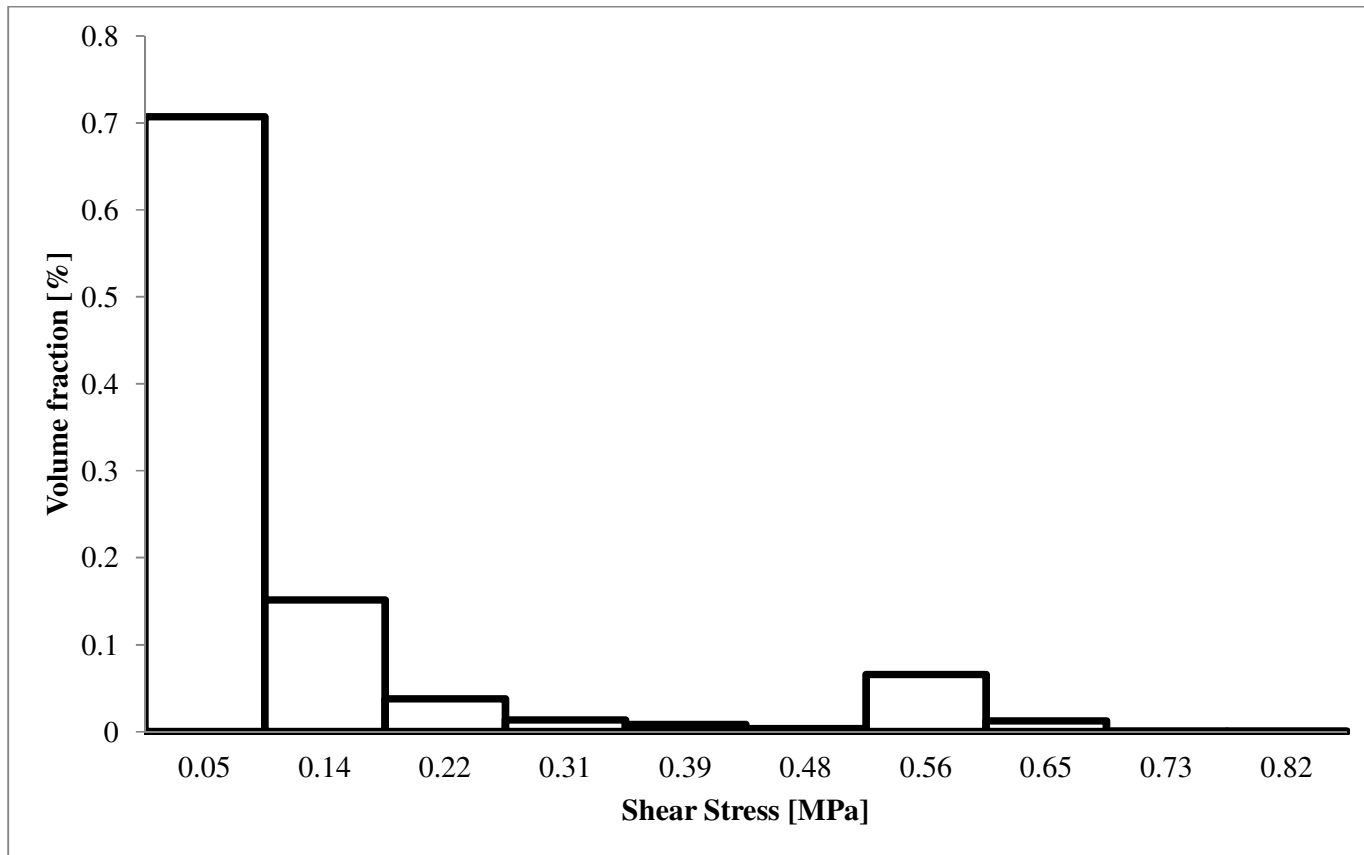


Figure 6.16. The Volume Distribution of Shear Stress for 75 mm Screw Pitch Length for Power Index 0.7

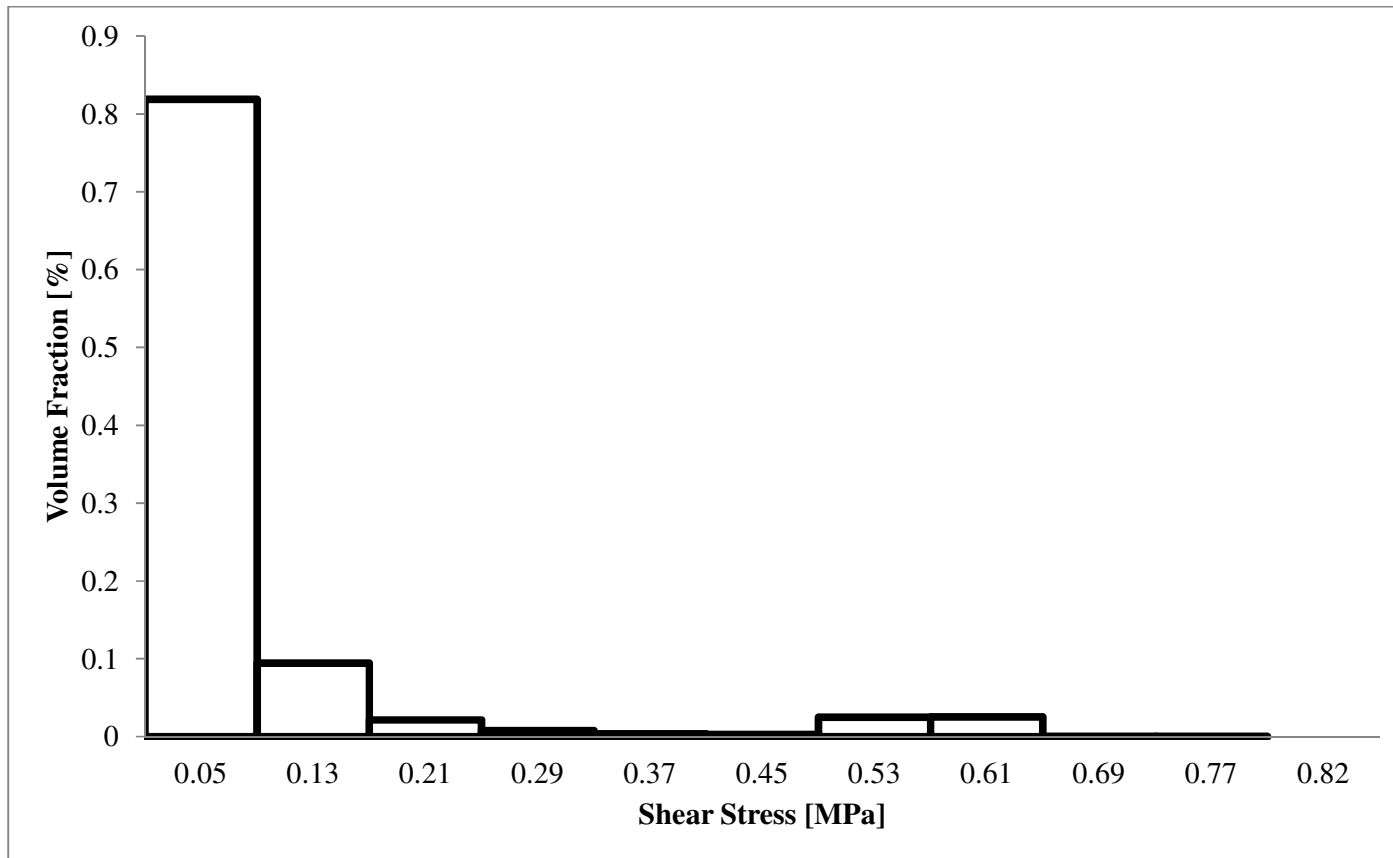


Figure 6.17. The Volume Distribution of Shear Stress for 105 mm Screw Pitch Length for Power Index 0.7

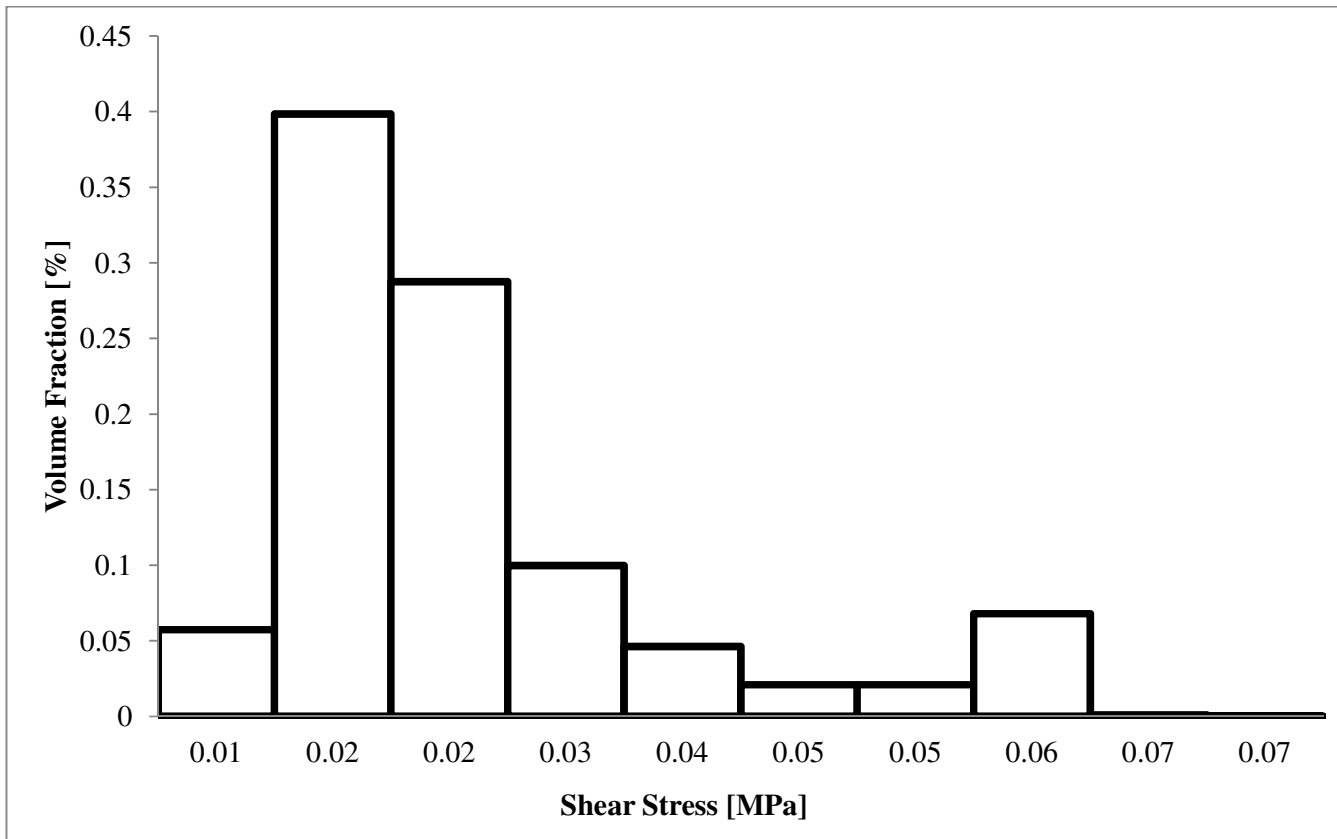


Figure 6.18. The Volume Distribution of Shear Stress for 75 mm Screw Pitch Length for Power Index 0.3

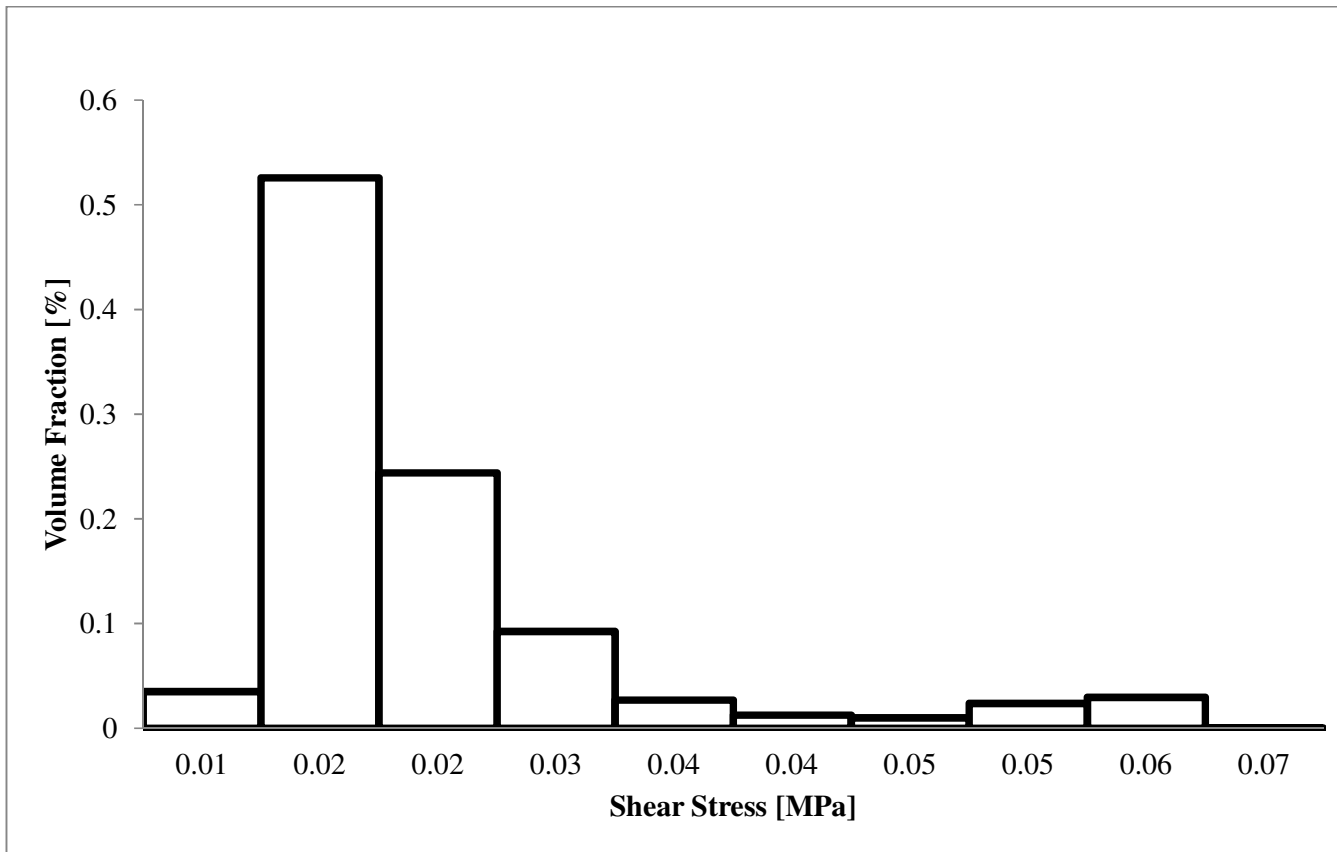


Figure 6.19. The Volume Distribution of Shear Stress for 105 mm Screw Pitch Length for Power Index 0.3

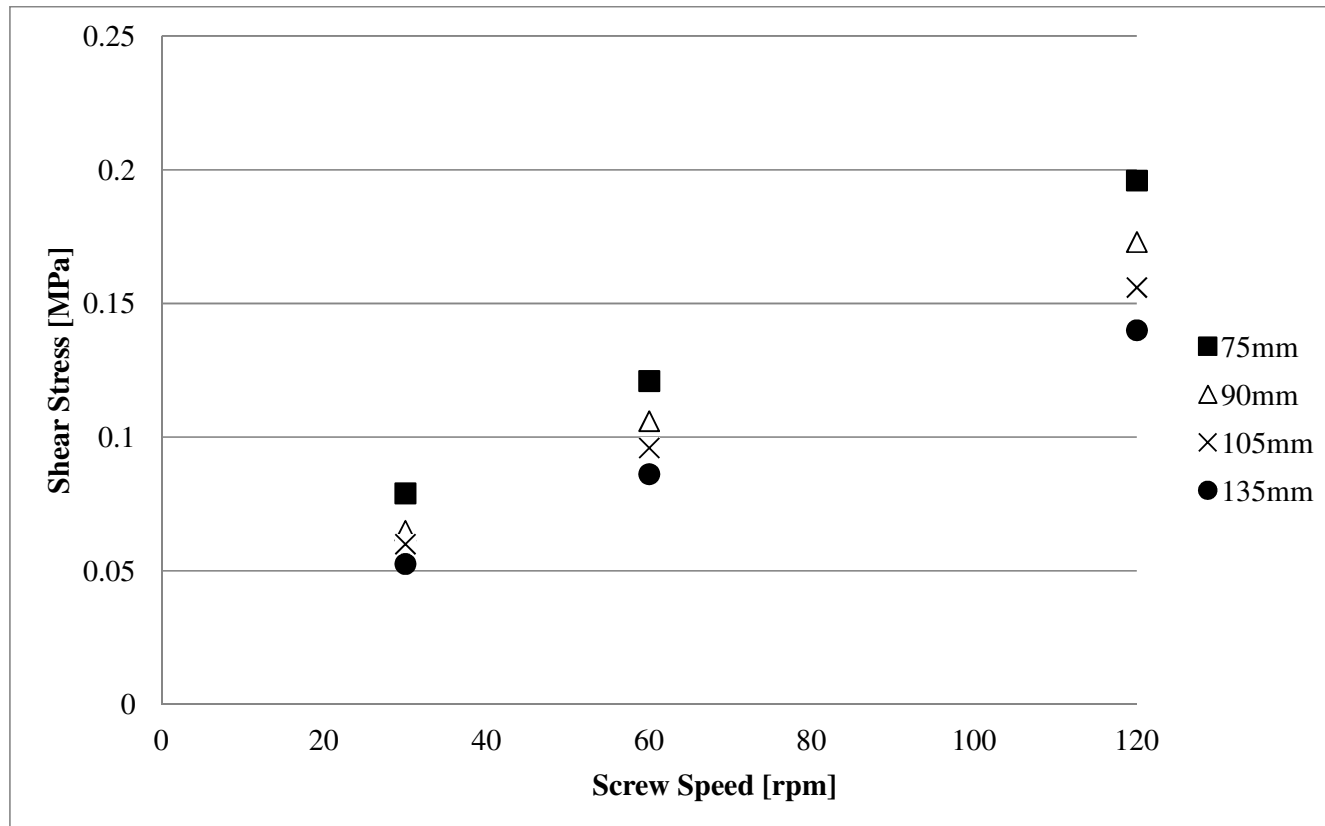


Figure 6.20. The Average Shear Stress for Various Screw Speed and Screw Pitch Length Power Index 0.7

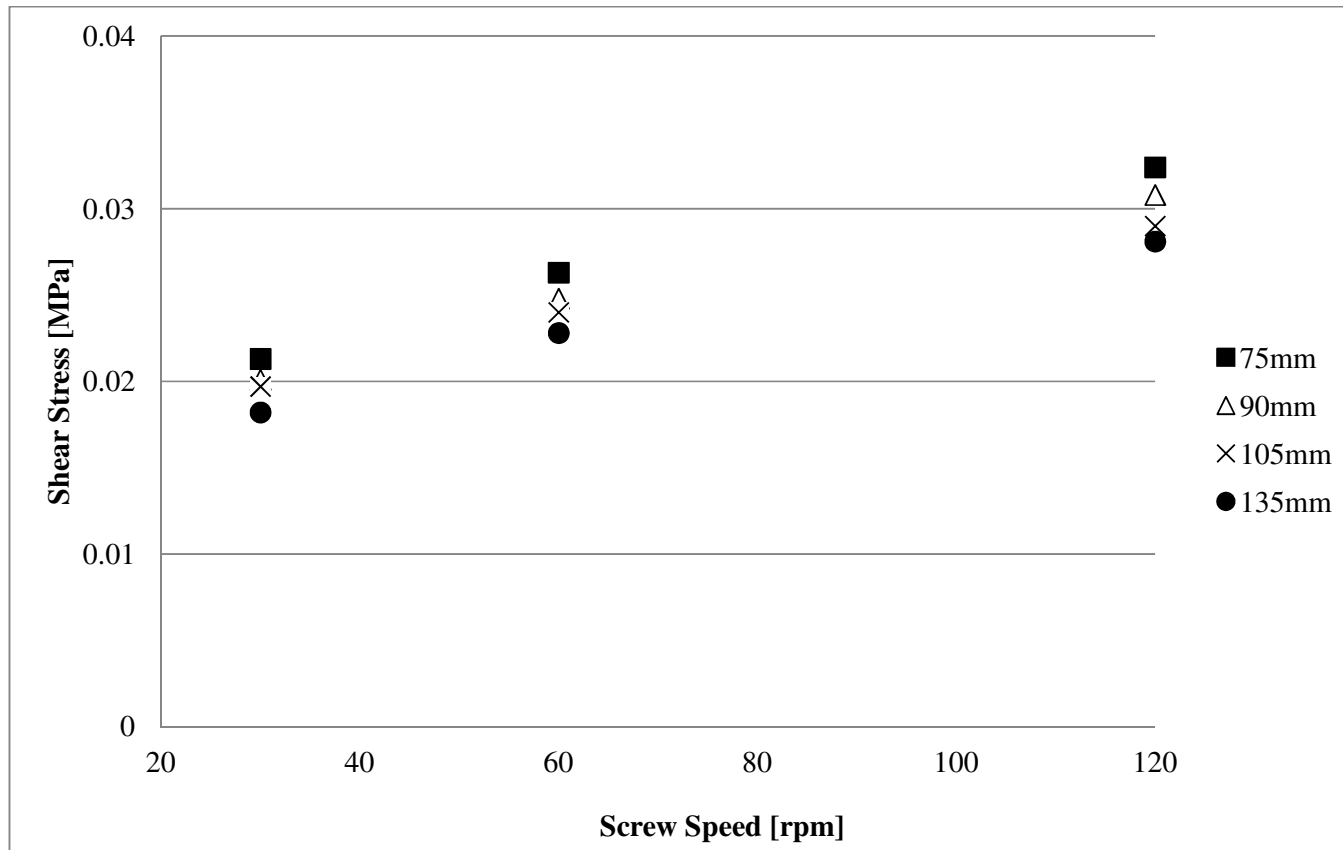


Figure 6.21. The Average Shear Stress for Various Screw Speed and Screw Pitch Length Power Index 0.3

6.4.2. Mixing Parameter Lamda

Manas-Zloczower et al. (1989, 1992) defined the mixing parameter, λ , as in Equation 6.2.

$$\lambda = \frac{|\dot{\gamma}|}{|\dot{\gamma}| + |\omega|} \quad (6.2)$$

$$\bar{\dot{\gamma}} = \overline{\nabla V} + (\overline{\nabla V})^T \quad (6.3)$$

$$\bar{\omega} = \overline{\nabla V} - (\overline{\nabla V})^T \quad (6.4)$$

$$|\dot{\gamma}| = \sqrt{\frac{1}{2}(\dot{\gamma}:\dot{\gamma})} \quad (6.5)$$

$$|\omega| = \sqrt{\frac{1}{2}|\omega:\omega|} \quad (6.5)$$

where $|\dot{\gamma}|$ is the magnitude of the rate of strain tensor and $|\omega|$ is the magnitude of the rate of vorticity tensor. $\dot{\gamma}$ and ω are related to the second invariants of the strain rate tensor and vorticity tensor. λ quantifies the elongational and rotational flow which are often thought to be more strongly relevant to dispersive mixing compared to shear. It has a value between 0 and 1, where $\lambda = 0$ indicates pure rotation while $\lambda = 1$ indicates pure elongation and $\lambda = 0.5$ corresponds to simple shear flow. The mixing parameter λ distribution is indicated from Figures 6.22 to 6.25 for various cross sections of the conveying element with 105 mm screw pitch and a fluid with power index of 0.7.

Li and Manas-Zloczower (1994) mentioned that simple shear flow dominated most of the flow region of their simulated 34 mm counter-rotating twin screw extruder. Figures 6.29 to 6.32 show that the mixing parameter λ was between 0.5 and 0.6 in most regions, indicating shear flow was dominant for this ICRTSE as well. Figures 6.22 to 6.25 imply that the maximum λ occurs in the intermeshing region due to a high rate of the strain tensor and low rate of the vorticity tensor. The intermeshing region was the most effective flow domain of the ICRTSE in terms of bringing about dispersive mixing because of its high shear stress and high mixing parameter λ .

The average values of the mixing parameter λ for all the geometries in a complete cycle are shown in Tables 6.4 and 6.5 for power indexes of 0.7 and 0.3 respectively. It is obvious in Tables 6.4 and 6.5 that the average mixing parameter λ increased slightly with increasing screw pitch length. Power index had little effect on the average mixing parameter λ for power index values from 0.7 to 0.3, indicating mixing is more geometry dependent than fluid dependent though larger differences in viscosity might produce different results. The average mixing parameter λ was between 0.533 and 0.555 for various screw pitch lengths. This means that shear flow dominant in the metering region of an ICRTSE.

The mixing parameter λ distribution over the volume of ICRTSE are expressed in Figures 6.26 to 6.29 for 75 mm and 105 mm screw pitch lengths with power indexes of 0.7 and 0.3 respectively. It is obvious from Figures 6.26 to 6.29 that the power index of 0.7 has a little wider distribution than the power index of 0.3 for the same screw pitch length. In addition, the mixing parameter λ distribution rarely changed with increasing screw pitch length.

The effects of screw speeds on mixing parameter λ are shown in Figures 6.30 and 6.31 for power index 0.7 and 0.3. It is obvious that mixing parameter λ does not depend on screw speeds.

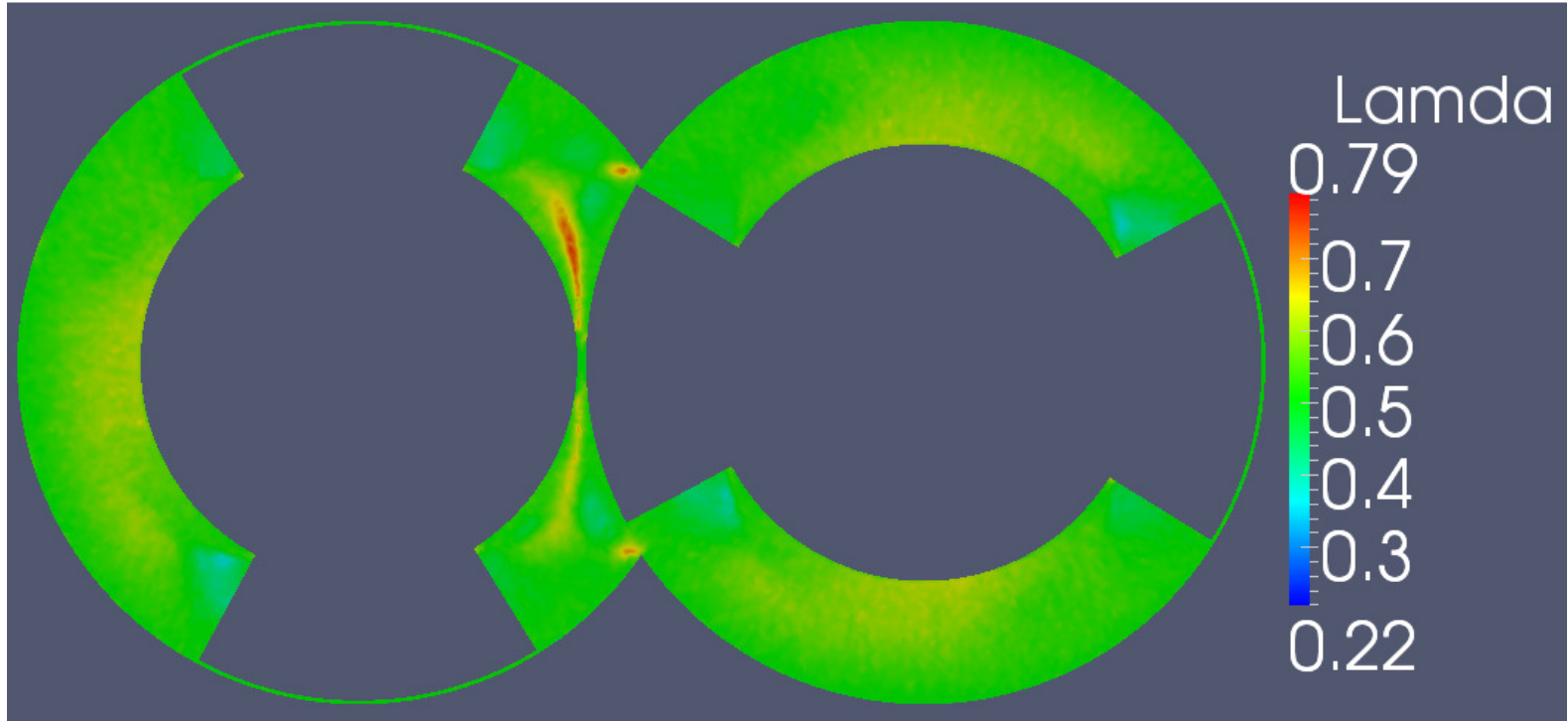


Figure 6.22. Mixing Parameter λ Distribution at Plane 1 $\alpha=90^\circ$ for 105 mm Screw Pitch Length Power Index 0.7

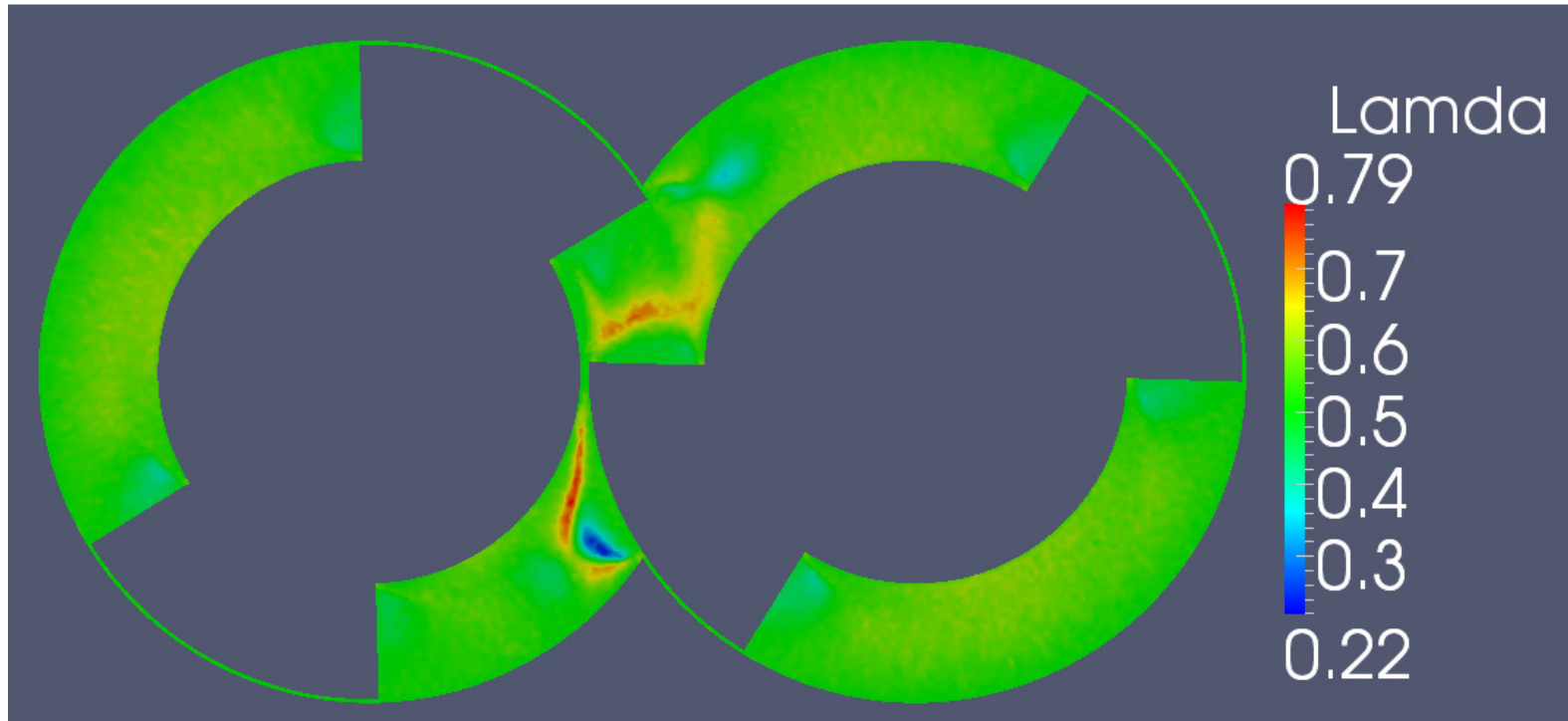


Figure 6.23. Mixing Parameter λ Distribution at Plane 2 $\alpha=90^\circ$ for 105 mm Screw Pitch Length Power Index 0.7

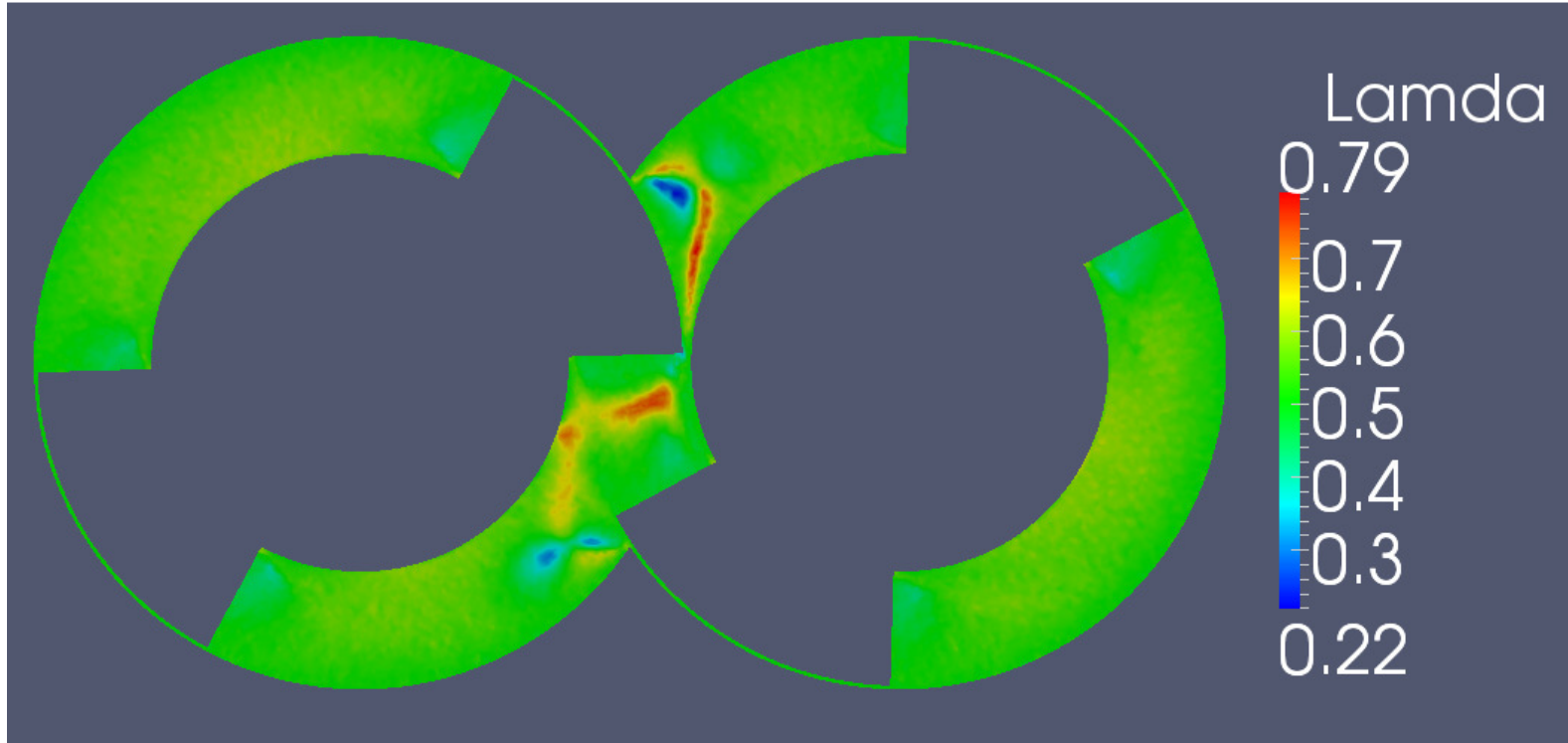


Figure 6.24. Mixing Parameter λ Distribution at Plane 3 $\alpha=90^\circ$ for 105 mm Screw Pitch Length Power Index 0.7

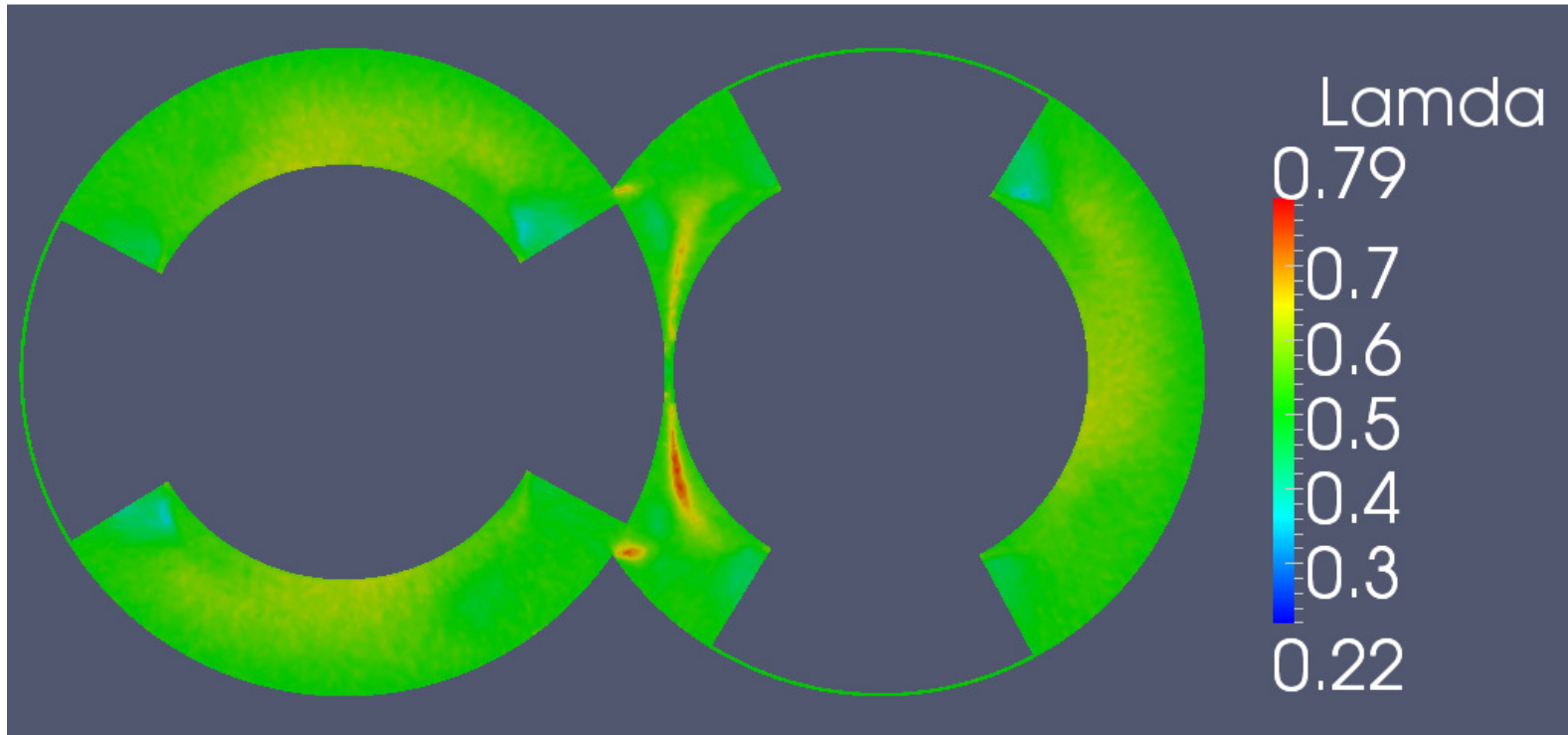


Figure 6.25. Mixing Parameter λ Distribution at Plane 4 $\alpha=90^\circ$ for 105 mm Screw Pitch Length Power Index 0.7

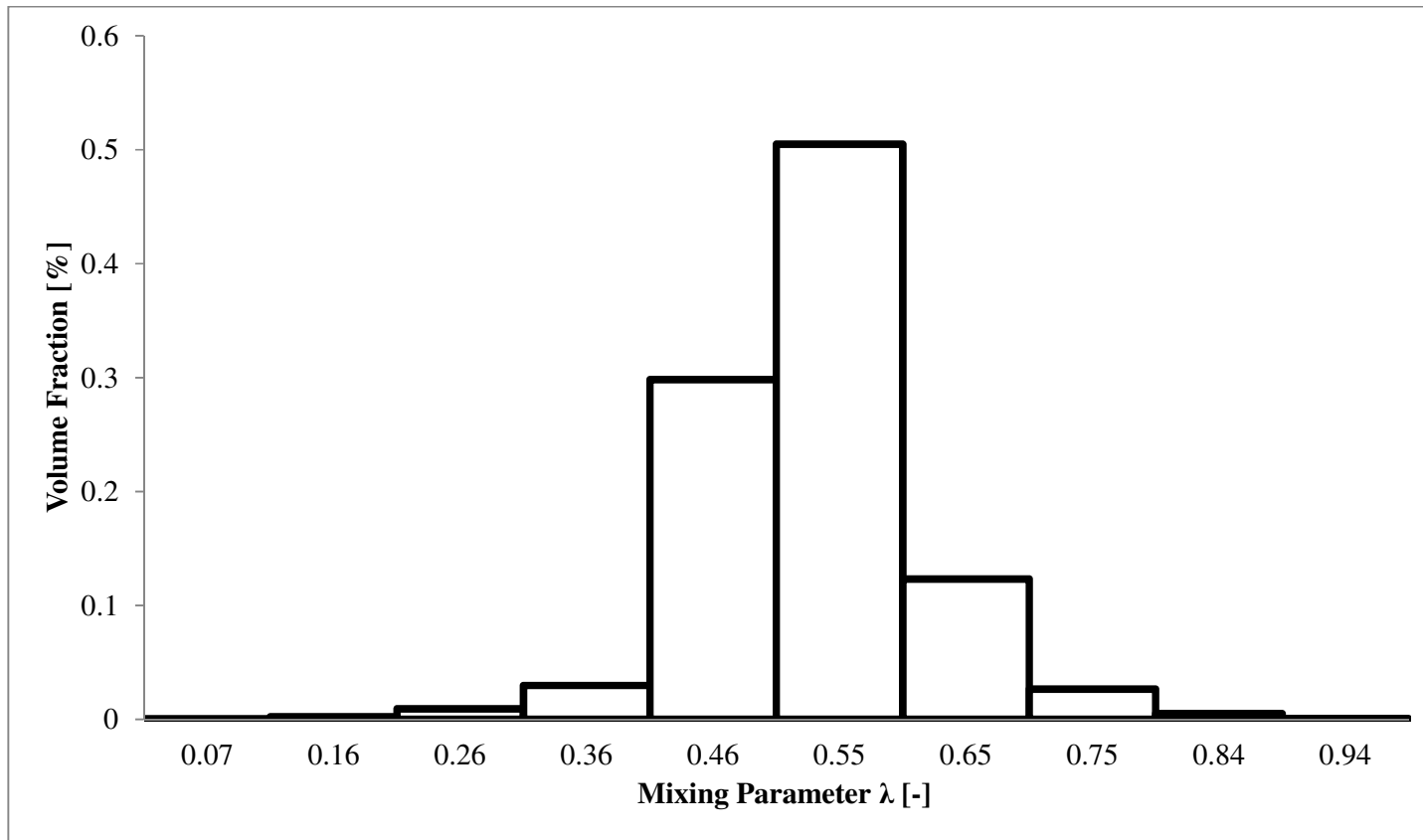


Figure 6.26. The Volume Distribution of Mixing Parameter λ for 75 mm Screw Pitch Length for Power Index 0.7

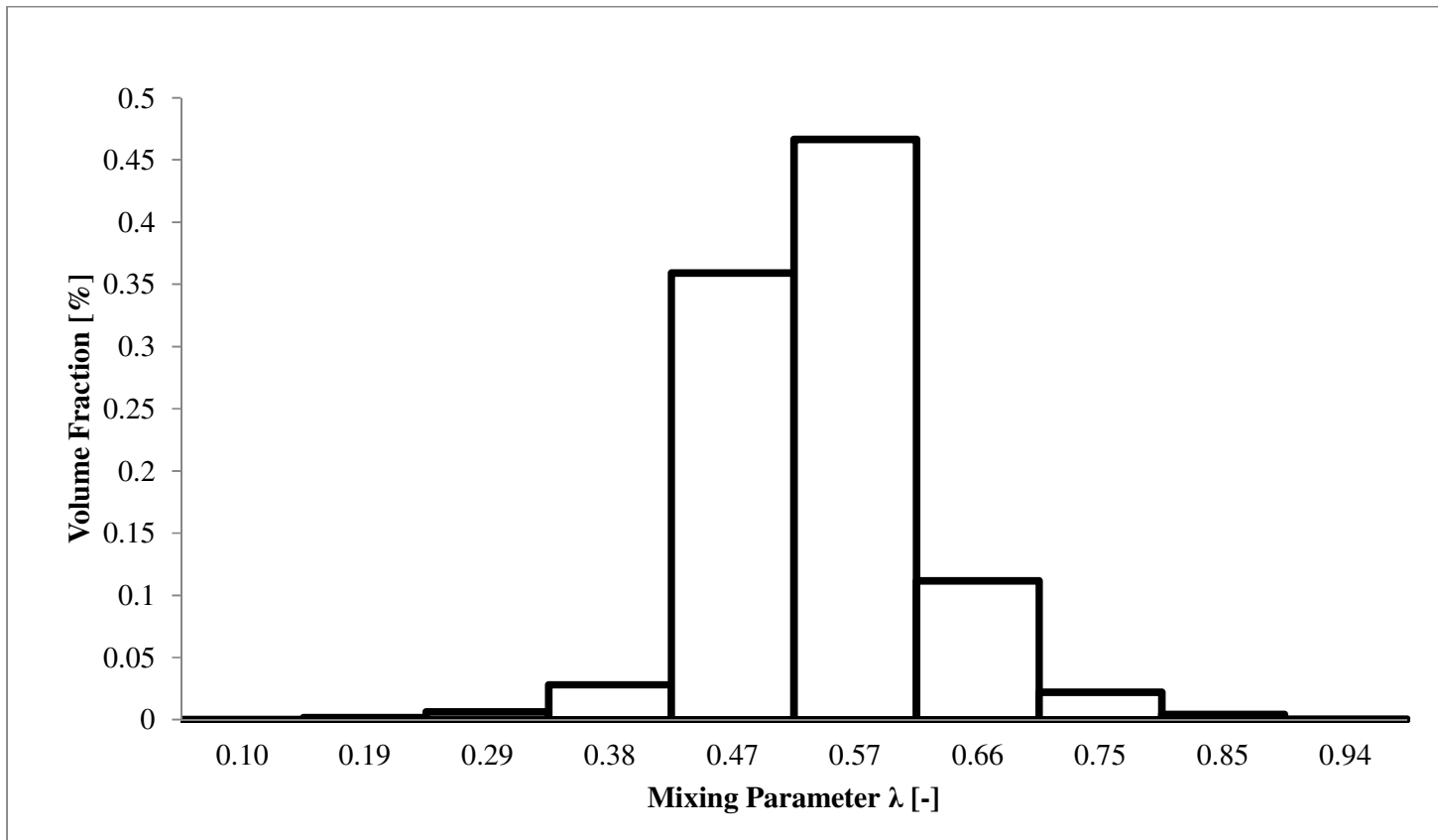


Figure 6.27. The Volume Distribution of Mixing Parameter λ for 105 mm Screw Pitch Length for Power Index 0.7

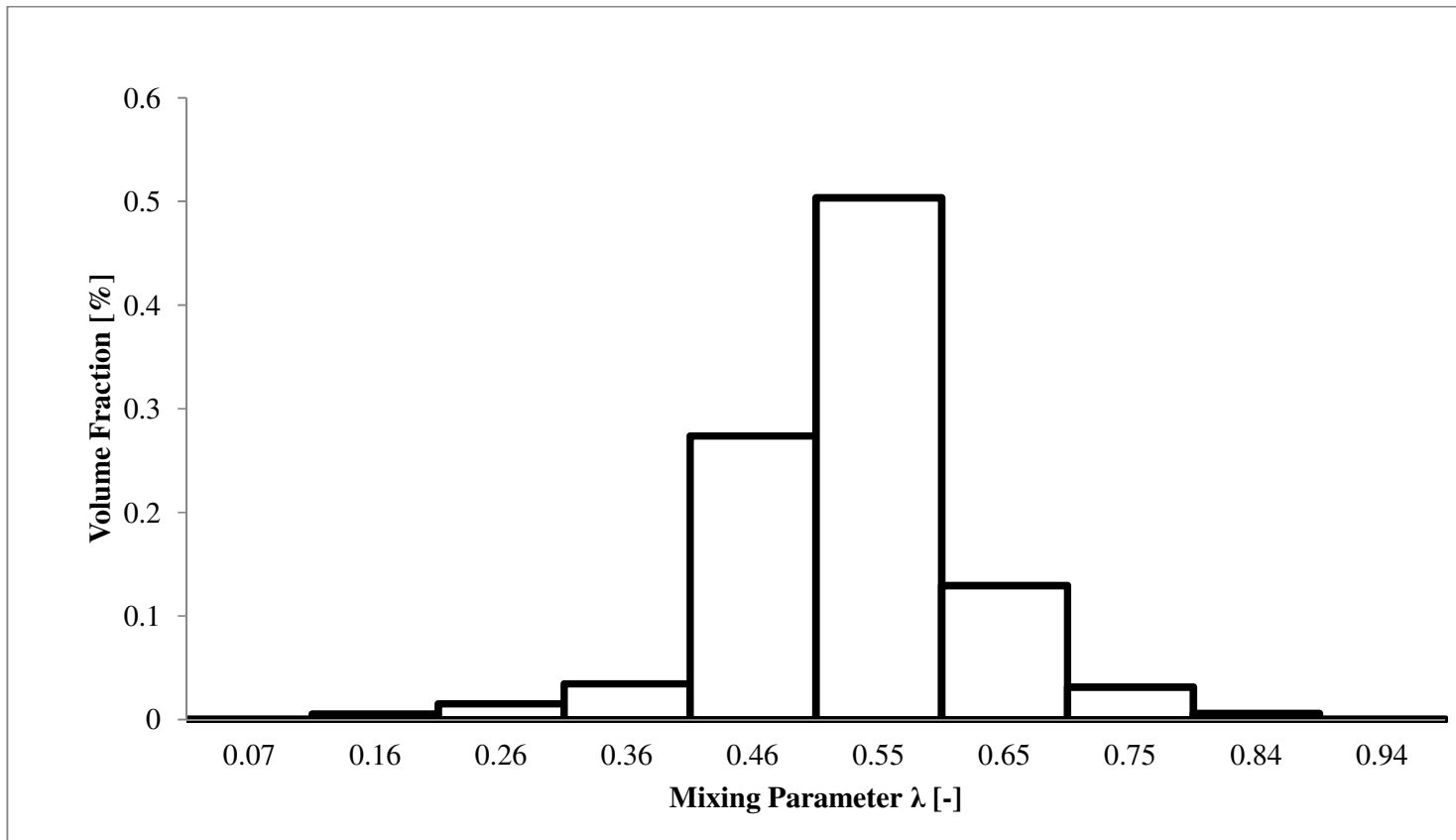


Figure 6.28. The Volume Distribution of Mixing Parameter λ for 75 mm Screw Pitch Length for Power Index 0.3

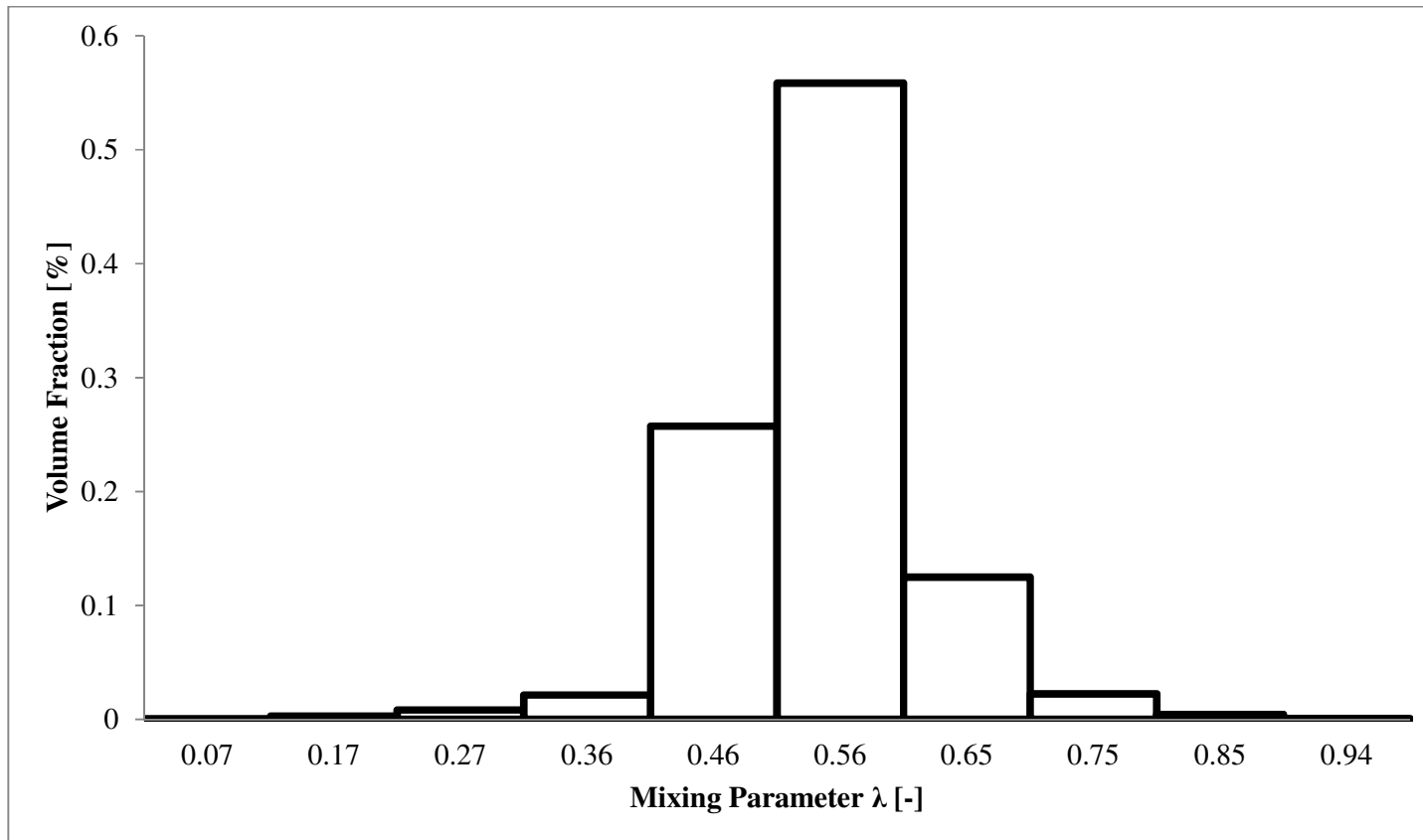


Figure 6.29. The Volume Distribution of Mixing Parameter λ for 105 mm Screw Pitch Length for Power Index 0.3

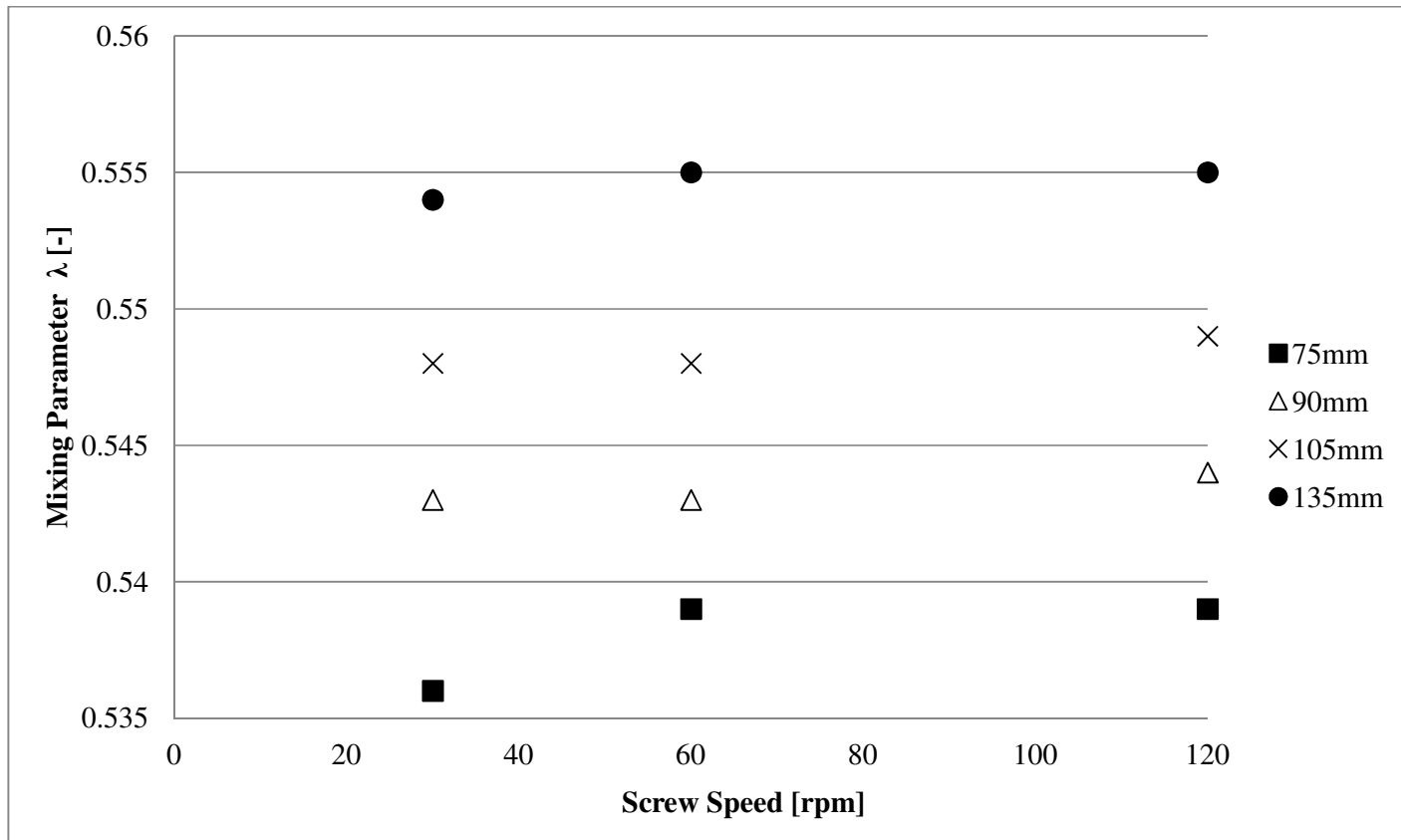


Figure 6.30. The Average Mixing Parameter λ for Various Screw Speed and Screw Pitch Length Power Index 0.7

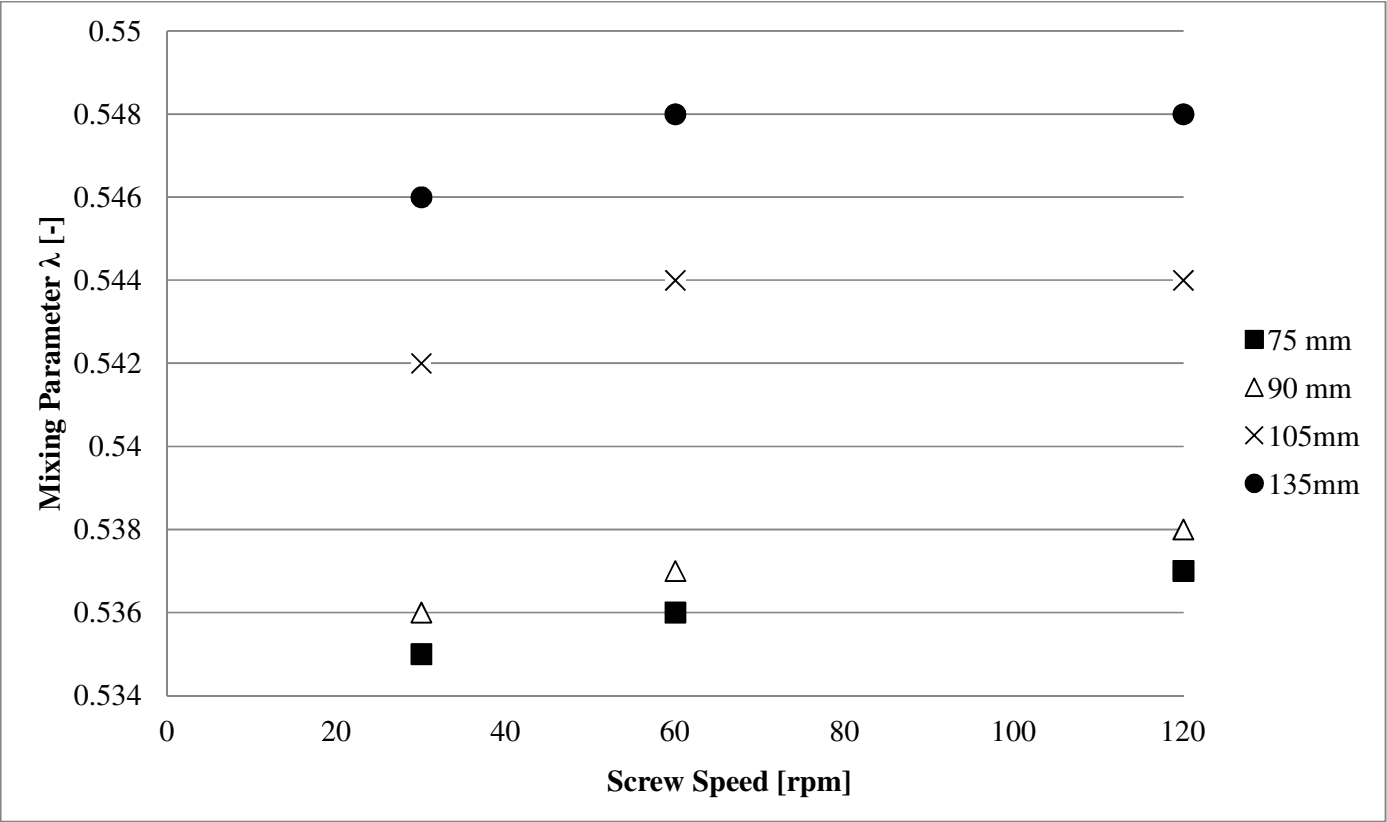


Figure 6.31. The Average Mixing Parameter λ for Various Screw Speed and Screw Pitch Length Power Index 0.3

Chapter Seven

COMPARASION OF SIMPLE FLOW MODEL AND COMPUTER SIMULATION

7.1. Introduction

In this chapter, simple flow model, which is explored in Chapter 3, is compared with computer simulation, covered in Chapter 6, in terms of flow behaviour. Different screw lengths, flight width-to-channel width ratios and screw speeds are compared for Newtonian fluid since simple flow model is only available for Newtonian fluids.

7.2. Comparison of the Effect of the Screw Pitch Length

Screw Pitch lengths of 75 mm, 90 mm, 105 mm and 135 mm were used for both simple flow model and computer simulation. Figure 7.1 indicates that both simple flow model and computer simulation increase gradually with increasing screw pitch length. Furthermore, increasing behaviour of mass flow rate decreases after 105 mm screw pitch length for both numerical and analytical solutions. Simple flow model and computer simulation also provide similar results for mass flow rate.

7.3. Comparison of the Effect of Flight Width-to-channel Width Ratio

The ratios of flight width-to-channel width of 0.35, 0.5, 0.636 and 0.875 were used. Figure 7.2 shows that mass flow rate decreases gradually with increasing the flight width-to-channel width ratio. It is obvious in Figure 7.2 that computer simulation and simple flow model provide very close mass flow rate results.

7.4. Comparison of the Effect of Screw Speeds

Screw speeds of 30, 60 and 120 rpm were investigated for both computer simulation and simple flow model. It can be seen in Figures 7.3 and 7.4 that mass flow rate increases proportionally with increasing screw speeds. Moreover, figures 7.3 and 7.4 indicate that numerical results match with simple flow model in the sense of mass flow rate.

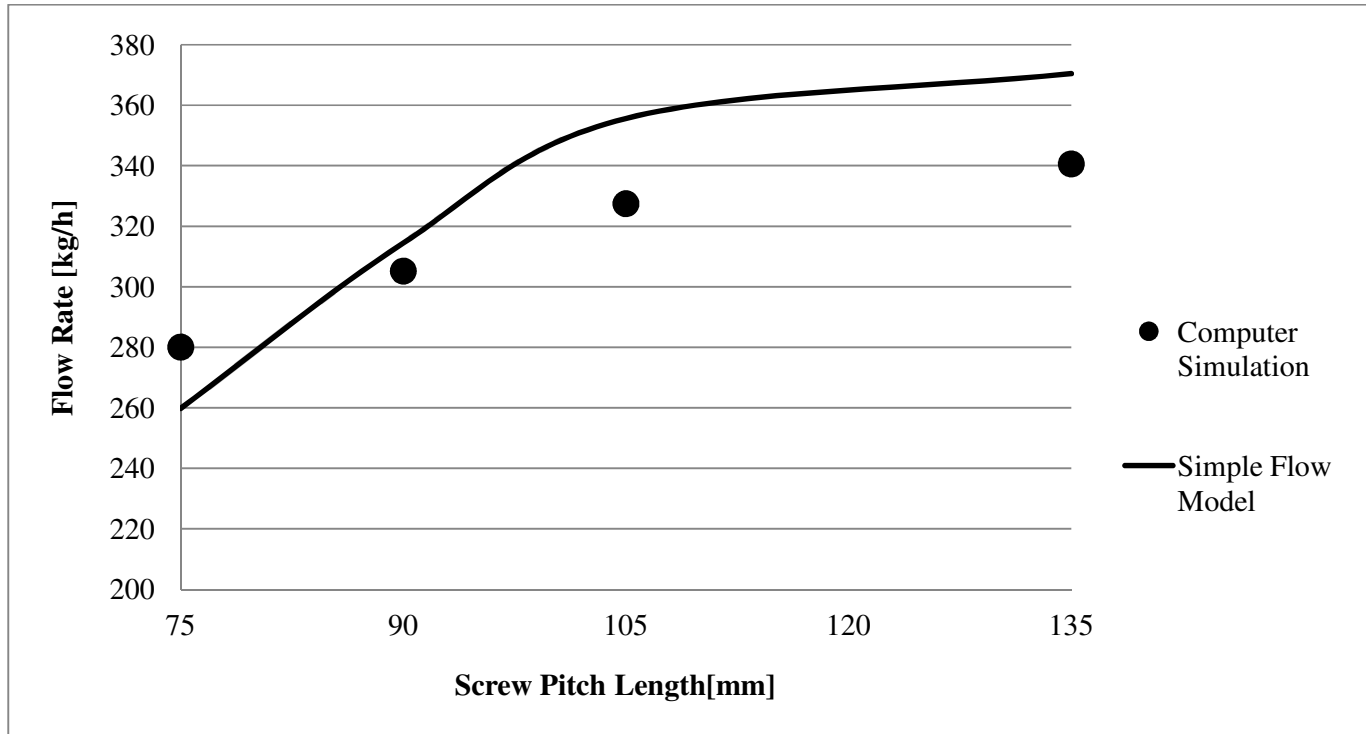


Figure 7.1. Comparison of the Effect of Screw Pitch Length for Computer Simulation and Simple Flow Model

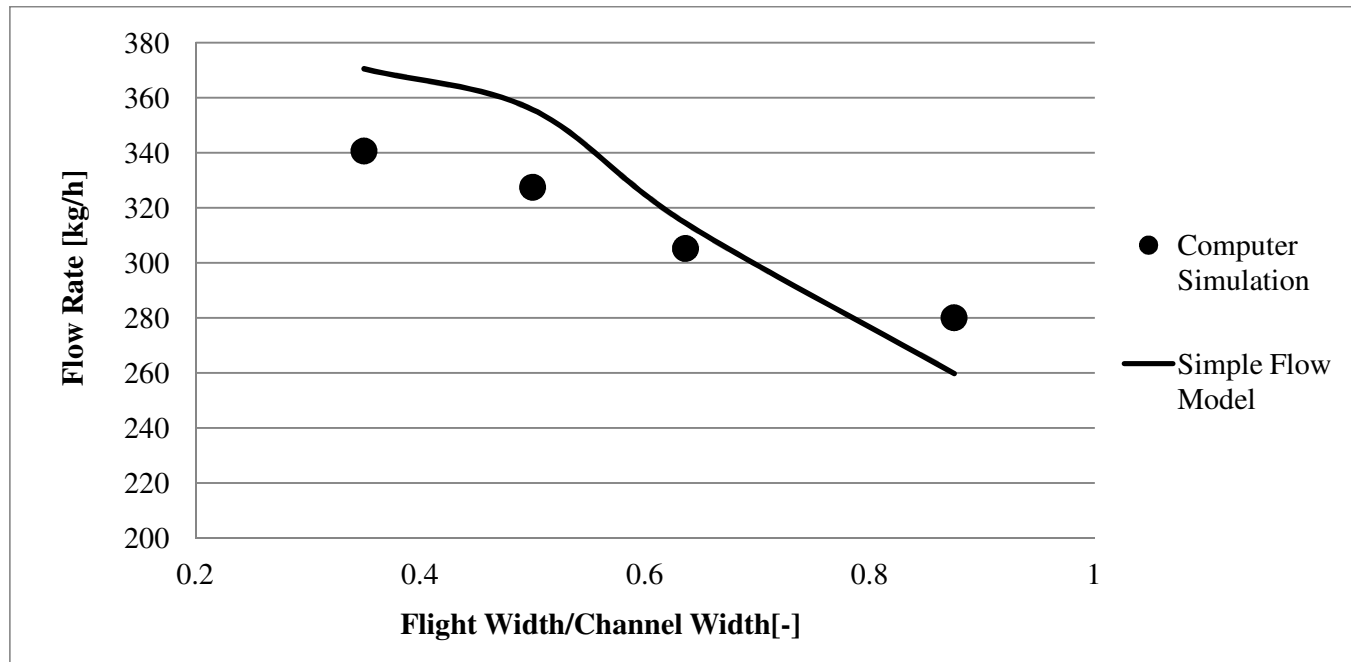


Figure 7.2. Comparison of the Effect of the Flight Width-to-channel Width Ratio for Computer Simulation and Simple Flow Model

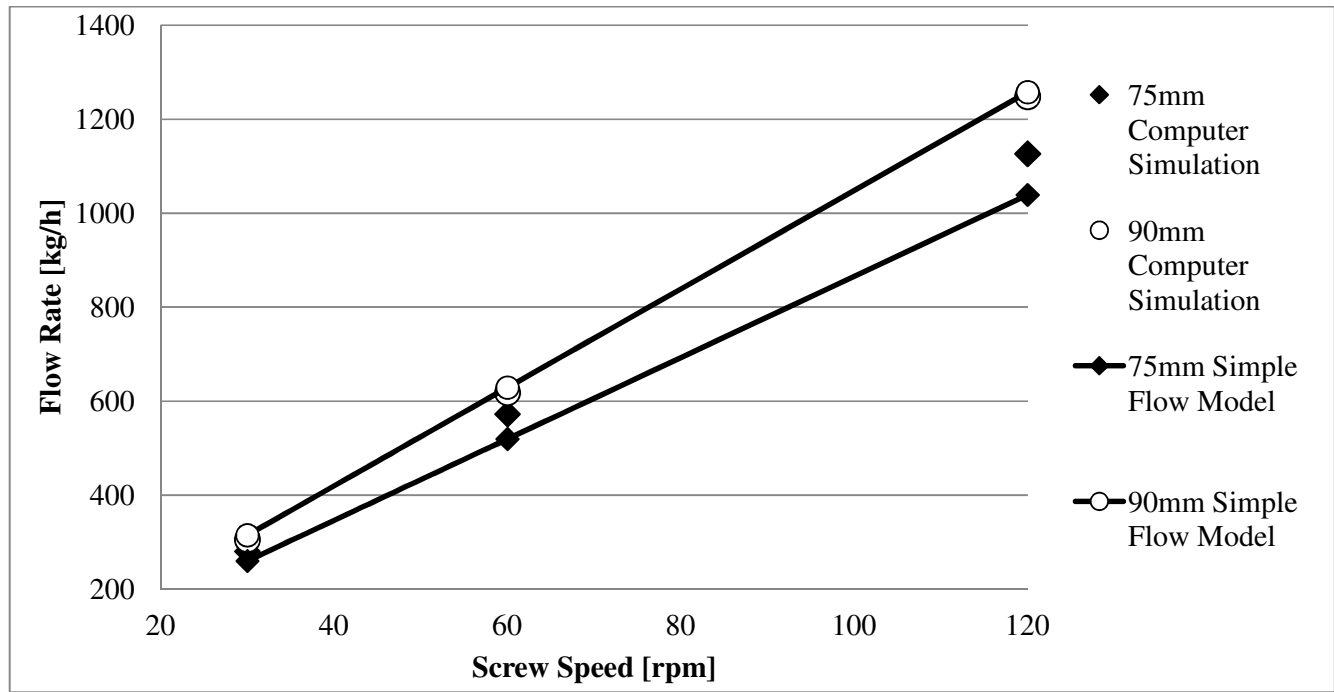


Figure 7.3. Comparison of the Effect of Screw Speed for 75 mm and 90 mm Screw Pitch Length for Computer Simulation and Simple Flow Model

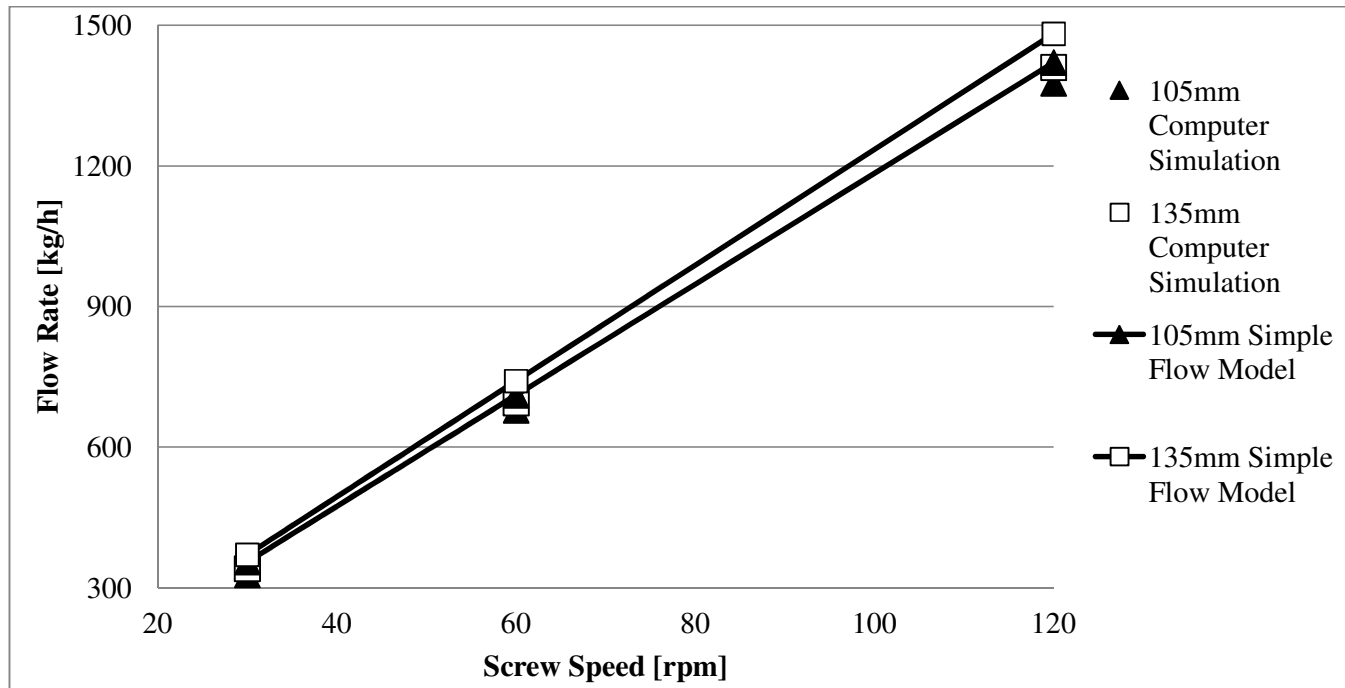


Figure 7.4. Comparison of the Effect of Screw Speed for 105 mm and 135 mm Screw Pitch Length for Computer Simulation and Simple Flow Model

Chapter Eight

CONCLUSION AND FUTURE WORK

8.1. Conclusion

The flow fields in the conveying section of the ICRTSE were obtained by using OpenFOAM®, a computational fluid dynamic package, based on the finite elements method. The problem of the time dependent moving boundaries was examined by selecting a number of sequential geometries to present a complete cycle. A good match was found between a simple analytical model and the computer simulation for the Newtonian flow condition, validating the simulation results in terms of pumping behaviour. For simple analysis, this analytical model appears a sufficient tool to start the design of the ICRTSE without necessitating the costly time to perform computer simulations. The computer simulation are however necessary for better understanding of the shear stress, shear rate and mixing etc. Design decision can be made to reduce pumping efficiency or shear stress level for shear sensitive material by using present model. The effect of different screw pitch lengths, flight width to channel width ratios, screw speeds and power indexes were investigated for pumping capacity and dispersive mixing behaviour of ICRTSE. Screw pitch length and ratio of flight width to channel width depend on each other geometrically, but it was decided to present the results for both parameters because it is useful for screw design purposes.

From the computer simulations, it was noticed that shear thinning behaviour of the fluid affects the pumping efficiency negatively. Secondly, pumping efficiency decreases with increasing screw pitch length. In addition, pumping efficiency goes up with increasing the ratio of flight width-to-channel width. Finally, screw speed almost does not affect the pumping efficiency at all.

Shear stress distribution was used to understand the dispersive mixing behaviour of ICRTSE. The average shear stress decreases gradually with increasing screw pitch length. Also, average shear stress is affected positively from the ratio of flight width-to-channel width. Average shear stress increase proportionally with increasing screw speed.

Dispersive mixing parameter lamda, λ , which quantifies the shear and elongational flow, was used to understand the mixing efficiency of different screw geometries and processing parameters. It is observed that the flow inside conveying element of ICRTSE is dominated by shear flow. The mixing parameter λ showed little variation by changing screw pitch length, ratio of flight width-to-channel width, screw speed or power indexes.

8.2. Recommendations

- The simulation of complete sections of the ICRTSE involving combination of mixing element and conveying element can be useful for better understanding.
- A better model would require a transient solver, temperature effects, distributive mixing and dispersive mixing for complete understanding of ICRTSE.

REFERENCES

Alsteens, B., Legat, V., Avalosse, T., Int. Polym. Proc., **XIX**, 207-217, (2004).

Bravo, V.L., Hrymak, A.N., Wright, J.D., Polym. Eng. Sci., **40**, 2, 525-541, (2000).

Bravo, V.L., Finite Element Simulation of Flow in Twin screw Extruder Mixing Elements, PhD Thesis, McMaster University, (1998).

Cheremisinoff, N.P., Polymer Mixing and Extrusion Technology, Marcel Dekker Inc. (1987).

Doboczky, Z., Plast. Verarb., **16**, 395 (1965²).

Doboczky, Z., Plast. Verarb., **16**, 57 (1965¹).

Dowson, D., Taylor, C. M., Ann. Rev. Fluid Mech., **11**, 35-66 (1979).

Eggen, S.S., Syre, A., Homogenizing Multimodal Polymer, European Patent EP1483311A1, (2004).

Fitzpatrick, H., Simulation and Characterization of Flow inside Twin Screw Extruders, PhD Thesis, Howard University, (2009).

Gonzales-Avila, S.R., Klaseboer, E., Khoo, B.C., Ohl, C., J. Fluid Mech., 241-260 (2011).

Gotsis, A.D., Ji, Z., Kalyon, D.M., Technical Papers SPE ANTEC, 139-142, (1990).

Gupta, M., Vivek, R., Kuehn, R., Technical Papers SPE ANTEC, 2350-2355, (2009).

Hong, M. H., White J. L., I., Int. Polym. Proc., **XIII**, 342-346, (1998).

Janssen, L. P. B. M., Twin Screw Extrusion, Elsevier, Amsterdam (1978).

Janssen, L.P.B.M., Mulders, L.P.H.R.M., Smith, J.M., *Plastics and Polymers*, **43**, 93, (1975).

Jiang, Q., Modeling Flow, Melting, Solid Conveying and Global Behaviour in Intermeshing Counter Rotating Twin Screw Extruders, PhD Thesis, University of Akron, (2008).

Jiang, Q., Wilczynski, K., White, J.L., Technical Papers SPE ANTEC, 491-496, (2007).

Juretic, F., Error Analysis in Finite Volume CFD, PhD Thesis, Imperial College, (2004).

Ilinca F., Hetu J. -H., I., Int. Polym. Proc., **XXV**, 275-286, (2010).

Ilinca F., Hetu J. -H., I., Int. Polym. Proc., **XXVII**, 111-120, (2012).

Ishikawa, T., Kihara, S.I., Funatsu, K., *Polym. Eng. Sci.*, **40**, 2, 357-364, (2000).

Kajiwarra, T., Nagashima, Y., Nakano, Y., Funatsu, K., *Polym. Eng. Sci.*, **36**, 16, 2142-2152, (1996).

Klenk, K. P., *Plast. Verarb.*, **17**, IV/1-IV/9 (1966).

Klenk, K. P., *Plast. Verarb.*, **22**, 33 (1971).

Lawal, A., Railkar, S., Kalyon D. M., *Technical Papers SPE ANTEC*, (1999).

Lee, C. C., Castro J. M., *Model Simplification*, in Chapter 3 from Charles Tucker III, *Computer Modelling for Polymer Processing*, Hanser (1989).

Li, T., *Analysis of Mixing Efficiency in Continuous Polymer Processing Equipment*, PhD Thesis, Case Western Reserve University, (1995).

Li, T., Manas-Zloczower. I., *Polym. Eng. Sci.*, **34**, 7, 551-558, (1994).

Ma, X., Shi, F., Geng, X., *Technical Papers SPE ANTEC*, 3288-3292, (2004).

Manas-Zloczower, I. And Feke, D.L., *Int. Polym. Proc.*, **II**, 185-190, (1988).

Manas-Zloczower, I. And Feke, D.L., *Int. Polym. Proc.*, **IV**, 3-8, (1989).

Menges, G., Klenk, K. P., *Plast. Verarb.*, **17**, 791 (1966).

OpenFOAM, *User's Guide*, Version 2.2.0, The OpenFOAM Foundation, (2013).

Ortiz-Rodriquez, E., Tzoganakis, C., *Technical Papers SPE ANTEC*, 171-175, (2009).

Ortiz-Rodriquez, E., *Numerical Simulations of Reactive Extrusion in Twin Screw Extrusion*, PhD Thesis, University of Waterloo, (2009).

- Potriefke, G., *Int. Polym. Proc.*, **XXI**, 61-72, (2007).
- Radl, S., Tritthart, T., Khinast, J.G., *Chem. Eng. Sci.*, **65**, 1976-1988, (2010).
- Sakai, T., Hashimoto, N., Kobayashi, N., *Technical Papers SPE ANTEC*, 146-151, (1987).
- Schenkel, G., *Kunststoffe Extrudertechnik*, Hanser Verlag, Munich (1963).
- Schenkel, G., *Plastics Extrusion Technology and Theory*, Iliffe Books Ltd., London, (1966).
- Sebastian, D.H., Rakos, R., *Technical Papers, SPE ANTEC*, 135-138 (1990).
- Shah, A., Gupta, M., *Technical Papers SPE ANTEC*, 443-447 (2004).
- Shon, K., Chang, D., White, J.L., *Int. Polym. Proc.*, **XIV**, 44-50, (1999).
- Sobhani, H., Nouri, M. R., Ghoreishy, M. H. R., *Iran. Polym. J.*, **19**, 143-154, (2010).
- Speur, J. A., Mavridis, H., Vlachopoulos, J., Janssen, L.P.B.M., *Advances in Polymer Technology*, **7**, 1, 39-48, (1987).
- Szydlowski, W., Brzoskowski, R., White, J.L., *Int. Polym. Proc.*, **1**, 207-214, (1987).
- Valette, R., Coupez, T., David, C., Vergnes, B., *Int. Polym. Proc.*, **XXIV**, 141-147, (2009).

Yang, H.-H., Flow Field Analysis of Batch and Continuous Mixing Equipment, PhD Thesis, Case Western Reserve University, (1993).

Yang, H. H., Manas-Zloczower, I., Int. Polym. Proc., **VII**, 195-203, (1992).

Yao, C. -H., Manas-Zloczower, I., Int. Polym. Proc., **XII**, 92-103, (1997).

Wang, C., Manas-Zloczower. I., Polym. Eng. Sci., **34**, 15, 1224-1230, (1994).

White, J. L., Twin Screw Extrusion: Technology and Principles, Hanser, NY (1990).

Wolf, D., Holin, N., White, D.H., Polym. Eng. Sci., **26**, 9, 640-646, (1986).